BAJECE

e-mail: editor@bajece.com

Balkan Journal of Electrical & Computer Engineering

International Referred Indexed Journal

www.bajece.com

Vol : 1
No : 1
Year : 2013
ISSN : 2147-284X

Sponsored by the

- Kirklareli University,
- Klaipeda University
- Inonu University
- Istanbul Technical University
- Kirklareli University Advanced Technologies Research and Application Center.

This journal is accredited by the Kirklareli University subsidy purposes. It is abstracted and indexed in Copernicus, Index Google Scholarship and the PSCR.

Aim & Scope

The journal publishes original papers in the extensive field of Electrical-Electronics and Computer engineering. It accepts contributions which are fundamental for the development of electrical engineering, computer engineering and its applications, including overlaps to physics. Manuscripts on both theoretical and experimental work are welcome. Review articles and letters to the editors are also included.
Application areas include (but are not limited to): Electrical & Electronics Engineering, Computer Engineering, Software Engineering, Biomedical Engineering, Electrical Power Engineering, Control Engineering, Signal and Image Processing, Communications & Networking, Sensors, Actuators Remote Sensing, Consumer Electronics, Fiber-Optics, Radar and Sonar Systems, Artificial Intelligence and its applications, Expert Systems, Medical Imaging, Biomedical Analysis and it's applications, Computer Vision, Pattern Recognition, Robotics, Industrial Automation.

BAJECE

Balkan Journal of Electrical & Computer Engineering

International Referred Indexed Journal

ISSN: 2147- 284X
Vol: 1
No: 1
Year: April 2013

CONTENTS

BALKAN JOURNAL OF ELECTRICAL & COMPUTER ENGINEERING
(International Referred Indexed Journal)

Contact
www.bajece.com
e-mail: editor@bajece.com
bajece@bajece.com

Phone: +90 288 214 05 14
Fax: +90 288 214 05 16

Kirklareli University, Department of Electrical & Electronics Engineering, 39060, Kirklareli-Turkey.

On Convergence of Carson Integral for Horizontally Layered Earth

T. Lazimov

***Abstract*—Convergence of the Carson integral for heterogeneous (horizontally layered) ground is researched in the article. This integral determines earth's contribution to the some parameters of double-wired aerial system, such as intensity of electrical field and mutual impedance and also to the magnetic vector potential of single aerial wire. Although there have been obtained several analytical expressions for the integral under consideration in the case of homogeneous ground and worked up some methods for it's calculation in the case of heterogeneous (horizontally layered) ground possibility of obtaining analytical solutions of the Carson integral for heterogeneous ground in general have not been researched yet and just a solution in the terms of principal value were once got. Almost all the other solutions obtained were got indirectly and have an approximate character, such as power series and asymptotical formulae.**

In the base of very general consideration it was shown in the article that this integral does not exist in the terms of general value.

Index Terms—**convergence, general value of integral, horizontally layered earth**

I. Introduction

IT is known that the Carson integral appears in problems concerned to taking into account influence of earth on long electrical lines' wave fields. It determines contribution of the earth into the some parameters such as electrical field intensity [1], magnetic vector potential [2], modified linear impedance [3, 4]. Some analytical expressions of the Carson integral have been obtained since 1926 after it was stated in [1]. These expressions were got either due to non-direct [1, 5, 6, 7] and direct [2 – 4, 8] integration. Some of these solutions e.g. ones presented in [2, 4, 5, 8] took into account longitudinal displacement currents in the earth i.e. they are appropriate for quasi-conductive earth.

It has always been especially interesting for researchers to obtain solutions of the Carson integral for horizontally layered earth. This is conditioned at first by the real structuring of the earth itself. Unfortunately obtaining of solutions under consideration is difficult theoretical problem. Some works may be noticed in this view.

T. Lazimov is with the Electric Supply and Insulation Department, Azerbaijan Technical University, 25 Huseyn Javid ave, AZ1073 Baku, Azerbaijan (e-mail: tahirlazim@gmail.com)

One of them is the article [9] which presented solution for the asymptotic range; another one is [10] in which the principal value of the Carson integral for horizontally layered earth had been presented. Survey of the sources concerned to the Carson integral has shown absence of its analytical solution in the terms of general value. For this reason it may be done an assumption on the possible divergence of the Carson integral for horizontally layered earth.

Note that we have not been able to find works dedicated to research of convergence of the integral under consideration itself. Obviously existence of the Carson integral for horizontally layered earth in the terms of principal value ascertained in [10] does not mean its existence in the terms of general value [11]. So research of the Carson integral's convergence seems very important since just dependently on the minded research it will be possible to consider conditions of the general values existence.

II. Research Of Convergence

Let us consider the following integral which is proportional directly to the Carson integral

$$I=\int_0^{\infty}\frac{\exp\left[-\left(h_k+h_m\right)\lambda\right]\cos a\lambda}{\lambda+\eta_1(\lambda)R(\lambda)}d\lambda, \tag{1}$$

where $\eta_1(\lambda)=\left(\lambda^2+k_1^2\right)^{\frac{1}{2}}$. For the arbitrary layer i.e. layer with index i it is written as

$$\eta_i(\lambda)=\left(\lambda^2+k_1^2\right)^{\frac{1}{2}}.$$

The function

$$R(\lambda)=th\left\{\eta_1 d_1+arcth\left[\frac{\eta_1}{\eta_2}cth\left(\eta_2 d_2+\ldots+arcth\frac{\eta_{n-1}}{\eta_n}\right)\right]\right\}$$

is one inversed to the so called modified impedance function.

E.g. for the three-layered earth it is written as

$$R(\lambda)=th\left\{\eta_1 d_1+arcth\left[\frac{\eta_1}{\eta_2}cth\left(\eta_2 d_2+arcth\frac{\eta_2}{\eta_3}\right)\right]\right\},$$

hk and hm are the mean highs of the two-wired system conductors with indexes k and m;

a is the projection of distance between these conductors to the horizontal plane;

λ is the integration variable;

di is the depth of the layer with index *i*. Note that at numeration of layers the index *i* is given to the layer closest to the earth surface;

n is the number of earth layers and consequently, in the same time the index of the last layer;

$k_i = \omega\left(\mu_i \varepsilon_i^{'}\right)^{\frac{1}{2}}$ is the wave number of the layer with index *i* determined via angular frequency $\omega\left(rad \cdot s^{-1}\right)$, magnetic permeability of the layer *i* $\mu_i\left(\Omega \cdot m^{-1}\right)$ and its complex dielectric permittivity $\varepsilon_i^{'}\left(F \cdot m^{-1}\right)$, at this

$$\varepsilon' = \varepsilon_i - j\gamma_i \omega^{-1}.$$

In the last expression $\varepsilon_i \left(F \cdot m^1\right)$ and $\gamma_i \left(Sm \cdot m^{-1}\right)$ are dielectric permittivity and specific conductivity of the layer with index i accordingly, j is imaginary unit.

Unlike the corresponding integral for electrically homogeneous earth researched in [1 - 4, 8] the integral under consideration contains the function $R(\lambda)$. Since this function is the function of hyperbolic tangent its change limits allows transformation of the integrand into infinity i.e. allows existence of the singular point inside the integration interval. Assume that the singularity inside the integration interval exists and denote it as λ_0. The existence of singularity may have been stated in research of the Carson integral existence will be obviously possible if we will find a point where the integrand in (1) transforms into infinity [12].

Divide the (0,∞) interval by parts, denote the integrand as $F(\lambda)$ and get

$$\int_0^{\infty} F(\lambda)d\lambda = \int_0^{\lambda_0} F(\lambda)d\lambda + \int_{\lambda_0}^{\infty} F(\lambda)d\lambda. \qquad (2)$$

Investigate convergence (i.e. existence in the terms of general value) of the right part of the last expression term by term.

For the first integral in the right part of (2) use known condition given in [13]. In accordance with the minded condition existence of improper integral with limited superior value requires an existence of the limited

$$\lim_{\lambda \to \lambda_0}\left[\left(\lambda_0 - \lambda\right)^{\alpha} \left|F(\lambda)\right|\right]$$

value for any α in the ($0 < \alpha < 1$) interval.

Forming the corresponding expression for a passage to the limit we will obtain

$$\lim_{\lambda \to \lambda_0}\left(\lambda_0 - \lambda\right)^{\alpha}\left[\frac{\exp\left[-\left(h_k + h_m\right)\lambda\right]\cos a\lambda}{\lambda + \sqrt{\lambda^2 + k_1^2 R(\lambda)}}\right] = \frac{0}{0}.$$

Use following denotations:

$$\varphi(\lambda) = \exp\left[-\left(h_k + h_m\right)\lambda\right]\cos a\lambda;$$
$$\psi(\lambda) = \lambda + \sqrt{\lambda^2 + k_1^2}R(\lambda).$$

In accordance with the L'Hospital rule,

$$\frac{d}{d\lambda}\left[\left(\lambda_0 - \lambda\right)^{\alpha}\left|\varphi(\lambda)\right|\right] =$$
$$= -\frac{\alpha}{\left(\lambda_0 - \lambda\right)^{1-\alpha}}\left|\varphi(\lambda)\right| - \left(\lambda_0 - \lambda\right)^{\alpha}\left\{a \cdot \exp\left[-\left(h_k + h_m\right)\lambda\right]\sin a\lambda + \right. \qquad (3)$$
$$\left. + \left(h_k + h_m\right)\exp\left[-\left(h_k + h_m\right)\lambda\right]\cos a\lambda\right\} / sign(\lambda)$$

$$\frac{d}{d\lambda}\left|\psi(\lambda)\right| = \frac{\left[1 + \frac{\lambda}{\sqrt{\lambda^2 + k_1^2}}R(\lambda) + \sqrt{\lambda^2 + k_1^2}\,\frac{dR(\lambda)}{d\lambda}\right]}{sign\,\psi(\lambda)}, \qquad (4)$$

where $sign\varphi(\lambda)$ and $sign\psi(\lambda)$ are the sign functions of the integrand's numerator and denominator accordingly. Their appearance in the formulae (3), (4) was conditioned by the differentiation of modulus of the functions.

Then for (3) and (4)

$$\lim_{\lambda \to \lambda_0 - 0}\left[\left(\lambda_0 - \lambda\right)^{\alpha}\frac{d}{d\lambda}\left|\varphi(\lambda)\right|\right] = -\infty \text{ for all the } \alpha < 1,$$

$$\lim_{\lambda \to \lambda_0}\frac{d}{d\lambda}\left|\psi(\lambda)\right| = \frac{1 + \frac{\lambda_0^2}{\lambda_0^2 + k_1^2} + \sqrt{\lambda_0^2 + k_1^2}\,\frac{dR(\lambda)}{d\lambda}}{sign\,\psi(\lambda_0)}. \qquad (5)$$

Since derivative of the $R(\lambda)$ function (i.e. the hyperbolic tangent function) is positive and limited in all the range of definition [14] then denominator of the integrand is limited. Moreover, at the left-side passage to the limit

$$sign\,\psi(\lambda_0) = -1,$$

i.e. limit of the denominator's derivative is negative under and the limit under consideration is diverged to the positive infinity. (k+∞)

Besides it means that above done assumption on existence of singular point into the Carson integral' integration interval has been turned right.

As it is known from the [13] source if limit

$$\lim_{\lambda \to \lambda_0}\left[\left(\lambda_0 - \lambda\right)\left|F(\lambda)\right|\right]$$

is equaled to limited positive number then integral is diverged.

Consider the following limit,

$$\lim_{\lambda\to\lambda_0}(\lambda_0-\lambda)\left|\frac{\exp\left[-(h_k+h_m)\lambda\right]\cos a\lambda}{\lambda+\sqrt{\lambda^2+k_1^2R(\lambda)}}\right|=\frac{0}{0}.$$

Use L'Hospital rule.

Derivative of the numerator is equaled to

$$\frac{d}{d\lambda}\left[(\lambda_0-\lambda)^{\alpha}\left|\varphi(\lambda)\right|\right]=$$
$$=-\left|\varphi(\lambda)\right|-(\lambda_0-\lambda)\{a\cdot\exp\left[-(h_k+h_m)\lambda\right]\sin a\lambda+. \quad (6)$$
$$+(h_k+h_m)\exp\left[-(h_k+h_m)\lambda\right]\cos a\lambda\}/\,sign(\lambda)$$

Limit of the numerator's derivative is equaled to

$$\lim_{\lambda\to\lambda_0-0}\frac{d}{d\lambda}\left[(\lambda_0-\lambda)\left|\varphi(\lambda)\right|\right]=-\left|\varphi(\lambda_0)\right|.$$

Taking into account the expression (5) in the right side of the first integral in the expression (2) we will get

$$\lim_{\lambda\to\lambda_0}(\lambda_0-\lambda)\left|F(\lambda)\right|=A>0.$$

Thus we have got the positive and limited number. It means that Carson integral for horizontally layered earth diverges, i.e. does not exist in the terms of general value in the interval $(0,\lambda_0)$. However, it is also necessary to consider the second integral in the right side of the formula (2) since at division of the integration interval by the even number of segments (2 in our case) there can take place the infinities cancellation. It would make difficult to do some conclusion on the Carson integral convergence $(0,+\infty)$.

Analyze the following limit

$$\lim_{\lambda\to\infty}\left[\lambda^{\alpha}\left|F(\lambda)\right|\right]$$

at any $\alpha>1$ and get

$$\lim_{\lambda\to\infty}\lambda^{\alpha}\left|\frac{\exp\left[-(h_k+h_m)\lambda\right]\cos a\lambda}{\lambda+\sqrt{\lambda^2+k_1^2}R(\lambda)}\right|=$$

$$\lim_{\lambda\to\infty}\lambda^{\alpha-1}\left|\frac{\exp\left[-(h_k+h_m)\lambda\right]\cos a\lambda}{1+\sqrt{1+k_1^2\lambda^{-2}}R(\lambda)}\right|.$$

Since $th(\infty)=1$ and the denominator has limited value we get the $\infty\cdot 0$ kind of infinity.

Assume for certainty $\alpha=2$ and get

$$\lim_{\lambda\to\infty}\lambda\left|\frac{\exp\left[-(h_k+h_m)\lambda\right]\cos a\lambda}{1+\sqrt{1+k_1^2\lambda^{-2}}R(\lambda)}\right|\sim\lim_{\lambda\to\infty}\lambda\left[-(h_k+h_m)\lambda\right].$$

Use L'Hospital rule and get

$$\lim_{\lambda\to\infty}\lambda\cdot\exp\left[-(h_k+h_m)\lambda\right]=\lim_{\lambda\to\infty}\frac{\lambda}{\exp\left[(h_k+h_m)\lambda\right]}=$$

.

$$=\lim_{\lambda\to\infty}\frac{1}{(h_k+h_m)\exp\left[(h_k+h_m)\lambda\right]}=0$$

Since the limit does exist then in correspondence with [13, 15] the second integral in the right side also exists.

Thus, the Carson integral for horizontally layered earth is diverged in the interval $(0,\lambda_0)$ and converged absolutely in the interval (λ_0,∞) that in general means the divergence of the integral under consideration.

Differed convergence of the Carson integral on separate intervals may be explained due to the known Abel condition for the first interval and the Dirichlet condition for the second one [11]. Note that direct application of the minded conditions to investigate the Carson integral existence instead of ones used in the present research is not expedient since they are just necessary ones not sufficient.

Remind that however the Carson integral does not exist in the terms of general value it does exist in the terms of principal value [10] that is important for solving different problems concerned to calculation and analyze the long line's wave fields.

Note that the principal value of Carson integral for horizontally layered earth obtained in [10] corresponds to the solution got in [9] for heterogeneous earth in high-frequency (asymptotic) area. It also corresponds to the approximate solution for the homogeneous ground obtained by Kostenko in [16].

The result presented in the article let to explain why the solution of the Carson integral for horizontally layered earth can be obtained just for asymptotical area of arguments [9]. While the argument λ is increasing then the hyperbolic tangent function is asymptotically approaching to 1. A physical analog of this is permanent decreasing of the skin-layer's thickness at increasing of frequency. As a result independently on the earth first layer's thickness the length of electromagnetic field can be much less in the asymptotical area of frequencies. Thus, increasing of frequency leads to growing proximity the parameters of horizontally layered earth with ones for electrically homogeneous earth with parameters the horizontally layered earth's first layer has i.e. the Carson integral for horizontally layered earth becomes similar to one for homogeneous earth in the asymptotical area (range of frequencies).

III. CONCLUSION

Despite the fact that the Carson integral for heterogeneous (horizontally layered) ground has been known since 1926 there have not been researched in general its existence (i.e. convergence) in the terms of general value. Some special problems concerned to this integral such as determination the intensity of electrical field and magnetic vector potential and mutual impedance of long electrical lines were researched in different years. It was found in particular the solution of the integral under consideration in the terms of principal value.

The present research stated that the Carson integral for horizontally layered earth does not exist in the terms of general value

REFERENCES

[1] Carson, J.R., "Wave propagation in overhead wires with ground return", *The Bell System Technical Journal*, Vol.5, No.4, 1926, pp.539-554

[2] Bursian V.R. Theory of electromagnetic fields used in electrical exploration. Leningrad: Nedra, 1972 (in Russian)

[3] Lazimov, T.M., "Analytical Expression of Carson Integral for Electrically Homogeneous Ground", *Electricity*, No.8, 1993, pp.66-72 (in Russian)

[4] Lazimov, T.M., "Analytical Expression for the Resistance of Electrically Homogeneous Ground Taking Account its Dielectric Properties", *Russian Electrical Engineering*, Vol. 66, No.2, 1996, pp.27-31

[5] Wise, W. H., "Propagation of free frequency currents in ground return systems", *Proceeding IRE*, Vol.22, No.4, 1934, pp.522-527

[6] Noda, T., "A double logarithmic approximation of Carson's ground-return impedance", *IEEE Transactions on Power Delivery*, Vol.21, No.1, 2006, pp.472-479

[7] Gary, C., "Approche complete de la propagation multifilaire en haute frequency par utilization des matrices complexes", *EDF Bulletin de la Direction des Etudes et Recherches*, Serie B, No.3-4, 1976, pp.5-20

[8] Perelman, L.S., "Refinement of wave propagation theory in the view of some technological problems", *NIIPT Transactions*, Vol.10, 1963, pp.103-120 (in Russian)

[9] Kaskevich, T.P., Puchkov, G.G., "Influence of horizontally layered earth's structure on mutual inductance coefficient between single-wired lines", *Transactions of SibNIIE*, Vol.33, 1976, pp.36-47 (in Russian)

[10] Glushko, V.I., "Methods for calculation magnetic influence between electric circuits taking into account finite conductance of earth", *Electricity*, No. 3, 1986, pp.6-18 (in Russian)

[11] Granino A. Korn and Theresa M. Korn., "Mathematical Handbook for Scientists and Engineers. Definitions, Theorems, and Formulas for Reference and Review". New-York: McGraw-Hill Book Co., 1967

[12] Lavrentyev M.A. and Shabat B.V., **"**Methods of the Theory of Functions of a Complex variable", Moscow: Nauka, 1973

[13] Gradshteyn I.S. and Ryzhik. I.M., "Table of Integrals, Series, and Products", San Diego, San Francisco, New York, Boston, London, Sydney, Tokyo: Academic Press, 2000

[14] Yahnke E., Emde F, Losch F., "Tables of higher functions", New-York: McGraw-Hill Book Co., 1960

[15] Prudnikov A.P., Brychkov Yu.A. and Marichev O.I., "Integrals and Series", Vol. 3: More Special Functions. New York: Gordon and Breach, 1989

[16] Kostenko, M.V., "Mutual impedances between overhead lines taking into account skin-effect", *Electricity*, No.10, 1955, pp.29-34 (in Russian)

Tahir Lazimov was born in Baku, Azerbaijan in 1955. He received the engineer qualification in electrical engineering from the Azerbaijan State Oil Academy, Baku, in 1977, Ph.D. degree in high voltage engineering from the Tomsk Polytechnic Institute, Tomsk, Russia Federation, in 1989 and D.Sc. degree in electrical engineering from the Azerbaijan Power Engineering Institute, Baku, in 1997. He has been a Professor since 2006 (Presidential Higher Attestation Commission).

From 1977 to 2004 he worked in the Power Engineering Research Institute, Baku, where he occupied the positions of Academic Secretary and Principal Researcher. Since 2004 he has been a head of the Electric Supply and Insulation Department in the Azerbaijan Technical University, Baku.

He is the author of about 160 scientific works including three books, dozens of articles and papers published in scientific journals and transactions and International conferences' proceedings, methodical works and inventions. His research areas include transitional processes in power electric systems and their computer simulation, power systems electromagnetic compatibility. Ph.D. and M.Sc. thesis are preparing under his supervision.

Professor T. Lazimov is the member of the Scientific Board on Power Engineering at the Azerbaijan National Academy of Science and also some other scientific councils and editorial boards in Azerbaijan and abroad.

Thermal Response of Power Transformer under Various Loading Conditions

Y. Çilliyüz, Y. Biçen, F. Aras

***Abstract*—Power transformers are major elements of the electric power transmission and distribution systems. Loadability of the transformer depends on the temperature affected by the loading variable and environment temperature. It is therefore essential to predict thermal behaviors of a transformer during normal cyclic loadings and particularly in the presence of overload conditions. This study presents a simple thermal model of a power transformer based on analogy between heat flow and current flow considering structure properties and operating conditions of the transformer. Top-oil temperature and thermal response of the transformer are determined and examined using the thermal model for different loads and time intervals.**

Index Terms—**Power transformers, thermal resistance, thermal capacitance, thermal analogy and thermal circuit**

I. INTRODUCTION

POWER transformers are major and expensive elements of the electric power transmission and distribution system. A transformer is operated at rated voltage and frequency, without exceeding the temperature rise due to overloads. The temperature rise is the most important parameter to determine the lifetime of transformer which has the thermal limitations of the core, winding, and insulation. Therefore, the loadability of the transformer depends on the maximum allowable temperature of the insulation known as hot-spot temperature [1, 2].

Recently, researchers have focused on monitoring and diagnosis of the power transformers because of the direct relationship between aging and temperature of the transformer [4]. The lifetime of the insulation is 1.0 under %100 load factor, continuous exposure to the hottest spot temperature, at 110^{o}C [3]. Lifetime of transformer insulation is halved by an increase in temperature range from 6 to 8^{o}C [1, 4]. Therefore, thermal modeling of the power transformer is very important to estimate the life time under any overload condition at certain time interval or determine the limit of overload rate.

This study is supported by the Scientific Research Projects Unit of Kocaeli University. Project number: 2010/33.

Y. Çilliyüz and F. Aras are with the Department of Electrical Education, Kocaeli University, Umuttepe, Kocaeli, Turkey (e-mail: ycilliyuz@kocaeli.edu.tr, faruk.aras@kocaeli.edu.tr)

Y. Biçen is with the DMYO, Industrial Electronics, 81010 Uzunmustafa, Duzce University (yunusbicen@duzce.edu.tr)

More accurate thermal model of a power transformer provides its reliable operation and should include following procedures;

- Structure, physical and electrical properties of transformers' parts
- Cooling operation system
- Insulation materials of transformers
- Operation conditions
- Environmental conditions

On the other hand, cooling system plays an important role to dissipate the heat in transformer. Therefore, a supplemental cooling system can be used during the overload transient conditions.

II. THERMAL CIRCUIT MODEL

It is well known that joule, eddy and hysteresis losses are caused with temperature rise in magnetic core and windings in a power transformer. Windings losses depend on load current and cause majority of the temperature rise. Therefore the generated heat is transferred during the operation since all insulation materials of transformer have thermal limitations [6, 7]. However, the insulations have ability to resist heat flow and store heat. Hence simple thermal model of a transformer is represented by a thermal resistance and capacitance similar to the electric circuit model. They are very important parameters to define thermal and loading capability of the power transformer [7, 8]. Particularly, thermal capacitance is considered calculating thermal rating under transient overloads.

A. Electrical-Thermal Analogy

A thermal circuit model is based on a fundamental similarity between the heat flow caused by the temperature difference and the electric current flow caused by a difference of potential, shown in Table 1. The thermal analogy uses formulations similar to electric equations as follows;

$$v = R_{el}.i \qquad i = C_{el}.\frac{dv}{dt} \tag{1}$$

$$\theta = R_{th}.q \qquad q = C_{th}.\frac{d\theta}{dt} \tag{2}$$

TABLE 1
THERMAL ANALOGY

Thermal		Electrical	
Generated Heat	q	Current	I
Temperature	θ	Voltage	V
Thermal Resistance	R_{th}	Resistance	R_{el}
Thermal Capacitance	C_{th}	Capacitance	C_{el}

A simple thermal circuit, shown in Fig. 1, includes a heat source, a thermal resistance and a capacitance as in electrical circuit.

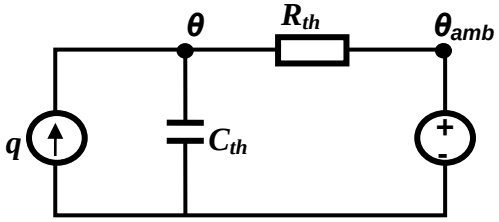

Fig.1. Thermal circuit

The thermal response of the circuit can be obtained using energy balance equation [5]:

$$q.dt = C_{th}.d\theta + \frac{\theta - \theta_{amb}}{R_{th}}.dt \tag{3}$$

$$q = C_{th}.\frac{d\theta}{dt} + \frac{\theta - \theta_{amb}}{R_{th}} \tag{4}$$

Where:

q is the heat generation, C_{th} is the thermal capacitance, q is temperature, R_{th} is the thermal resistance, θ_{amb} is the ambient temperature.

The thermal capacitance is directly related to the material's properties and used for solid and liquid materials as follows [1, 8]:

$$C = c_p.\rho.v \tag{5}$$

Where:

c_p is the specific heat of material (c_p=1.8 kJ/kg.K for oil and c_p= 0.5 kJ/kg.K for metal parts as core or windings[8]), ρ is Density of material, and v is Volume of the material.

B. Thermal Equivalent Model

Thermal equivalent circuit of the transformer can be defined as shown in Fig. 2. Using this model, a Simulink model was created to analyze according to the loading conditions of the power transformer.

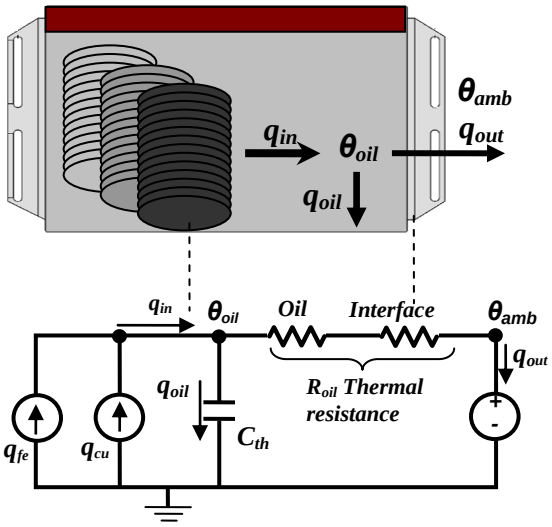

Fig. 2. Thermal equivalent circuit model [5]

Where;

q_g is total losses, q_{fe} is no-load losses, q_{cu} is load losses, $C_{th\text{-}oil}$ is equivalent thermal capacitance of the oil, θ_{oil} is top-oil temperature, and θ_{amb} is ambient temperature.

III. CASE STUDY

As a case study, a 250 MVA power transformer is selected and some of its values, shown in Table 2 [9], have been used to calculate the parameters in thermal model.

Thermal response of the power transformer is determined for three loading conditions shown in Table 3 as follows;

- Condition 1: Constant load factor for different time periods.
- Condition 2: Variable load factors for the same time period with condition 1.
- Condition 3: Random variable load factors for different time periods. For instance, load factor is increased 4 times in the period between 480_{th} and 492_{nd} minutes.

TABLE 2
PROPERTIES OF THE POWER TRANSFORMER 250 MVA

Power Losses			
Winding(DC) Losses		Eddy losses	Stray Losses
P_w (W)		P_E (W)	P_S (W)
411780		29469	43391
Masses			
Winding	Core	Tank and connectin	Oil
m_{wdn}(kg)	m_{fe}(kg)	m_{mp}=M_{Tank} (kg)	m_{oil}=M_{Fluid} (kg)
29181	99389	39760	73887

TABLE 3
LOADABILITY STATE OF 250MVA TRANSFORMER DEPEND ON TIME FOR 3 TYPES OF CONDITIONS

Condition 1		Condition 2		Condition 3	
Time (minute)	*Load Factor (p.u)*	*Time (minute)*	*Load Factor (p.u)*	*Time (minute)*	*Load Factor (p.u)*
0-120	1	0-120	0,5	0-300	1
120-240	1	120-240	0,25		
240-360	1	240-360	0,30	300-480	1,2
360-480	1	360-480	0,35		
480-600	1	480-600	0,50	480– 492	4
600-720	1	600-720	0,60	492-780	0,7
720-840	1	720-840	0,55	780-1080	1,2
840-960	1	840-960	0,60		
960-1080	1	960-1080	0,60	1080-1260	1,2
1080-1200	1	1080-1200	0,55		
1200-1320	1	1200-1320	0,65	1260-1440	1,5
1320-1440	1	1320-1440	0,7		

A. *Simulation Results*

According to the guide for loading of transformer of IEEE Standard [3], hot-spot temperature of 110°C and ambient temperature of 30°C are assumed. Simulations were started at t=0 (the transformer put into the service first time).

Top-oil temperature and losses versus loading time of the power transformer for % 100 load factor given as condition – 1 is shown in Fig. 3. It can be seen that the top-oil temperature reaches saturation point between 350 and 500 minutes at constant load factor. This type of loading is considered to determine capability and life-time of the transformer.

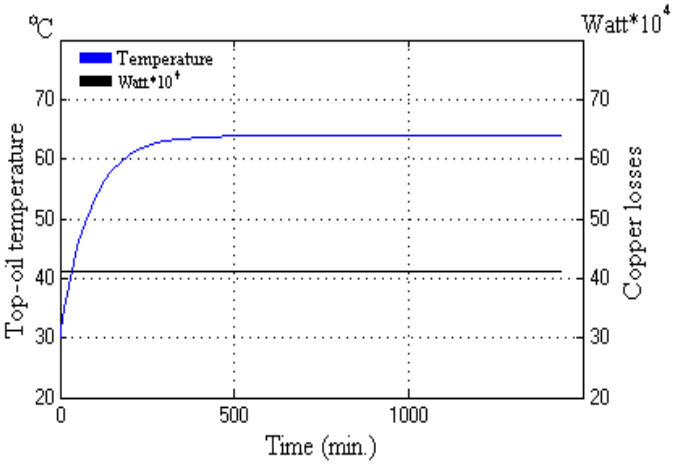

Fig. 3. Operating condition of steady state

The top-oil temperature rise versus daily loads for condition 2 is shown in Fig. 4. The response of temperature increases slower than the load current due to thermal capacity of transformer insulation. Particularly, this situation is important for short duration emergency overloads in condition 3 as shown in Fig. 5. Although the rate of increase of load factor is approximately four times between 480_{th} and 492_{nd} minutes, it is seen that temperature rise cannot same respond. It means that heat dissipation rate changes slowly due to the thermal capacitances of the materials. These overloads accelerate the aging of power transformer.

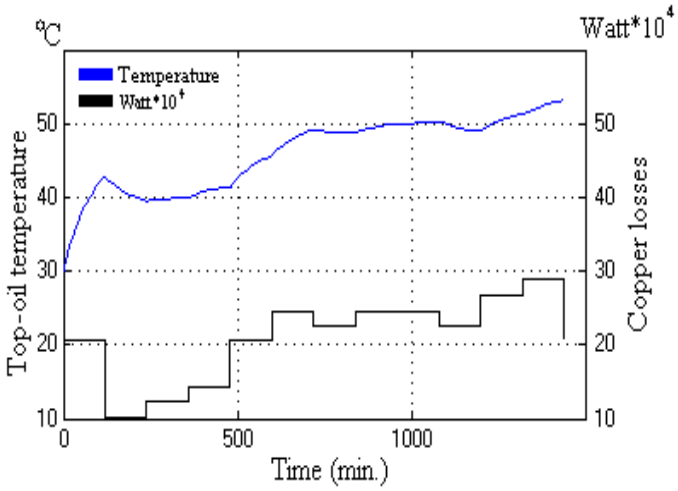

Fig. 4. Operating condition dependence on daily load factor

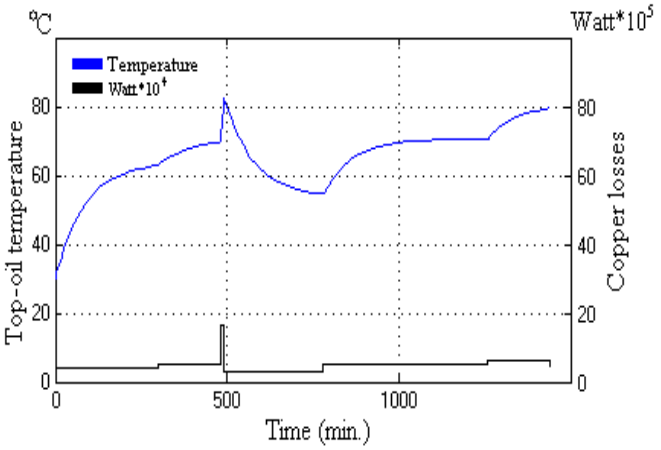

Fig. 5. Operating condition under variable and overloads

IV. CONCLUSION

The temperature rise is directly related to load current and thermal characteristics of power transformer. Therefore, the thermal modeling based on analogy between heat flow and electric current is very important to examine the thermal behavior of power transformer. Using this model, thermal response of a power transformer can be obtained easily under various loading conditions, and it is reliably operated.

REFERENCES

[1] Raymond, T. C., "Power Transformer Thermal Ratings – An Overview", IEEE Transmission & Distribution Conference – Dallas, Texas, 2003, pp. 1017–1021.

[2] Kömürgöz, G., Güzelbeyoğlu, N., "Kendi Kendine Soğuyan Kuru Tip Güç Transformatörlerinde Sıcaklık Dağılımının Belirlenmesi", itüdergisi/d mühendislik, Cilt 1, Sayı 1, 2002.

[3] IEEE Guide for Loading Mineral-Oil Immersed Power Transformers, IEEE Standard Institute of Electrical and Electronic Engineers, New York NY, 1995.

[4] Hunt, R., Giordano, M. L., "Thermal Overload Protection of Power Transformers – Operating Theory and Practical Experience", 59. Annual Protective Relaying Conference,Georgia Tech, Atlanta, Georgia, 2005, pp. 1-32.

[5] Swift, G., Molinski, T. S., Lehn, W., "A Fundamental Approach to Transformer thermal Modeling – Part I: Theory and Equivalent Circuit", IEEE Transactions on Power Delivery, Vol.16, No.2, 171 – 175, 2001.
[6] Susa, D., Lehtonen, M., Nordman, H., "Dynamic Thermal Modeling of Power Transformers", IEEE Transactions on Power Delivery, Vol. 20, No. 1, 2005, pp. 197 – 204
[7] Susa, D., "Dynamic Thermal Modeling of Power Transformers: Further Development – Part II", IEEE Transactions on Power Delivery, Vol. 21, No. 4, 2006, pp. 1971 – 1980
[8] Tang, W. H., Wu, Q. H., Richardson, Z. J., "A Simplified Transformer Thermal Model Based on Thermal – Electric Analogy", IEEE Transactions on Power Delivery, Vol. 19, No 3, 2004, pp. 1112 – 1119,
[9] Susa, D., "Dynamic Thermal Modeling of Power Transformers", Doctoral Dissertation Helsinki University of Technology Department of Electrical and Communications Engineering Power Systems and High Voltage Engineering, Finland, 2005.

Yusuf Çilliyüz was born in Bursa, Turkey. He received the BSc. degree in Electrical Education Marmara University in 2002, master degree from Kocaeli University in 2006. His PhD. education is in progress at Institute of Science of Kocaeli University, Turkey. He has worked as a Research Assistant in Department of Electrical Education. He is interested in solid and liquid dielectric aging and power transformers, distribution and transmission systems.

Yunus Biçen was born in Kastamonu, Turkey. He received the MSc. degree in Electrical Education from the University of Kocaeli in 2006 and received the PhD degree in 2012 at the same university. His research interests are in power transformer condition monitoring, fault diagnosis, power transmission, high-voltage equipment and aging. Moreover he has papers related computer applications to power system. From 2004 to 2008, he was a Research Assistant with the Department of Electrical Education, University of Kocaeli. He is presently working at the Department of Industrial Electronic in the University of Düzce.

Faruk Aras was born in Ardahan, Turkey in 1970. He received the BSc degree from Marmara University, Electrical Education Department, Istanbul, Turkey in 1994, the MSc and PhD degrees from Kocaeli University, Kocaeli, Turkey in 1996 and 2001, respectively. He is an associate professor teaching undergraduate and graduate courses at the Department of Electrical Education of Kocaeli University. His current research interests are in the area of electrical education, development of setup system and teaching materials for high voltage power system, cables and transformers. Assoc. Prof. Aras is a member IEEE Dielectrics & Electrical Insulation Society since 2011.

Development of a new integer hash function with variable length using prime number set

F. Aydin, G. Dogan

***Abstract*—This study presents a new integer hash function which generates a hash value with N-bit length from a key value which is N-bit in length as N is an element of the natural numbers space. A mix function in the structure of the proposed hash function is developed by using prime numbers. A common algorithm for all bit lengths in the hash function is used to both remove the probable conflicts and provide a good distribution in the hash table and also maintain the performance. In this study, the developed hash algorithm is compared with the existing ones in the literature, then obtained the results are analysed intimately.**

***Index Terms*—Integer Hash function, prime number, ROTATE operation, XOR operation.**

I. Introduction

Many applications require a dynamic set that supports only the dictionary operations. A hash table is an effective data structure for implementing dictionaries. A hash table is a generalization of the simpler notion of an ordinary array. An index is generated by means of Key used in hash tables and with this index; any data of the string can be reached. Key is unique and hence cannot be existed in another record. However, data can be the same with former ones. If the hash function does not generate the same hash code for two different keys, the hash table is said to be with the direct address.

There have been various applications where the hash table can be used in practice. Proxy server and server software can be given as examples. Proxy servers keep the web pages (visited before) in a local disc and then next connection to these pages is made through the disc. To go to the web content in the disc, proxy server generates a hash value by taking the desired address as key and with the hash value the web pages are displayed. In order to reach the correct data, the content should be saved in the index previously generated by the same function. Furthermore, server software's employ the dynamic hash tables to prevent the attacks of DoS (Denial of Service), DDoS (Distributed Denial of Service) and brute force. In the get and post type attacks against which firewall is usually ineffective and useless, in order to avoid the excessive load on the server and also to get over the server, user who sends such a request is added to the black list. Even if the user goes on sending request to the server, the user gets an answer like "http 403 forbidden" and also server will not be more tired of making such a treatment.

Hash function generates an index through the hash table by using a key. Locations of the data in the table are determined by the hash function. The hash function uses key as input and generates hash code or a hash value as output.

A hash function is called an integer hash function if it gets an integer number as a key and finally generates an integer hash value. An integer hash function is either a well-defined function which generates a hash value from an integer key with variable bit length, or a mathematical function. Hash functions are used in various treatments such as quick placement of a given search key on a data record, the treatments of file organization, determination of similarities among the matches of DNA array, detection of double records or similar records in the data structure and geometrical hashing and cryptology. A hash function has some properties expressed below coarsely.

- Calculation cost of a hash function applied to get hash-based solutions should sufficiently be small. For instance, binary search can locate an item in a sorted table of n items with $\log_2 n$ key comparisons. Therefore, a hash table solution will be more efficient than binary search only if computing the hash function for one key cost less than performing $\log_2 n$ key comparisons.
- A hash function must be deterministic. In other words, it must always generate the same hash value for any given input.
- One key or more does not yield the same hash value all the way.
- Hash function has not a complex structure.

There have been several hash functions (each one has different characteristics) used in various fields. These hash functions can be classified basically as following.

- Cyclic redundancy checks (CRC [1])
- Checksums (Fletcher's checksum [2], Luhn Algorithm [3], Verhoeff algorithm [4])
- Non-cryptographic hash functions (Jenkins hash function [5], Pearson hashing [6], The Goulburn Hashing Function [7], Integer Hash Function [8], Zobrist hashing [9])
- Cryptographic hash functions (HAVAL [10], MD6 [11], SHA-3 [12])

Several hash functions have been developed based on the aforementioned methods. Donald E. Knuth [13] introduced the multiplicative hashing as a way of forming a good hash function. It has been adopted as a method for development of many hash functions. For example, 32-bit mix functions by

F. Aydin, is with the Software Engineering Department, Kirklareli University, Kirklareli, Turkey (e-mail: fatih.aydin@kirklareli.edu.tr).

G. Dogan, is with Vocational School of Technical Science, Kirklareli University, Kirklareli, Turkey (e-mail: gokhandogan@kirklareli.edu.tr).

Robert Jenkins [5] and Thomas Wang [8] are based on the multiplicative method. Thomas Wang has 64-bit functions and Robert Jenkins has 96-bit functions except for 32-bit integer hash functions. Different approaches were regarded in the development of these hash functions. One of them is called the magic constant. Use of the magic constant approach supplies a good distribution in the hash table. The developed hash functions are defined as separate functions for key values of 32-bit, 64-bit and 96-bit. But, this situation reduces its flexibility. In addition, these hash functions have complex structure.

The developed hash function is described as a set of functions. Thus, behaviour of the function may be easily examined. Eventually, it helped us develop the intended hash function.

II. DESCRIPTION OF A NEW N-BIT INTEGER HASH ALGORITHM

One of the problems encountered during the development of Hash function is associated with the analyses of the function behaviour. The most important factor which makes the analyses of Hash function difficult is the complexity of the function. To overcome this complexity of the hash function, it is divided into sub-functions. Thus, behaviour of each function is examined easily. A hash function can be defined as the function set as following.

$$h : K \rightarrow \mathbb{N} \quad (1)$$

Where, *K* is key value and h is a hash function.

Hash function can be defined as a combination of two functions labelled f and g, or more functions. Let *f* be a function which is defined by a relation taking *K* to integer number space, Z.

$$f : K \rightarrow \mathbb{Z} \quad (2)$$

Let g be a function with a relation taking integer number space, *Z* to Natural number space, *N*. The function is expressed as following.

$$g : \mathbb{Z} \rightarrow \mathbb{N} \quad (3)$$

Hash function can be basically defined with both *f* and *g* functions as following.

$$h = g \circ f \quad (4)$$

In this context, hash value of *K* is calculated using the following formulation.

$$h(x) = g(f(x)) \quad (5)$$

Above formulation is only valid for a hash function excluding mix function. It must be formulated in the generalized form in the hash function (which has been developed by us) since it may involve mix functions, which is expressed as follows.

$$h(x) = g(f(g(f(g(f(\dots)))))) \quad (6)$$

Hash function has been basically developed by using two fundamental functions. First function is *f* function which rotates the bits of input value right while the other one is *g* function which applies *XOR* operation to two values. Regarding the relationship between *N* which means the bit width of key value inside algorithm, and set of prime numbers, an *f* and *g* function define a nested function and calculates *M* value which is the product of the mix function. Later, *M* value is put into *XOR* operation with *K*, thus the hash value is obtained.

Accordingly, function *f* rotates *k* input value *x*-bit right and is defined as following.

$$f(x) = k \ggg x \quad (7)$$

g function is acquired via *f* function's *XOR* with *k* input value. This is shown on formula (8).

$$g(f(x)) = k \oplus f(x) \quad (8)$$

With set of *P* as prime sets' subset, *f(x)* function is defined as $\forall x \in P$. There are two reasons for x to be chosen from prime set; firstly, prime numbers are not constantly ranging numbers. Secondly, the difference between two sequential prime numbers is narrow. For example, in Fibonacci numbers [14], Kaprekar numbers [15], etc, the gap between the numbers increases as the series proceed. This effects the hash table's distribution's efficiency. First 10 terms of the prime sets are shown at (9).

$$P = \{2, 3, 5, 7, 11, 13, 17, 19, 23, 29, \dots\} \quad (9)$$

f and *g* functions complexity in algorithm is calculated as: a subset is composed starting from the first element in the *P* set.

Total of this subset's elements should be equivalent or higher than *N* and at the same time should be constituting of the elements that have the closest values. Thus, all bits are converted into minimum *N*-bit length. For example, elements' set to be chosen for a key value of 32 bits are shown at (11).

$$(P_{32}) \subset P \quad (10)$$

$$P_{32} = \{2, 3, 5, 7, 11, 13\} \quad (11)$$

$$N \leq \sum_{i=0}^{5} (P_{32})_i \quad (12)$$

The relation between Fig. 1 $s(P_{32})$ and *N* bit number. Accordingly *f* and *g* functions for 32 bit numbers are used 6 times. This process is appropriate and useful number that repeating for creating 32 bit hash values. This method also creates appropriate values for the other bit length.

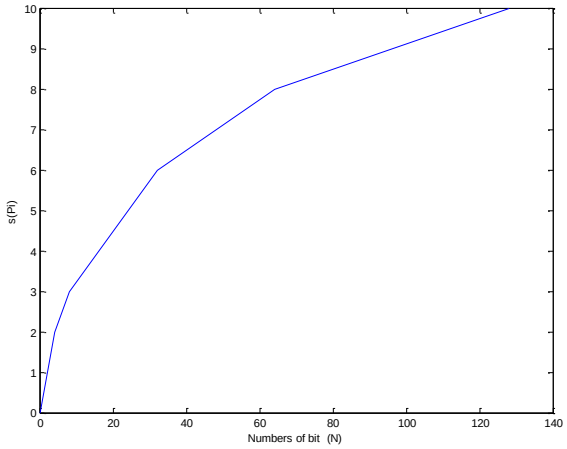

Fig. 1. The relationship between $s(P_{32})$ and N-bit is seen at the figure.

The calculation of hash value which will be created for *N-bit* key value is below:

$$K'_0 = K \oplus (K \ggg (P_N)_0) \quad (13)$$

$$K'_1 = K'_0 \oplus (K'_0 \ggg (P_N)_1) \quad (14)$$

$$K'_2 = K'_1 \oplus (K'_1 \ggg (P_N)_2) \quad (15)$$

$$\vdots$$

$$K'_{i-1} = K'_{i-2} \oplus (K'_{i-2} \ggg (P_N)_{i-1}) \quad (16)$$

$$K'_i = K'_{i-1} \oplus (K'_{i-1} \ggg (P_N)_i) \quad (17)$$

$$M = K'_i \quad (18)$$

After this step, the values of *M* and *K* are subjected to *XOR* and the value of hash is obtained.

$$H = (K \oplus M) \quad (19)$$

TABLE I
Obtaining Hash Value from 32 bit Key Value

Operations	Values	Results
K	0000 0000 0000 0000 0000 0000 0000 0001	0x00000001
$K \ggg 2$	0100 0000 0000 0000 0000 0000 0000 0000	0x40000000
K'_0	0100 0000 0000 0000 0000 0000 0000 0001	0x40000001
$K'_0 \ggg 3$	0010 1000 0000 0000 0000 0000 0000 0000	0x28000000
K'_1	0110 1000 0000 0000 0000 0000 0000 0001	0x68000001
$K'_1 \ggg 5$	0000 1011 0100 0000 0000 0000 0000 0000	0x0b400000
K'_2	0110 0011 0100 0000 0000 0000 0000 0001	0x63400001
$K'_2 \ggg 7$	0000 0010 1100 0110 1000 0000 0000 0000	0x02c68000
K'_3	0110 0001 1000 0110 1000 0000 0000 0001	0x61868001
$K'_3 \ggg 11$	0000 0000 0010 1100 0011 0000 1101 0000	0x002c30d0
K'_4	0110 0001 1010 1010 1011 0000 1101 0001	0x61aab0d1
$K'_4 \ggg 13$	1000 0110 1000 1011 0000 1101 0101 0101	0x868b0d55
K'_5	1110 0111 0010 0001 1011 1101 1000 0100	0xe721bd84
K	0000 0000 0000 0000 0000 0000 0000 0001	0x00000001
M	1110 0111 0010 0001 1011 1101 1000 0100	0xe721bd84
H	1110 0111 0010 0001 1011 1101 1000 0101	0xe721bd85

IntegerHasFunction shown as Pseudo code is at Fig. 2.

```
Function: IntegerHashFunction
Input: K: Integer
Output: H: Integer
Algorithm:

1:    n ← sizeof(K) * 8
2:    p ← GetLoopCount(n, primeList)    // Section 1
3:    temp ← K

4:    for i ← 0 to p      // Section 2
5:          do     K ← K ^ (K >>> primeList[i])

6:    H ← K ^ temp // Section 3
7:    return H
```

Fig. 2. Pseudo code of IntegerHashFunction function.

GetLoopCount() function on the row Section 1 on Fig. 2 returns the element number of the subset $s(P_n)$. The presentation of this function as Pseudo code is shown on Fig. 3.

```
Function: GetLoopCount
Input: n: Integer and primeList: Array of Integer
Output: p: Integer
Algorithm:

1:    p ← 0
2:    total ← 0

3:    for p ← 0 to primeList.Length
4:          do     if (total >= n)
5:                       then   break
6:                 else
7:                       total ← total + primeList[p]

8:    return p
```

Fig. 3. Pseudo code of GetLoopCount Function.

A. *Mathematical model of the hash function behaviour*

f(x) and *g(x)* functions which calculates the hash value of hash function are defined with bitwise operators. This process doesn't give an idea to us about function behaviours. Because of this, on the trials we have done with the numbers that have short bit length, we tried to learn function behaviours by comparing the results of function. For instance, the results coming from 4-bit numbers turning 1-bit to right was examined. When the results were examined, it was seen that the numbers increases with certain rate and then cropped. For instance, as well as turning 1-bit to right, it was seen that the numbers increases with 8 growth and when the number passes $(2^4 - 1)$ value, the process of mod operated. We expressed function behaviours as mathematical on equation (20). On this equation n equals to how many bits the number is, equation *x* equals to how many bits the number is going to be turned to right and finally *k* equals to input value.

$$f(x) = (k.2^{n-x}) \bmod (2^n - 1) \quad (20)$$

When we examine equation (20), we can make these analyses. Our number increases in the form of multiple of (2^{n-x}). But if this growth value is bigger than $(2^n - 1)$ value, the process of *mod* will be performed. Even so, the numbers show sequence with certain pattern.

g(x) function was expressed as the being subjected of *k* input value with *XOR* in *f(x)* function. We can show *XOR* logic operator by using mathematical and logic expressions on equation (21).

$$XOR(x, y) = x + y - (2 * x \wedge y) \quad (21)$$

When equation (21) was examined, $(x \oplus y)$ expression gives the difference of *x* and *y* bit sets to us. $(x \wedge y)$ expression which defined in *XOR* expression gives the intersection set of both numbers bit to us. We showed the expression mathematically on (22).

$$\sum_{i=0}^{n} \left(\frac{xy}{2^{2i}} \bmod 2\right) 2^i \quad (22)$$

We have summarized the statement at equation (22) with examining the multiplying the bits of two numbers at Fig. 4. As seen at Fig. 4, *AND* result of each bit is shown red. This method's equation is shown at (22). The result of *AND* process is always equal or less than less of two numbers. This is shown at (23).

$$(x \wedge y) \leq \min(x, y) \quad (23)$$

```
    1001
∧   1011
-------
    1001
   1001
  0000
 1001
-------
 1 0 0 1
```

Fig. 4. AND process of two 4-bit numbers.

We can find the result at (24) for *n-bit* numbers via induction method by processing *XOR*.

$$g(f(x))_{i=0 \text{ to } (2^{n-1})-1} = g(f(x))_{i=2^n-1 \text{ downto } 2^{n-1}} \quad (24)$$

The $M(x) = g(f(g(f(g(f(\dots)))))$function calculating the combination value at the Hash function showing a proper distribution for values at *n-bit* length is seen at Table I. To optimize the distribution, prime numbers set is used. Prime numbers set is shown at (25) and set of D_p which is the difference the set between the elements of this set.

$$P = \{2, 3, 5, 7, 11, 13, 17, 19, 23, 29, 31, \dots\} \quad (25)$$

$$D_p = \{1, 2, 2, 4, 2, 4, 2, 4, 6, 2, \dots\} \quad (26)$$

Prime numbers' forming series in this way enables a proper distribution at optimum step. Prime numbers series do not follow a known pattern in natural numbers. However, Riemann hypothesis claim that there is a solution at the complex plane on a straight line [16]. There is an important argument by Louis de Branges for the proof of Riemann hypothesis [17].

When 4 bit numbers are examined, it is seen that *M* value forms symmetry and there are two of each value. In order to prevent this intersection, *M* values and *K* values are processed with *XOR*. Hence, $H(x) = (K \oplus M(x))$ function enables us to produce hash value without intersection. After this *XOR* process, a satisfactory distribution is obtained as well.

III. Results and Discussions

Two variables are selected for the complexity analysis of the algorithm at Figure 1. The first one is *p* which is the elements of set of P_n that are chosen for *n-bit* and the second is *n* which is the bit width of the key value to be calculated. Running time of the *n-bit* integer hash function related to *p* and *n* is shown at (27) and (28).

$$T(n, p) = T'(n, p) + 15np + 3n \quad (27)$$
$$T(n, p) = 9np + 15np + 3n \quad (28)$$

Running time of *GetLoopCount* function that is defined in Fig. 1. Section 1 is related to *p* and *n* and it is *9np*. Running time of the lines defined in Section 2 is *15np*. Finally, running time of the statement defined at Section 3 is *3n*. If asymptotic attitude of (28) equivalence is stated in terms of Big-Oh notation, running time of the algorithm is *O(np)*.

When the *p* value of *O(np)* is $1 \leq p < n$, algorithm's complexity is *O(n)*. When *p* is $n \leq p < n^2$ algorithm's complexity is $O(n^2)$. But $s(P_n)$ value equal to all chosen values at *n*-bit length is always less than *n*. This is because the prime numbers are infinite [18, 19, 20, 21].

Non-collision possibility of *n-bit* integer hash function is proved at mathematical analysis section. Additionally, collision and distribution tests are made for 8, 16, 32 and 64 bit sets. After the tests, there is no collision for 8 and 16 bit sets. There aren't any collisions determined for 32 and 64 bit sets in 2^{23} values. Also, hash values produced for 8, 16, 32 and 64 bit sets show a proper distribution. Table III shows current integer Hash functions' comparisons.

TABLE II
Comparison Table of the Integer Hash Functions for 32-bit

Key Value	Algorithms				
	Thomas Wang (January 2007 version)	Thomas Wang (last version 3.1)	Robert Jenkins	Knuth	Our
0x000000d7	0x07568e43	0x47162bbc	0x139faf13	0x609733a7	0x9f4e4b4d
0x000002d9	0x5c7f5c7f	0x7a483c15	0x888c9a2a	0x0bf98909	0xb7fd21b0
0x00016e0f	0x0586ac91	0x7a94aa7c	0xcdb5d637	0x153b2f5f	0xa1dccdd0
0x003c89aa	0xd132d132	0x03a14ca9	0xbefd9a95	0x4672888a	0x03ee8f82
0x1cc4844e	0xba91ba91	0x37cd7a70	0x41719047	0x572a57ee	0xc8d9b0b3
0x2d80a6ec	0x99f899f8	0x2a1b39fd	0xb46a1299	0x498cf52c	0xf6a757e1
0x7fffffff	0x07d8396a	0x22e84a14	0xeb5744b1	0x61c8864f	0x0c6f213d

Bit variance (avalanche) comparison between key values and hash values that are produced with integer hash algorithms compared at Table II are shown at Table III. When avalanche values are examined, it is seen that developed integer hash algorithm results positively. The highest average avalanche in algorithms belongs to developed hash algorithm.

TABLE III
The comparison of bit variance between hash and key values of algorithms

Algorithms	Key Values							Average Avalanche
	0x000000d7	0x000002d9	0x00016e0f	0x003c89aa	0x1cc4844e	0x2d80a6ec	0x7fffffff	
Our	18	20	20	10	18	18	17	17,29
Thomas Wang (January 2007 version)	14	20	14	13	20	16	17	16,29
Thomas Wang (last version 3.1)	16	16	17	13	18	16	21	16,71
Robert Jenkins	18	14	16	18	14	18	15	16,14
Knuth	14	16	11	9	17	11	18	13,71

The integer hash function developed via the results does a proper hashing. Our algorithm is also an effective one in terms of performance and complexity.

IV. CONCLUSION

In this study, it is aimed to develop a new, integer hash function with the length of *n-bit*. It is fairly clear that no conflicts and disagreement has been encountered during all tests performed to seek the validation of the developed hash function. Added to them, in the part of mathematical analysis, it was proven that no disagreement occurred between the results compared other methods. The hash values which are the product of the hash function provided a good distribution inside the hash table. Besides all these, there has been no loss of the performance of the developed hash function and it also operates with other hash functions simultaneously. As creating the hash function, *XOR* operation was used and operation of rotate was done with respect to the array of prime number. Also running time of the algorithm is *O(n)* and average avalanche value for 32-bit key values is 17,29. Finally, a simple and easy understandable hash function was developed.

REFERENCES

[1] W.W. Peterson and D. T. Brown. (1961, January). Cyclic Codes for Error Detection. Proceedings of the IRE. 7(4), pp. 228-235.

[2] J. G. Fletcher. (1982, January). An Arithmetic Checksum for Serial Transmissions. IEEE Trans. on Communications. 30(1), pp. 247-252.

[3] H. P. Luhn, "Computer for Verifying Numbers," U.S. Patent 2 950 048, Aug.23,1960.

[4] J. Verhoeff, "Error Detecting Decimal Codes," in Mathematical Centre Tract 29, Amsterdam, CA: The Mathematical Centre, 1969, pp. 118.

[5] Bob Jenkins, "A hash function for hash table lookup". [Online]. Available: http://www.burtleburtle.net/bob/hash/doobs.html. [Accessed: 08.12.2009]

[6] P. K. Pearson. (1990). Fast Hashing of Variable-Length Text Strings. Communications of the ACM. 33(6), pp. 677.

[7] M. Patel. (2006, August). Random numbers for computer graphics. In ACM SIGGRAPH 2006 Sketches (SIGGRAPH '06). ACM, New York, NY, USA, Article 135. DOI=10.1145/1179849.1180018. Available: http://doi.acm.org/10.1145/1179849.1180018.

[8] T. Wang. (1997, March). Integer Hash Function. Available: http://www.concentric.net/~Ttwang/tech/inthash.htm. [Accessed: 08.12.2009].

[9] A. L. Zobrist, "A Hashing Method with Applications for Game Playing," Computer Sciences Department, University of Wisconsin, Madison, Wisconsin, Tech. Rep. 88, 1969.

[10] Y. Zheng, J. Pieprzyk and J. Seberry, "HAVAL - A One-Way Hashing Algorithm with Variable Length of Output," in Proc. Advances in Cryptology - AUSCRYPT '92. 1993, pp. 83-104.

[11] R. L. Rivest. The MD6 hash function -A proposal to NIST for SHA-3, Submission to NIST, 2008.

[12] NIST. [docket no.: 070911510751201] announcing request for candidate algorithm nominations for a new cryptographic hash algorithm (SHA3) family," Federal Register, November 2007.

[13] D. E. Knuth, The Art of Computer Programming: Sorting and searching. CA: Addison-Wesley Publishing Company, 1973.

[14] M. Beck and R. Geoghegan, The Art of Proof: Basic Training for Deeper Mathematics. New York, CA: Springer, 2010.

[15] D. Kaprekar. (1980). On Kaprekar Numbers. Journal of Recreational Mathematics. 13(2), pp. 81-82.

[16] H. M. Edwards, Riemann's Zeta Function. New York, CA: Academic Press, 1974.

[17] L. B. Bourcia. Apology for the proof of the Riemann hypothesis. Available: http://www.math.purdue.edu/~branges/apology.pdf. [Accessed: 17.02.2013]

[18] P. Ribenboim, The new book of prime number records. New York, CA: Springer-Verlag, 1995.

[19] H. Furstenberg. (1955). On the infinitude of primes. American Mathematical Monthly. 62, pp. 353.

[20] C. K. Caldwell. Proofs that there are infinitely many primes. Available: http://primes.utm.edu/notes/proofs/infinite/. [Accessed: 17.02.2013]

[21] F. Saidak. (2006, December). A new prof of Euclid's theorem. American Mathematical Monthly. 113(10).

Fatih Aydın was born in Malatya-Turkey, in 1982. He received the B.S. degrees in computer engineering from Firat University, in 2004 and M.S. degrees in computer engineering from Trakya University in 2011. He is Ph.D. candidate.

From 2006 to 2008, he was a software expert with the STS Security and Information Systems in Gebze, Turkey. From 2008 to 2013, he has been a Lecturer in Vocational School of Technical Sciences, Kirklareli University. Since 2013, he has been a Lecturer in the Software Engineering Department, Kirklareli University. His research interests area, Machine Learning and Computational Number Theory.

Gökhan Doğan was born in Malatya, Turkey, in 1979. He received the B.S. degrees in computer engineering from Firat University, Elazig, Turkey. He has been now studying the Ph.D. degree in computer engineering at Istanbul Aydin University. And he has been working for 3 years at Kirklareli University as head of information technology and lecturer.

Evaluation of the Electrical Power Systems Laboratory In Terms Of the Lighting Properties and Ergonomics

B. Dursun

***Abstract*—The aim of the lighting in educational environment both ensures the optimum visual environment and supports the teaching and learning processes for both students and teachers in classes and laboratories. From the ergonomic aspect, the visual environment in classes and laboratories should meet not only ideal view conditions required while making any performances but also emotional and psychological needs of students. In this study, the relationship between ergonomics and lighting is presented and the lighting properties of the electrical power systems laboratory are investigated considering ergonomic parameters. With DIALux lighting software, it is aimed to provide the optimum visual environment in terms of ergonomic conditions, to analyze the optimum lighting level of this laboratory, and to obtain light intensity curves occurring on working plane.**

Index Terms—**Lighting, Ergonomics, Educational Environment, DIALux**

I. Introduction

CHANGE can be seen everywhere as a result of the developing technology. The change diversifies and develops the human abilities in the working places from the physical and mental aspects. Furthermore, humans have some structural (anatomic), dimensional (anthropometric), and psychological properties. As a result of these human properties and also necessary needs, Ergonomics, defined as Engineering of Human Factors or Science of Work, has been constituted as a discipline trying to establish the basic laws of the system efficiency and human-environment consistency against organic and psycho-social stresses which can result from the effects of all factors in the working environment [1].

The word ergonomics is originated from the Greek words “Ergo” and “Nomic”. Ergo means work and Nomic means rules. Therefore, Ergonomics can be defined as “providing optimum working conditions for human” [1]. In terms of Ergonomics, defined as the evaluation of human and environment, not only evaluating the environment perceived by human, but also the factors affecting the perception of human should be considered. Major factor affecting the perception of the human is the sight. There are some criteria about assessing the eye sight and the most important one of these criteria is lighting.

Lighting is an art as well as a science. It should meet aesthetic, emotional as well as economic and functional requirements concurrently. Providing a good and efficient lighting system requires co-ordination between the architect, the consultant and the lighting engineer. A good and efficient lighting system should provide adequate lighting with uniform light distribution all over the working plane, to provide light of suitable color and avoid glare and hard shadows as far as possible. Earlier conventional offices used to include just reading or writing documents on horizontal plane, but with the introduction of computers in modern offices, the lighting designer has to take into consideration more factors like glare, static & dynamic imbalance etc. [2].

A well designed lighting system that applied to any places increases the working performance and productivity of people, makes up a suitable atmosphere for people and reduces fatigue. On the other hand, disadvantages of the lighting systems designed improperly include rapid fatigue, lethargy, headaches, eyestrain, eye burn and overall visual impairment [3]. The process of lighting design for any facility is quite complex. These process starts by calculating the volumetric dimensions of the room and then applying various formulae, depending on the method selected and the use for which the room is intended, in order to arrive at the average lighting level per square area required in the room. The light characteristics of various fittings are then compared and the selected fitting is subjected to further calculations to determine the optimum number of fittings required in the room. The layout of these fittings within the room can then tax the creativity of the best of architects. When the dimension of energy bills is added to this complex process, it is normal that the facility designers throw up their hands in exasperation. The most commonly used method for arriving at the lighting layouts & designs (as per the results of the market survey) is the use of thumb rules & experience [2].

Looking at the recent developments in Lighting Technology, these technologies available today have enabled many lighting manufacturers to develop and market numerous energy efficient equipments. However, the high initial investment & lack of knowledge about their quick payback periods has inhibited the use of these equipments. Lighting accounts for 20% to 30% of the total energy consumption in software industry. For any typical lighting system, energy cost

B.Dursun is with the Electrical Engineering Department, Technology Faculty, University of Kırklareli, Kırklareli, 39300,Turkey, (e-mail: bahtiyar.dursun@kirklareli.edu.tr).

is about 80% to 90% of the annual cost & 65% to 85 % of the life cycle cost. So while designing the system more emphasize should be put on reducing the running & recurring costs as compared to reduction of the initial cost. One can save more than 30% of energy consumed in lighting system by efficient use of 'right amount of light, at right place & right time'. Energy efficient upgrades along with the use of modern control systems offer almost 50% energy savings with little or no user impact [4-6].

Lighting design software have been available in developed countries for many years, but in most developing countries, these software are used by the lighting manufacturers merely as a marketing tool for selling their lighting products. As a result, the aesthetic aspects of lighting designs were gaining greater interest as compared to the energy efficiency aspects. However, the recent interest in global energy saving efforts has led to the development of various software solutions for the professionals to analyze the energy saving potential in lighting designs[7,8]. Europic, Calculux, Silicht, Relux, and Dialux are some of the lighting programs. The most popular and preferred one of these programs is Dialux. The DIALux lighting computer program has been developed by the German Applied Light Technique Institute in order to gather armature data from companies and standardize the calculations made by using different methods. There are many versions of the DIALux program. The latest version is DIALux 4.4. DIALux includes the armature and lamp information from many companies, such as AEG Lichttechnik, Zumtobel, Regiolux, Siemens, Thorn, Erco, Wila, Ridi, LBM and Idman, in its database[9, 10]. DIALux which is a lighting simulation program supports many room shapes, such as rectangular, square, polygon, L shaped or the shapes designed by the user, and allows the user to choose from among those shapes. The program, which supports the addition of more than one piece of furniture to the place, also takes into consideration factors such as lighting level, reflection and glitter which can be seen on the furniture [10-12].

II. THE IMPORTANCE OF THE LIGHTING AND ERGONOMIC IN EDUCATIONAL ENVIRONMENT

The most important parameter in eye sight is providing the optimum view conditions. It is clear that the optimum sight conditions can be performed by good lighting. Lighting is an indispensable element for good sight conditions for some circumstances like limited or unlimited places with conditions of inefficient or non-sunlight or insufficient optimum conditions. The good sight conditions, mainly based on the lighting technique, should present aesthetically successful images under the aspects of architecture and art according to the properties of lighting subject. In the scope of emotional and perceptive data of human, lighting and visional perception have an important place. Between 80%-90% of these, all perceptions are done by sight. Sight perceptions are originated by color and light activators. For this reason, performing the educational and training activities in optimal lighting conditions is important for humans' eye health and saving the sight ability. As it is known, eye is the most important sensor for perceiving the facts [13-14].

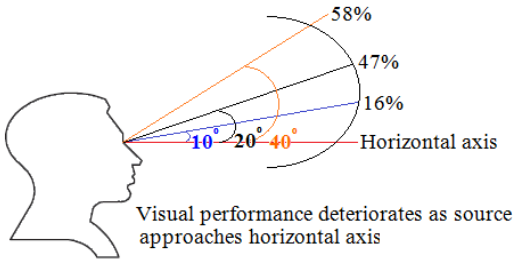

Fig1. Visual Area [24]

The area perceived by eyes when the head is fixed called "visual area" in ergonomics. Visual area is assessed in three parts. These are:

- Sharp sight area angles 1^0 vertically
- Middle area angles 40^0 vertically
- Surrounding area angles 40^0-70^0 vertically (Figure 1).

One of the conditions to maintain a relaxing environment for an effective working is lighting. In the transition from normal or excessive lighting to less illuminated environments, a time for the adaptation to the environment is needed. If sufficient time is spent for the adaptation, in sudden transitions from excessive illuminated environments to less illuminated environments, falling, slipping and bumping can occur. At this point, the lighting level appears as a critical factor for the adaptation mechanism[24]. The closest distance for the vision of the objects is classified in below according to age.

- 8 cm for 16 years old
- 12,5 cm for 32 years old
- 25 cm for 44 years old
- 50 cm for 50 years old
- 100 cm for 60 years old [14].

25~30 minutes is needed to get 80% adaptation in transition to a dark environment from an environment where you exposed to day light. Most of the tiredness that is caused by work is thought to be eye exhaustion. There are a lot of parameters that affect the ergonomic conditions of the environments where education takes place. One of the parameter is lighting. For both students and instructors to carry out healthy, safe and efficient education activity, lighting of the classroom, library and education environments should be performed properly [15].

The pleasant and enlivening effect of good lighting is a known fact that increases the working efficiency, encouraging learning of people along with affecting the users' behavior in positively. Ergonomics and lighting is closely related with each other in educational institutions. Insufficiently illuminated class or laboratory environment causes students face with lots of problems. The problems could be defined as hardly seeing of the board because of the insufficient level of lighting of the students, lack of eye contact of instructors with the students, lack of interest and curiosity of students what instructors told. In contrast to this situation, similar situations can occur in an environment that is illuminated more than

enough. If the students cannot see the board because of excessive lighting or dazzling, as a result of the exposure of the students' and instructors' eyes to excessive lighting intensity, they can face with problems like eye health malfunction. Unless lighting, which is a parameter of ergonomics, is proper, obviously, there can be many obstacles. If people don't work in sufficiently illuminated environments in a proper way to see the details of their work, it would be the possible reason for the increase of the risks in the working environments and the reduce of efficiency and effectiveness of work. For the effective and efficient lighting in the education activity, the height of the table and studying surface should be properly determined and the distance between the sitting height should be properly evaluated (Figure 2) [14].

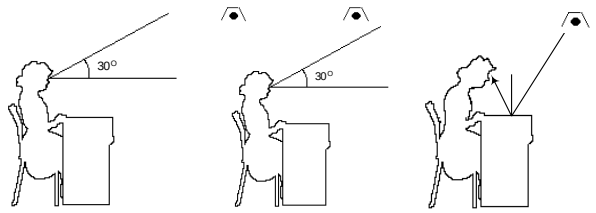

Fig 2. Working Settlings

It has been observed that people, who work in environments where light vibrations occur, have perception problems, and they perceive the rotation of the machine as if it slowed down or even reversed. This situation is caused by the lighting fixtures that are not properly chosen in working environments and it is known as "Stroboscopic effect". There are lighting fixtures that are designed for the places where people could be exposed to stroboscopic effects. Yet, problem can be solved to a certain level via energization of the lighting fixtures by connecting them to different phases.Another problem in illuminating which directly effects working efficiency is shadowing. Unless lighting is not properly done as it is needed, depending on the random shadowing it can cause perception mistakes. The brightness, however, the low or excessive intensity of lighting affect students in a positive or negative way [15].

The suitability of lighting source to environment colors, in education environments at the visualization process, has an increasing or decreasing effect. Lamps show variation in their characteristic spectrum features. However, the specific colors of the light have to be differentiated and the returning index of color to be attended. The returning index of color is highly important especially in performing color based works. When this value increases, the evaluation rate and effectiveness increase. In illuminating sources where the returning color index is below 60, it is accepted that the color based applications will be insufficient [16]. This feature is important in terms of performing an activity in different people that work in illuminated environments. Thus, warm and peaceful atmosphere can be created by lighting sources that have different color features. Besides, this atmosphere also affects stimulating and encouragement for work. Direct lighting is the most appropriate one in classroom where the education activity takes place. In direct lighting, the light that comes from the lighting fixture is directed to bottom via special reflectors with various angles. This comprehension is the opposite of classical lighting. Light distribution is obtained via configuration of various veiling surfaces [14]. Owing to directed lighting, energy can be saved and high efficiency can be obtained with the lighting fixtures that have low light flux. Direct lighting is not only economical but also maintains the best and the ideal lighting of the environment. The light flux of artificial lighting in classrooms where everyone can sit freely is appropriate if the light comes in the same direction parallel with the day through the window [16-18]. In the positioning of the lighting fixtures with such kind of lighting, all the students that sit facing the board sit back at the classroom and whose backs are towards the window has proper vision conditions in their desks.

III. STUDIES ON THE LIGHTING PROPERTIES AND ERGONOMICS FOR VARIOUS WORKING PLANE

Educational institutions which give technical education in addition to theoretical knowledge have to obtain working areas in which knowledge can be transformed into skills during teaching-learning periods. As applications are done in these areas, they are expected to have enough technical equipment such as machines and also adequate lighting and ergonomic conditions. Because, during lessons, it is important to provide students to get the right idea in a comfortable way, and efficient lighting is the only way to prevent accidents which may occur by misunderstanding. By good lighting, sight becomes better, eye fatigue and carelessness decrease. As workers feel better and more comfortable, their attention for the subject and success get higher. What's more, optimum lighting conditions must be chosen, in other words it is very important to provide the most comfortable and economic lighting [15]. There is little paper on examining by means of lighting and ergonomic in working area. Some of them are below:

Aksoy and Kelesoglu argued the ergonomic qualities of the laboratory in the construct, machine and metal education depending on systematic information and scientific methods, for the aim of proceeding appropriate working conditions for students. The lighting level, noise level and air condition of those laboratory are basically investigated [19]. Another study is done by Demirci and Armagan[20]. They evaluated physical environment components such as lighting, air condition, noise, temperature and humidity, and examined to influence upon the workers of these factors. Walavalkar and De analyzed the impact of the new trends in energy efficient lighting design practices on human comfort and productivity in the modern IT offices. They conducted a scientific project which is named Joint Research Project on Ergonomic Evaluation of modern IT Offices for 15 months, in India during year 2000-2001. They took inputs data from the Energy Management program run by Walavalkar for the various offices of Tata Infotech in India during 1998-2001, for analyzing the impact of efficiency and ergonomics [2].

IV. LIGHTING DESIGN CRITERIA FOR INDOOR MEDIA

A. The choice of Artificial Lighting Type

One of the primary functions of a luminaire is to direct the light to where it is needed. The light distribution produced by luminaires is characterized by the Illuminating Engineering Society as follows:

- Direct lighting,
- Semi-direct Lighting,
- General Diffuse or Direct-IndirectLighting
- Semi-indirect Lighting
- Highlighting

In the direct lighting, 90 to 100 percent of the light is directed downward for maximum use. However, in the indirect lighting, the light spreads over the mass reflecting from a surface, a part of it is absorbed depending on the light reflecting factor of the surface it is reflected. If not needed with aesthetic concerns and other reasons, especially in the institutions where day length lighting is required, direct lighting should be preferred. At the universities where engineering education is given, in the classrooms and labs, direct lighting should be preferred. The entire light sent is conveyed to workplace without meeting any obstacle, thus, the learning motivations of students are positively affected. In indirect lighting, 90 to 100 percent of the light is directed to the ceilings and upper walls and reflected to all parts of a room. While 60 to 90 percent of the light is directed downward with the remainder directed upward in the Semi-Direct lighting, the equal portions of the light are directed upward and downward in General Diffuse or Direct-Indirect Lighting. Finally, the beam projection distance and focusing ability characterize this luminaire in the highlighting [21,22].

B. The Choice of Lamp, Armature and Secondary Devices

In the education environment, the choice of lamp, armature and secondary items has been the most discussed issue in terms of the efficient energy use. Lamps occupy a huge place in the energy consumption with their efficiency values. Although the incandescent lamps are preferred for their color characteristics, they consume energy more than the other lamps because their efficiency values are quite low. In the education environment, such types of lamps are not preferred to be used. Instead of them, in laboratory, classes or the multifunctional used places, preferably, it is possible to obtain the same light flow by consuming less energy with compact florescent lamps that are designed similarly in terms of color properties, having E27 heading, electronic igniter and ballast. CFLs which are used during day time or at nights permanently or for a long time in the facilities have the demanded quality in terms of color among the lamps. Moreover, the choice of the lamp with high efficiency value is important for the influential use of enlightening energy. Armatures are the devices that regulate the light spread of the lamp, prevent glare, protect the lamp and sub-materials against outer factors and contribute to the aesthetical values of the environment they are found. In the armatures that reflect the light coming out of bare light and/or transmit it to the environment, the absorption of a certain amount of the light with this reflection and transit is also in question. Due to this absorbed light, the light flow emitted from the armature will be less that the light flow coming from the lamp, and this rate completes the productivity of armature. Thus, in the choice of armature, the productivity of armature should be taken into consideration. With respect to the effectual use of energy, in such buildings like education centers where electricity load is generally for enlightening purposes high productive armatures should be chosen [21,22].

In the education buildings, because of high efficiency factor, fluorescent systems are commonly used. For this reason, the type of ballasts to be used with florescent lamps and the extra powers they get from mains are important factors we see in terms of energy consumption. While 36W fluorescent lamp used with inductive ballast withdraws 46W powers, the power that the same lamp withdraws from mains when used with electronic ballast remains as 36W again [23].

C. Volume Inner Surface Colors and the Choice of Light Reflecting Factors

The light reflecting factors of inner volume in buildings is one of the variants that enormously affect the volume's lighting productivity. The magnitude of total light flow necessary to provide lighting levels determined as the necessity of comfort of the user within the volume is counted depending on the lighting productivity of the volume. When the inner surfaces are covered with light colors, in other words the light reflecting factors of the inner surfaces are large, the light will be less absorbed and therefore in the working level, the required lighting level will be provided by a system that uses less power. When the inner surfaces are covered with darker colors, since the light keeping factors of the surfaces will be bigger, it will result in the withdrawal of more electricity energy from mains to reach the desired lighting. In particular, in the indirect, semi-indirect, mixed and semi-direct lighting systems, because a part of the light flow coming out of devices will reach the working level reflecting from the inner surfaces, such kinds of systems should not be preferred in educational environment.

D. Determination of Proper Armature Locating Heights

The locating heights of the armatures, especially in the lighting systems set through ceilings are a variant that directly impact the gratitude of the total light flow expected from devices. As known, in accordance with the law of "distances law", lighting levels change in inversely proportional to the square of the distance of lighted surface. In the educational constructions visited until now (the universities), armatures have been integrated into ceiling. In an area lighted from ceiling, the more the distance between the working level and armature is the more the total light flow that the armatures are to give. Accordingly, since more lighting armatures will be necessary, the energy consumption will increase. For this reason, on the condition that glare control is made, the height between working level and armature should be decreased to

lowest level that is allowed [21,22].

E.The Selection of the Lighting Programs to be used

In the design process of lighting system, a wide kind of calculation models which were developed based upon "light flow method" or "light intensity method" are used. As the majority of the developed programs use the self-productions of the instrument manufacturers as data, in the situation when it is used for a different product, it can give highly incorrect results. As a result of this, a setting power table that is bigger than required may be encountered. For this reason, the programs to be used in calculations should be correctly selected and data of devices and lamps should be carefully added into the calculations [21].

F. Consideration of Maintenance Factor

Maintenance factor is important because the performance of the environment inner surfaces and armatures decreases after a certain period of time. Since the dirtiness that dust and similar items will make on the surfaces inner environment will reduce the reflection properties, firstly, the determination of high repair factor and thus the way of decreasing setting load should be preferred. Besides, as a result of the fact that the components of armatures that reflect or transmit light are polluted due to the air pollution and other environmental factors and thus their performance of light reflecting and transmitting accordingly decreases and their efficiency declines. Therefore, either the demanded comfort conditions are not provided or more energy consumption is needed to enable the desired conditions. For this reason, the regulations that will be done about increasing the frequency of repair periods of armatures should be kept as high as possible with firm projects or directives, the first setting load of the system should not reach upper values unnecessarily because of this reason [21].

V. INVESTIGATION OF ELECTRICAL POWER SYSTEMS LABORATORY IN TERMS OF THE LIGHTING PROPERTIES AND ERGONOMICS

The department of Electric and Energy Technologies has electrical power systems laboratory. The courses of the electric circuits, electric power systems, and energy transmission and distribution are conducted in this laboratory. Electrical power systems laboratory comprises analysis and design of electric and integrated power systems including their planning, design and operation. In this study, considering the lighting properties, a laboratory that can provide ergonomically the most proper laboratory conditions will be designed and built. Besides ameliorating the conditions of an existing laboratory, ergonomically, it will also be designed in the way to appeal to the visual comfort, psychological relief and aesthetic emotions of people.

In this research, the electrical power systems laboratory which is one of the most important laboratories in Electric and Energy Technology at Kırklareli University is investigated for its ergonomic conditions. There are six tables in this laboratory and there are six active working students at each table. Compact fluorescent lighting fixtures were used for lighting system. Six lighting fixtures from 2x36W fluorescent lamps are in use. Walls and ceilings are painted white and light white in order. Lighting intensity for working areas like laboratories has been specified by International Commission on Lighting (CIE) as 700 lux. The settling position of the laboratory is shown below.

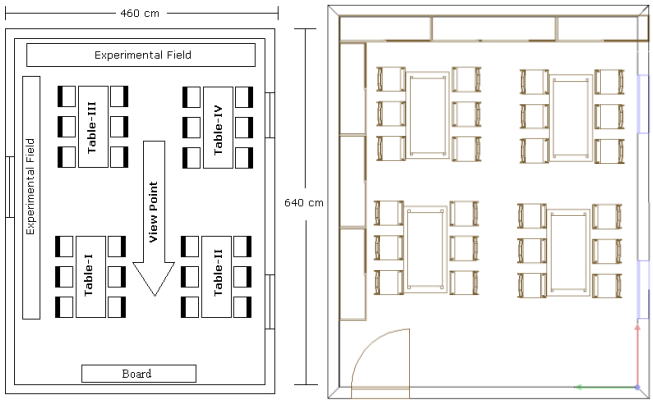

Fig 3. The placement Electrical Power Systems of Laboratory

In general, working students in front of the table are more important than writings on the board in laboratories. In an ergonomic lighting condition, the experimental arrangements on the table have to be seen clearly while students are performing or watching the action to enhance their learning activity. For this reason, as students do open seating during experiments, it is necessary to maintain suitable lighting conditions at each table. In classes, the board and walls with windows must not be parallel positioned to avoid dazzling caused by the sunlight coming from the windows. In this system, positions of the lighting fixtures with windows are changed from parallel to vertical to take the advantage of sunlight. Standard TL-D model fluorescent lamps and lighting fixtures without reflectors were used in the laboratory. Color discrimination index and efficiency factors of these lamps are low. If they use TL-5 serial new generation lamps which have high efficiency factors and long lasting lamps with electronic ballasts, a good lighting condition with less lighting fixtures will be provided.

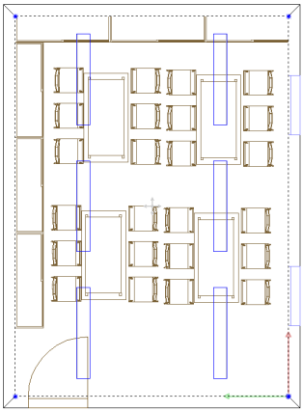

Fig 4. Lighting Fixture Positioning of the New Laboratory Design

DIALux lighting computer program was used to specify optimum ergonomic lighting system for this laboratory. If you enter necessary parameters to DIALux lighting computer program, you can calculate some parameters which effect human ergonomics such as optimum lighting intensity, lighting fixture number, light flux occur at working height. DIALux, prepared this DIALux computer program for German Practical Light Technique Institute (DIAL) to collect lighting fixture data of companies and to standardize these data. DIALux program has lots of versions. The last version is DIALux 4.9. DIAlux program has lots of companies having lighting fixture and lamp information such as, AEG Lichttechnik, Zumtobel, Regiolux, Siemens, Thorn, Erco, Wila, Ridi, LBM and Idman. DIALux program which is also a simulation program, makes possible to form rectangular, square, polygon, L-shaped and user desired/designed room types. The program which makes possible to add one or more furniture into the environment, considers also the factors such as lighting level, reflection and sparkle.

Table 1The Information about the Laboratory

Length (a)	6,40 m	Ceiling Reflection Coefficient	0,70
Width (b)	4,60 m	Wall Reflection Coefficient	0,50
Height (h_1)	2,20 m	Floor Reflection Coefficient	0,20
Working Height (h_2)	0,80 m	Dirtiness Factor	1,00
Hanger Length (h_3)	0 m		

The information about our laboratory is shown in Table 1. The light intensity which is desired in the laboratory environments has been accepted as 700 Lux by commissions such as CIE (Commission Internationale de L'Eclairage) and IES (The Illuminating Engineering Society of America). When the information given above as parameter and the type of the lighting fixture are entered into DIALux program, required optimum calculation is carried out by program. Generally, fluorescence light fixtures are preferred in the laboratory working areas. Among these lighting fixtures, a better lighting level can be obtained with new generation TL-5 series lighting fixtures having higher color separation index and activity factors, longer lifetime and electronic ballast.

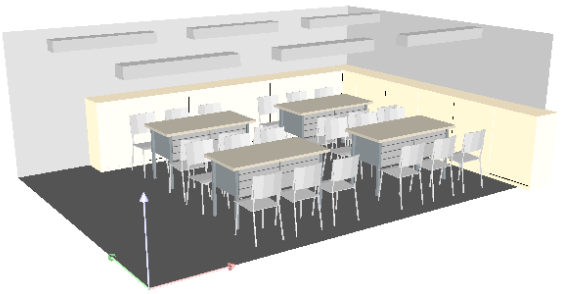

Fig 5. Render Image of the laboratory with DIALux Program

Without changing the number and the type of lighting fixtures used in the current system, the situation of which isohyps are given below is observed in the current environment by putting reflector on to each lighting fixture. Here, the amount of light flux at every point of the environment is seen. If the isohyps are examined carefully, the light intensity is increased especially on the tables which the experimental works have been carried out on.

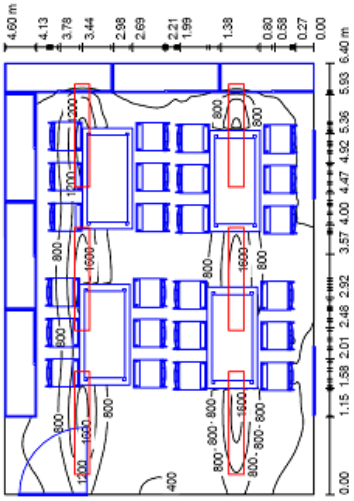

Fig 6. The isohips image of Light Flux Curves of Laboratory Environment

By putting reflector on the current lighting fixtures or replacing the lighting fixtures with TL-5 series fluorescent lamps, desired light intensities would be obtained in the experiment areas. Adequate and suitable lighting in terms of ergonomics, in the laboratory environment, is made by maintaining desired light intensity. Desired light intensity is defined as the level of optimum lighting in which a person can see around.

VI. CONCLUSIONS

Lighting is the most important parameter to provide an optimum visual environment in terms of the ergonomics. In this study, necessary arrangements have been made by taking on the necessary parameters, to optimize the lighting properties in a current environment. The conditions such as the localization of the lighting fixtures of the current system and how to position them according to the window have been evaluated one by one. For efficient use of energy in the present lighting system, lamps in the lighting fixtures were replaced with TL-5 series lamps. The effects of the factors such as the colors of walls, ceiling and the floor, on the instructor and the students in the process of active learning and teaching, were examined. Necessary arrangements have been made to maintain the optimum ergonomic environment.

REFERENCES

[1] W.E Hathaway, "Effects of school lighting on physical development and school performance", *Journal of Educational Research*, vol.88, no. 4, 1995, pp.228-242.

[2] R. Walawalkar and M. Mittal, "It applications for energy efficient lighting designing", *International Conference On 'Energy Automation and Information Technology"*, Kharagpur, India, 2001.

[3] R. Walawalkar, D. Amitabha, T. Mogare, J. Sahariya, "Effect of efficient lighting on ergonomic aspects in modern it offices", *International Right Light 5 Conference*, Niece, France, 2002.
[4] B. Dursun, S. Kocabey, "İç aydinlatma da etkin enerji kullanimi ve bir uygulama örneği" 3e *Electrotech Elektrik Elektronik Enerji Dergisi*, vol.127, 2004, pp.76-80.
[5] EIE, "Elektrik Işleri Ve Etüt Idaresi Genel Müdürlüğü, Enerji Tasarrufu Çalişmalari", Access from: http://www.eie.gov.tr/turkce/en_tasarrufu/konut_ulas/en_tasarruf_bina_ay.html
[6] R.Walawalkar, "Energy management in software industry", *All India Seminar on Electrical Energy Systems Management - Indian Scenario*, 1998.
[7] N. Ekren, B. Dursun, E. Aykut, "Lighting computer programs in lighting technology", *Gazi University, Journal of Science* , Vol.21 No.1,2008, pp.15-20.
[8] 8 R. Walawalkar, M. Mittal, "Computer aided efficient lighting design practices in developing countries, *International Right Light 5 Conference*, 2002, Nice, France, pp.149-157.
[9] D. Enarun, "Aydınlatma tekniği ile ilgili bilgisayar programları", 3e *Electrotech Elektrik Elektronik Enerji Dergisi*, vol.86, 1994, pp.52-56.
[10] Anonymous, Dialux version 4.4 user manual, DIAL Gmbh publishing, Deutsches Instituts Angewandte Lichttechnik, Lüdenscheid, 2007, pp.19-117.
[11] Anonymous, "Dialux Handbook Ver. 4.9", DIAL Gmbh publishing, Deutsches Instituts Angewandte Lichttechnik , Lüdenscheid, 2006, pp.3-5.
[12] Anonymous, "Dialux, The new software standard for lighting calculations",DIAL Gmbh, Deutsches Instituts Angewandte Lichttechnik, Version 2.6, 1989.
[13] A. Aytuğ, "Mimaride ergonomik faktörler, YTU publishing, 1991, Istanbul, Turkey.
[14] F.D. Cetin, B. Gumus, B. Ozbudak, "Aydınlatma özelliklerinin ergonomik açıdan değerlendirilmesi", II. *Ulusal Aydınlatma Sempozyumu*, 8 Ekim 2003, Diyarbakır, Türkiye.
[15] I. Güney, Y. Oğuz, S. Kocabey, Aydınlatmanın öğrenme sürecindeki katkısının incelenmesi, *4.Ulusal Aydınlatma Kongresi*, 5 Ekim 2002, Istanbul, Turkey.
[16] C. Guler, "Ergonomiye giriş", Ankara Tabip Odası Yayını, 2001, Ankara, Turkey.
[17] Anonymous, "Philips lighting manual", Philips Lighting B.V., 1993.
[18] A. Brett, O. Lee, L. Sorhaindo, "Effect of field-based technology laboratory on pre-service teachers, Knowledge, Attitudes, And Infusion Of Technology, University of Miami Florida", *Journal of educational research*, vol. 37, no.1, 1997.
[19] U.T. Aksoy, O Kelesoglu, "The scrutiny of the ergonomic qualities of the workshops at the faculty of technical education in the Firat University", *Fırat University Journal of Social Science*, vol.14, no. 2, pp.167-173, 2004.
[20] K. Demirci, K. Armağan, "Bürolarda fiziksel ortamın düzenlenmesi ve olumsuz çevresel faktörlerin çalışanlar üzerindeki etkisi", *Dumlupınar Üniversitesi Sosyal Bilimler Dergisi*, vol.7, pp.179, 2002.
[21] M.Ş. Küçükdoğu, Aydınlatmada etkin enerji kullanımı", *II. Aydınlatma Sempozyumu*, 08-10 Ekim 2003, Diyarbakır, Türkiye.
[22] F.B. William, Light in design – an application guide- IES CP-2-10, Access from: http://www.iesna.org/pdf/education/lightindesign.pdf
[23] H.D. Einhorn, "School lighting – a new approach" vol.4, 1982, pp. 98-100.
[24] D.A. Attwood, J.M. Deeb, M.E. Reece, "Ergonomic solutions for the process industries", Chapter-4, Gulf Professional Publishing, Elsevier, 2004, USA.

Bahtiyar Dursun was born in Istanbul in Turkey. He received the B.Sc. and M.Sc. degrees from Marmara University, Turkey. He obtained the Ph.D. degree in 2010 from Kocaeli University. From 2004 to 2008, he worked at Gebze Institute of Technology as a Research Assistant. Since 2008, he has been with the Electrical - Electronics Engineering Department of Kırklareli University, Turkey as an Assistant Professor.

Education Purpose Design of User Interface (Matlab/GUI) for Single Phase Trigger Circuits

M. Ak, M. Tuna, A. Ergun Amac

***Abstract*—In this study, a graphical user interface has been designed for the simulations of single phase trigger circuits which take place within the syllabus of power electronics course given in the engineering and technical education faculties and it has been conveyed to vocational education. The simulation of the circuit was realized with MATLAB Simulink and the design of the interface was made with MATLAB GUI. The interface prepared enables the user to select the type of whatever circuit he wants. Besides this, arranging the input parameters of the circuit to the values he desires, the user can view the results on the same interface numerically and graphically. Furthermore, since animations are used in the interface, the effects of parameter changings can be watched visually. Thus, the simulation process carried out and the obtained results are presented to the user in a short time and in coherence and much negativity that decrease productivity in education are prevented.**

Index Terms—**Matlab, Simulink/Simpower Systems, GUI, Vocational Education**

I. INTRODUCTION

IT is known that the visual elements used in educational environments help permanent learning. Then, it is obvious that the visual course materials used in the right place and in an effective way make it possible for education to reach its aim in a shorter period of time. At the head of these materials, undoubtedly computers come. With the use of computers in the field of education, many studies are being carried out to make education more productive, generalize and individualize it [1-2]. Such kinds of studies which are a part of computer-supported education have gained acceleration and become more interesting.

Computer-supported education is the general name of the practices in teaching process of computer technology. The major ones of these practices are; to provide information, to tutor, to contribute the improvement of a skill. The computers commonly used in every field of education have a special importance in vocational and technical education.

M. Ak, Elimsan Switchgear and Electromechanical San. and Tic. Co. Uzuntarla, Kocaeli / Turkey (email: muhlis.ak@elimsangroup.com)

M. Tuna, Kirklareli University, Technical Education Faculty, Department of Electrical Education Kirklareli / Turkey, (email: murat.tuna@kirklareli.edu.tr

A. Ergun Amac, Kocaeli University, Technical Education Faculty, Department of Electrical Education Kocaeli / Turkey, (email: ayseergun@kocaeli.edu.tr)

There are a lot of advantages of using computers for education. Its providing possibility to individual studies and each student to increase his/her learning speed.

Computers are commonly used in the education environments due to the fact that they make saving from student's learning time as they provide instant feedback, they enable the students to repeat the missed course or subject whenever desired, they facilitate teacher's duty providing students' active participation in the class, they enable the students to repeat the missed course or subject whenever desired, they facilitate teacher's duty providing students' active participation in the class, they help the teacher making even the most boring courses easier and more enjoyable. In the technical fields, one of the facilities provided by computers is to be able to make the simulations of many systems before production thanks to the improved softwares. Thus, many experiments which are impossible to be carried out in educational environment are made in virtual platform [3-4]. In this study, the modelling of single phase trigger circuits known as dimmer circuit and the use of the model for educational purposes by being inspected by the user interface designed have been emphasized. Thus, a sample program has been made relating to the use of MATLAB program in education.

II. THE SIMULINK MODEL OF DIMMER CIRCUIT

In the Simulink model of Dimmer circuit, while one thyristor is used for half-wave supervision, in full-wave supervision, two thyristors were linked inverse parallel [5]. The simulink model prepared for dimmer circuit has been shown in Fig. 1. In the Simulink model, it is quite difficult to observe results for various values and use these results for education. To open the dialogue window of the block whose parameter change is made for each simulation, to write a decimal numerical value in the relevant parameter, to confirm it, to activate the start button of the simulation, to open the scope screen where curves appear include rather long and complicated processes. These processes both consume time and cause a big disconnection in the observation of the influence of the change on the output.

Especially, in educational environments, these situations lead to both ineffectual use of time and students' losing their attention. In this study, to eliminate such kinds of negativities and facilitate the simulation of a circuit model

prepared in simulink, a user interface has designed [6-8].

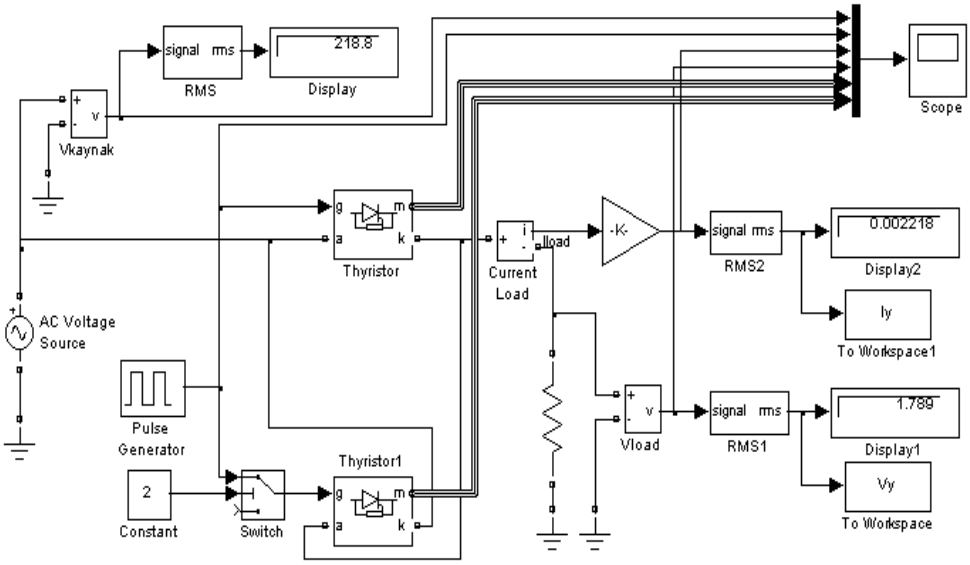

Fig. 1. The Simulink model of Dimmer circuit.

III. THE CREATION OF INTERFACE IN MATLAB/GUI

Matlab is a platform that provides the graphic based applications prepared by the programmer of Graphical User Interface, in other words, Matlab GUI, Matlab to reach the last user interactively through mouse and keyboard interface. Today, Matlab GUI applications have been needed because of the fact that the applications are graphic based and these applications provide user with the facility of usage. Besides, Matlab GUI is an easy application so much as to be created by everyone who prepares m-file or m-function [9-14].

To reach the previously prepared program, there needs to enter dimmer in the command line of Matlab and confirm it or to open the file named dimmer with the help of file opening icon. Completing this process, the interface and loading bar seen in Fig. 2 comes to screen.

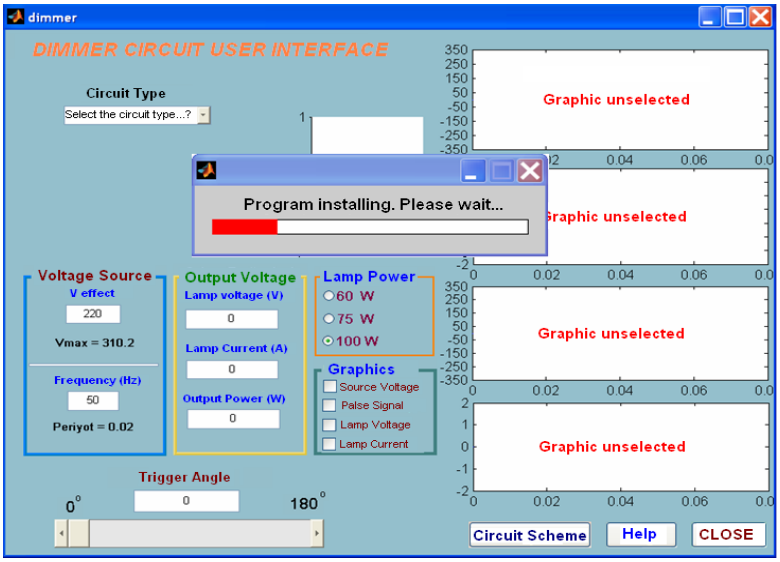

Fig. 2. Opening interface composed in GUI.

Some choices concerning the circuits and graphics in the opened window are needed to be activated. At the head of these, the circuit type choice seen in Fig. 3 comes. Here two different dimmer circuits, full-wave (with triac) and half wave (with thyristor) have been designed. According to the ype of chosen circuit, just under the choice menu, a picture showing the circuit model is opened.

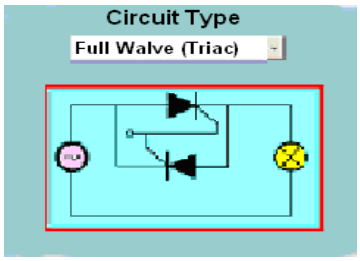

Fig. 3. Choice of Circuit type.

Later coming to the interface in Fig. 4 where source voltage and trigger point take place, the efficient value of the voltage and its frequency are arranged to the desired value. This part has been designed counting the peak value of the voltage and period of the frequency automatically in such a way to demonstrate them just below the relevant parameters. The voltage, current, and power of the lamp obtained after simulation are numerically seen in the section of output values.

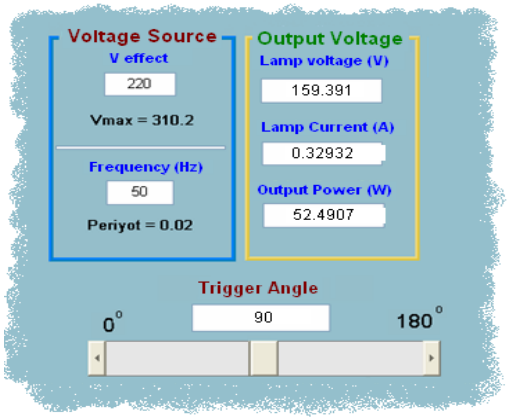

Fig. 4. The interface showing the input and output values.

In the interface, two different choices have been presented to determine the trigger point. One of these choices is the textbox that the user can directly enter the trigger point; the other one is the sliding bar that represents potentiometer. The textbox makes it possible to enter the trigger point at certain value with the help of keyboard. The voltage, frequency and trigger point parameters chosen in this section are required to be within certain limits. For, the values entered as very big or very small may cause over extension of simulation time and even the lockout of the program. For this reason, there are warning windows that will provide the simulation to be realized between certain parameters in the design. For instance, when a value that is not suitable for trigger point is entered by the user, the warning window in Fig. 5 is opened. Similar warning messages have also been designed for source voltage or frequency parameters.

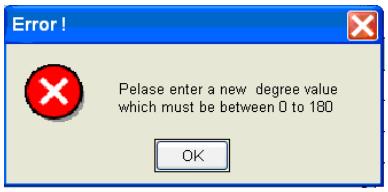

Fig. 5. Warning window for erroneous trigger point.

With the move of mouse on the sliding bar, the trigger point can be more easily changed. Thus, after each parameter change, simulation is immediately realized and the results and graphics are conveyed to the interface. The lamp symbol on the interface shown in Fig. 6 stand for the load in the circuit. The lamp power can be chosen as 60W, 75W or 100W from the choice list.

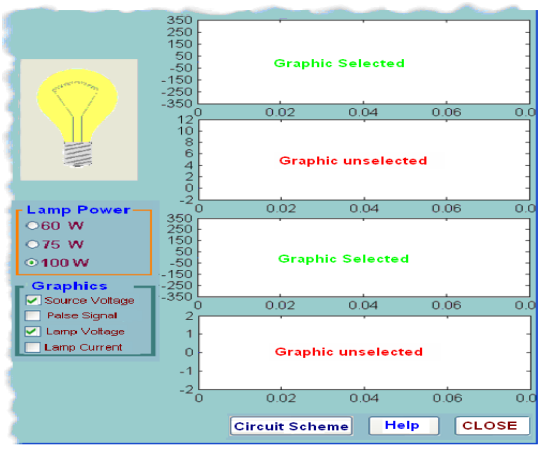

Fig. 6. The interface demonstrating the choice of lamp power and graphics.

As a result of the simulations implemented the colour tone of the lamp changes according to the output power. Thanks to this design, the user has the possibility of seeing the output parameters visually, numerically and graphically on the same interface. The displays of the graphics belonging to input and output parameters in the chart area have also been left to the choice of the user, whether the chart is chosen or not has been given in written in the relevant area. Pressing on the 'Circuit Schema' icon on the right down corner of the interface, a new window seen in Fig. 7 is opened. In this window is found the basic principle schema of the circuit. In the designed interface, when it is pressed on 'Information' icon, a document including theoretical information about alternative phase transducers is opened. With the help of this document shown in Fig. 8, the user easily has an access to all of the subtitles and mathematical calculations he needs.

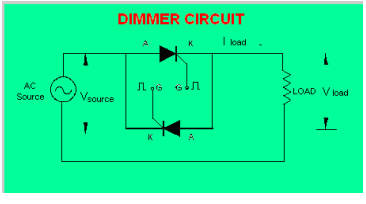

Fig. 7. The window demonstrating the basic principle schema of dimmer circuit.

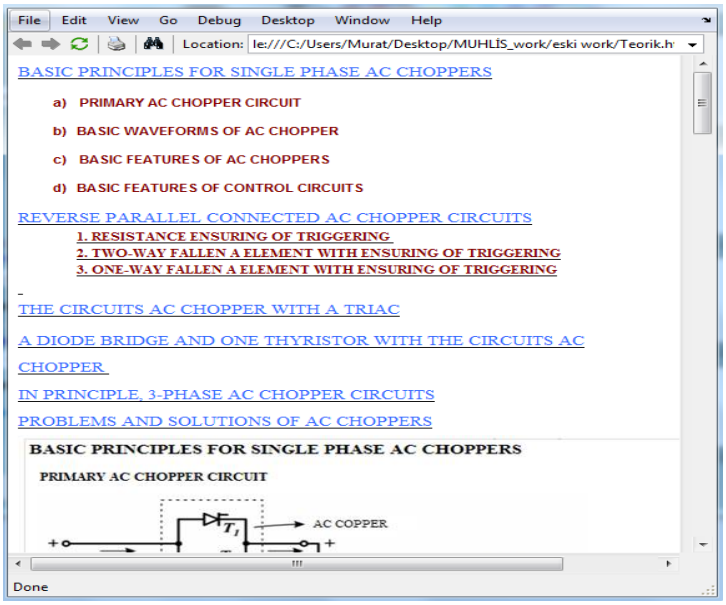

Fig. 8. The window demonstrating theoretical information about phase splitter.

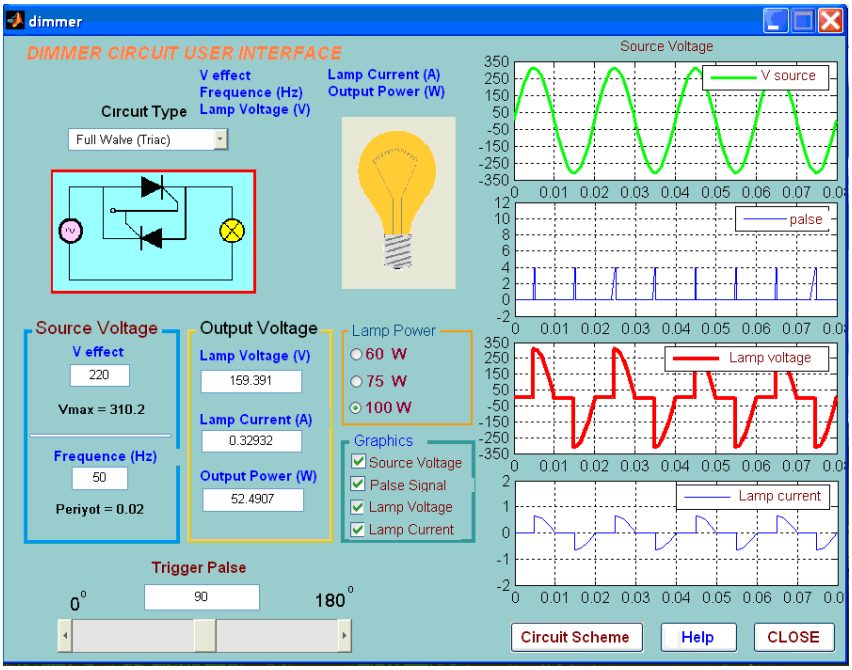

Fig. 9. The simulation results obtained in the designed interface

As a sample application, full-wave control of a 100 Watt lamp connected in series to a 50 Hz - 220 V voltage source has been made at 90 degree. The output values and the graphics obtained have been shown on the interface in Fig. 9.

IV. CONCLUSION

The dimmer circuit used in this study is an important sample in terms of students' learning how thyristor and triac run. In this essay, the models of different dimmer circuits have been designed on Matlab Simulink at first, and then shown in a single window by constituting an interface with the help of GUI. Via this interface, students;

- Have a good command of the subject of dimmer circuit,
- Can observe the impact of the of circuit parameters' changing on output voltage and output current instantly,
- Get rid of losing attention because there is visually in the interface.

In addition to these, while the user is transferring information dealt with the subject; such factors that negatively affect learning as decrease of attention, loss of time have been minimized.

In this study, it is possible to adapt the user interface constituted only for dimmer circuit to other subjects, even to use it for checking the models of the systems found outside the electricity science. It is believed that such kinds of user interfaces will raise the quality in education.

REFERENCES

[1] Kılıc R., "Design Principles of Visual Teaching Materials",Journal of Education, Number 136, 1997.

[2] Usun S., "The world and in Turkey, Computer-Aided Teaching", Ankara Pegem Publishing, 2000.

[3] Yalın H.I., "Teaching Technology and Material Development", Ankara Nobel Publication Distribution, 2000.

[4] Demirel O., Seferoglu S.S., Yagcı E. "Educational Technologies and Material Development", Ankara Pegem Publishing, 2001.

[5] Ak M., Tuna M., Ergün Amaç A., "Education Purpose Design Of User Interface For Single Phase Trigger Circuits", UMES'2007 symposium, Kocaeli University.

[6] Uzunoglu M., "Easy Lecture with Advanced Matlab", Istanbul Turkmen bookshop, 2002.

[7] Trip N.D., Lungu S., Popescu V., "Modelling of Switched Mode Fly-back Supply for Engineering Education", Advances in Electrical and Computer Engineering Volume 10, Number 1, 2010.

[8] Bodur H., "Power Electronics Applications I", Yildiz Technical University, Lecture Notes.

[9] Marchand P., Thomas Holland P., "Graphics and GUIs with MATLAB", Third Edition, 2003.

[10] Bogdanova, I., Khan, R., and Kunt, M., "Graphical User Interface and MATLAB Web Server for Multimedia Teaching on www", Signal Processing Laboratory, Swiss Federal Institute of Technology (EPFL), CH-1015 Lausanne, Ecublens, Switzerland, 2001.

[11] Patrick March and O. Thomas Holland; "Graphics and GUIs with MATLAB®, 3rd Edition", 2002.

[12] Postalcioglu Ozgen S., "Graphical User Interface Aided Online Fault Diagnosis of Electric Motor – DC Motor Case Study", Advances in Electrical and Computer Engineering Volume 9, Number 3, 2009.

[13] Koc S., Aydogmus Z., "A Matlab/GUI Based Fault Simulation Tool For Power System Education", Mathematical and Computational Applications, Vol. 14, No. 3, pp. 207-217, 2009.

[14] www.mathworks.com

Muhlis AK was born in Sivas in 1982. He completed his primary and secondary education in Istanbul. He started to Maltepe Kucukyali Technical High School and completed at first degree in 1999-2000 training period. He graduated from the Department of Electrical Training Faculty of Technical Education at Kocaeli University in 2004 at first degree at the department and faculty. One year later he started to master of Science at Kocaeli University Institute of Science. He started to work life at Elimsan Switchgear Equipments & Electromechanical Industry and Trade Inc which produces medium and high voltage electrical equipment, besides mastering education in 2008. He completed mastering education in 2009. He is still going on to work at same company as a Research and Development Chief.

Murat Tuna was born in 1982 in Bursa, Turkey. He was accepted into department the electrical teachers, faculty of technical education, Kocaeli University in 2000. Later, the Institute of Electrical Education in Science at the same university in 2005 continued his education at the master program. From 2007 to 2009 master's degree worked at department research and development in the field of Medium and High Voltage Switchgear Elimsan-KOCAELI company. In 2008 completed his master studies. Kirklareli University Technical Education Faculty since 2009 has been working as academics Electrical Training section. Mr. Tuna's current research interests are electric vehicles, fuzzy logic, neural networks, and automatic control.

Ayşe Ergün Amac (S'97-M'03) received the B.S degree (with honors) in electrical education from Marmara University, Istanbul, Turkey in 1994 and the M.S. and Ph.D. degrees in electrical education from Kocaeli University, Kocaeli, Turkey in 1997 and 2003 respectively. From 1995 to 2003, she was a research and teaching assistant in Department of Electrical Education in Kocaeli University, Technical Education Faculty. From 2002 to 2004, she was in the Electric and Power Electronics Center and the Grainger Laboratories, Illinois Institute of Technology, Chicago as a research scholar to study active filters and uninterruptible power supplies. Since 2004, she has been with the Department of Electrical Education, Kocaeli University, Technical Education Faculty Kocaeli, as an Assistant Professor. Dr. Amac's current research interests are hybrid electrical vehicles and computer based learning approaches in teaching power electronics courses.

Experimental Investigation of Corona Discharge Technique With RF

T. Dindar, N.F. Oyman Serteller, T. Ç. Akinci

***Abstract*— In this study, corona discharges occurring on insulators, the factors affecting the discharge of corana and corona effects may occur after discharge were investigated experimentally. Especially increased rate of moisture in the air or rainy weather is higher than the corona effect, for these conditions discharge was investigated.**

In this study; corona discharge, representing the humid airs rain droplets on insulators (electrodes) is examined, graphical results, with the help of the horn antenna technology removed. The results of; theoretical knowledge compared with previous experimental results, observed in full compliance.

Index Terms—**Corona voltage, horn antenna, gas-discharge**

I. INTRODUCTION

Energy transmission lines reductions of faults and in terms of ensuring the continuance of the process of energy flow, insulation of power transmission lines, break and short-circuit is very important to investigate the events [1-6]. High-voltage power transmission lines, Insulators to protect against external and internal over-voltage [1] lines or power transmission lines is very important to detect short circuit events in advance. In this way, dimensions of the insulation in high voltage devices are possible. Power lines and bus of transformer stations from each other are separated by air gaps. Air gaps with drilling of high-voltage lines, short circuits occur. In general, in an inert gas protected from external influences transmit electricity. However, a voltage is applied between the two electrodes and the voltage gradually increased, the voltage of a specific value is a sudden increase in current, and thus, the air loses its insulation property. This is a change of state of a gas or air, is called discharge event [3-14].

In this study, similar to the corona discharge (self-sustaining) discharge event between two water droplets, the water droplets were applied to 5-10KV voltage value After corona discharge, the voltage is held to raise the voltage of certain value, the full discharge occurs.

T.Dindar, is with the Ankara University, Nallıhan Vocational School, Department of Electronics&Automation, Ankara,Turkey. (e-mail: tdindar@ankara.edu.tr).

N.F.O. Serteller, is with Marmara University, Technology Faculty, Department of Electrical&ElectronicsEngineering, Istanbul-Turkey. (e-mail: fserteller@marmara.edu.tr)

T.Ç. Akinci, is with Kirklareli University, Engineering Faculty, Department of Electrical & Electronics Engineering, Kirklareli-Turkey. (e-mail: cetinakinci@hotmail.com)

In this study, short circuit isolators without the prior discharges, with the help of the experimental horn antenna, the computer tries to explain graphically.

II. THEORETICAL KNOWLEDGE ABOUT THE GAS-DISCHARGE AND CORONA DISCHARGE

Damp and foggy weather, power transmission line, the phase conductors is ionized air to the surface of the purple-collared, illuminated rings are seen. This is a result of the corona phenomenon. On the surface of the conductor in contact with each other if this purple colour and light cylinders, are perforations on the surface of the conductor. In the meantime, the sound vibrations can be heard. This phenomenon is rather less than the radiuses of the distance between the conductors 15 are found on the phase conductors.

Peek, normal weather conditions, the intensity began to ionization by collision, 30 kV / cm as a given. A larger value of the voltage, becomes conductive light throughout and it is called the corona voltage is indicated by Uk.

The voltage is increased further, the full discharge between the electrodes, that is, short-circuit occurs. That the value of the voltage is called breakdown voltage is indicated by Ud. [1-19]. There are many factors that affect the corona voltage, and some of them; are conductor radius, roughness, clearance between the conductors, air conditions.

Of voltages and field strengths given above, there are the following equations.

$$U_K = U_0 . m . \delta \left(1 + \frac{0{,}301}{\sqrt{r . \delta}}\right) \quad (1)$$

$$E_K = E_0 . m . \delta \left(1 + \frac{0{,}301}{\sqrt{r . \delta}}\right) \quad (2)$$

Here, E0=21,2 KVef/cm, δ=0,392 p/T (mm.Hg/K) ve r(cm) shows that the radius of the conductor.

Power transmission systems, insulators used as insulation property loss is caused by discharges. Mentioned in this study, RF (radio frequency) antenna is used, the transmission lines would be expected to prevent the losses that may occur. In this study, a high voltage corona discharge are reviewed, maintain the distance of 1 meter from for full access to the data produced during the discharge of the electrical field and RF antenna is placed on the test system while maintaining the distance. Electrical field, inter-electrode distance and pressure changes. In this study, the pressure is fixed by changing the distance between the corona discharge electrodes are examined. The distance between two water drops changes,

volume and surface condition of this experimental observations insulator infected (Figure 3, 4).

Changes in the frequency spectrum of 800 MHz - 900 MHz and 1.25 GHz - 1.4 GHz measurements were made. These values are sufficient values to observe the corona discharge and to determine insulators used in high-voltage transmission lines. [11-29].

Insulators used in high voltage transmission lines, are made of gelmiflt material. Although these are non-conductive material, they sometimes, can cause electrical discharges. One of the reasons that is, there maining water droplets on insulators. As long as these drops remain, high-voltage transmission lines where the discharge occurs due to insulators. These discharges occurring on insulator (discharges), insulator is harm.

This is the situation in order to determine in advance, horn antenna is used, or RF (radio frequency) sensors are recommended. [19-34]

III. EXPERIMENTAL STUDY AND SPECTRAL ANALYSIS

5-10 KV voltage source voltage is used. In Figure 1, input voltage 100 V (TR1), the output voltage 15 KV (TR2), which are high-voltage transformer, voltage divider resistors, isolation transformer and measuring instruments to make a high voltage transformer stability control, established circuit arrangement shown. After checking the robustness of transformer, circuit resistance is extracted.

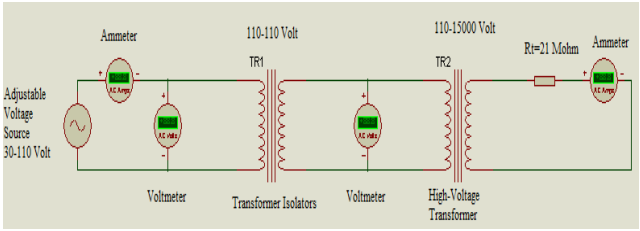

Fig. 1. Test Scheme for the Control of High Voltage Transformer

In Figure 2, horn antenna, RF (radio frequency) link is shown using corona discharge to obtain spectral analysis. Full picture of the experiment, high voltage test is not given here, occupies a large place, but given schematically in Figure 4.

a) b)

Figure 2. Values were obtained with Horn Antenna and Connection Diagram

The main task of insulators, high voltage power transmission system is to isolate portions of the bottom. In addition, the second most important task is to carry the mechanical loads. Insulators, usually made with mechanical handling the task successfully, although not able to sometimes as insulation. Capacitive-resistive leakage current to flow from the surface of the insulator-featured, providing that disrupts the distribution of the surface contamination, high voltage insulators, and therefore often causes a short-circuit events occur in the incident energy shortages and economic losses. [8-10]. The layer of dirt becomes, wet because of rain, fog humidity and so an. And this dirty layer causes leakage currents and energy loss.

Energy loss is greater than the intensity, especially in the narrow parts of the insulator polluted regions and more heated dry "dry belt" leads to the formation of the so-called parts. As a result, deterioration of voltage distribution across the surface, the structure becomes non-uniform. [10-19].Dry-band regions of the air resistance of the voltage drop occur exceeded pre-discharges. Pre-discharges will often, in some circumstances, give rise to the surface by spreading a short circuit resulting in the jump event.

In this study, the normal weather conditions, as a result of omissions caused by water droplets formed on insulators, corona discharge experiments were performed in order to investigate the problem of damaged insulators to perform this experiment, the same volume of the droplet of water in a two nano - to composite materials were dropped through a dropper. Displaced both water drop contact metal electrodes 15 KV 50 Hz. AC transformer output. Electrodes connected to the water droplets is shown in Figure 3.

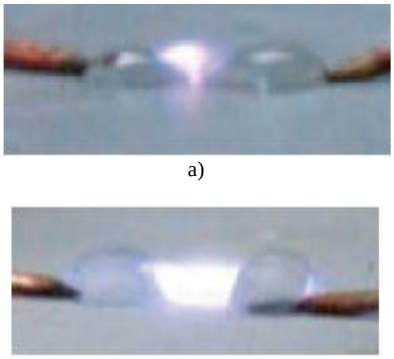

a)

b)

Fig. 3. Electrode Connection with Water Droplets

The electrical field signal that creates corona discharge is detected via the horn antenna 1 meter away. Pay attention to the frequency settings while experimenting with 0-2.5 GHz frequency has to be achieved between try lifelike graphics, Experimental mechanism is shown in Figure 4.

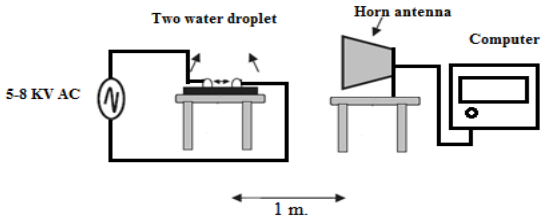

Fig. 4. Experiment Mechanism

In the experiment, a sample of epoxy on different distances for each test consisting of the water droplets in the discharge was recorded with the help of the horn antenna.[11-15]. Carried out the experiment, 0.2 ml, 0.4 ml, 0.6 ml, weight is given a high voltage of the two water droplets. (Figure 5).

a) b) c)

Fig. 5. 0.2-0.4-0.6 ml Used experimental Style (a), (b), (c), respectively, of the

An experiment carried out when the distance between two water droplets is 1.5-2-2.5 cm. carried out the experiment. The spectrum analysis of each experiment is shown in Figure 6, 7 and 8.

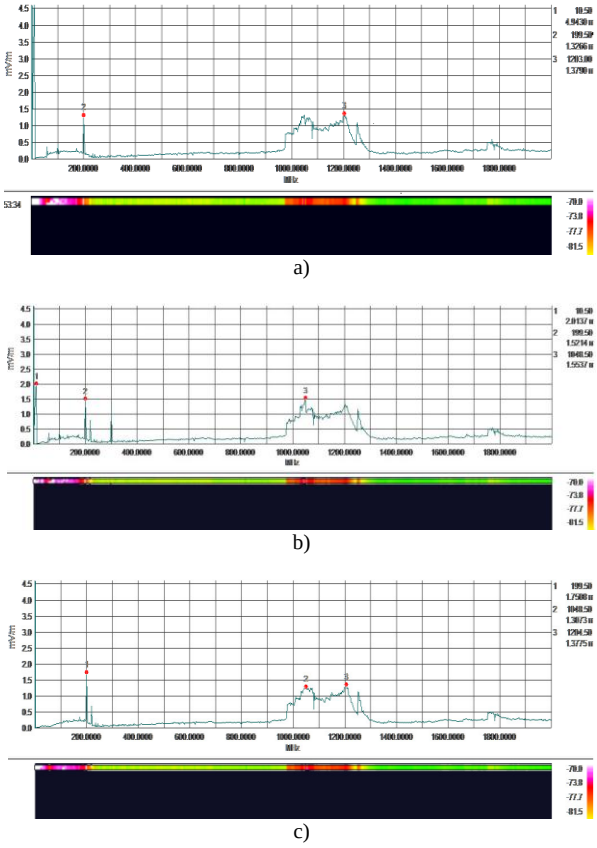

a)

b)

c)

Figure 6. 0.2 ml of water droplet corona discharge performed
a) 1,5 cm b) 2 cm c) 2.5 cm

Figure 6, Figure 7 and Figure 8, the horizontal axis the frequency, the vertical axis is the electric field values. Located under the colored parts of the graphics states that the spectral values of the electric field. There are some colors under the horizontals axis. There colors are sometimes constant. This is because the horn antenna sometimes receives other frequencies.

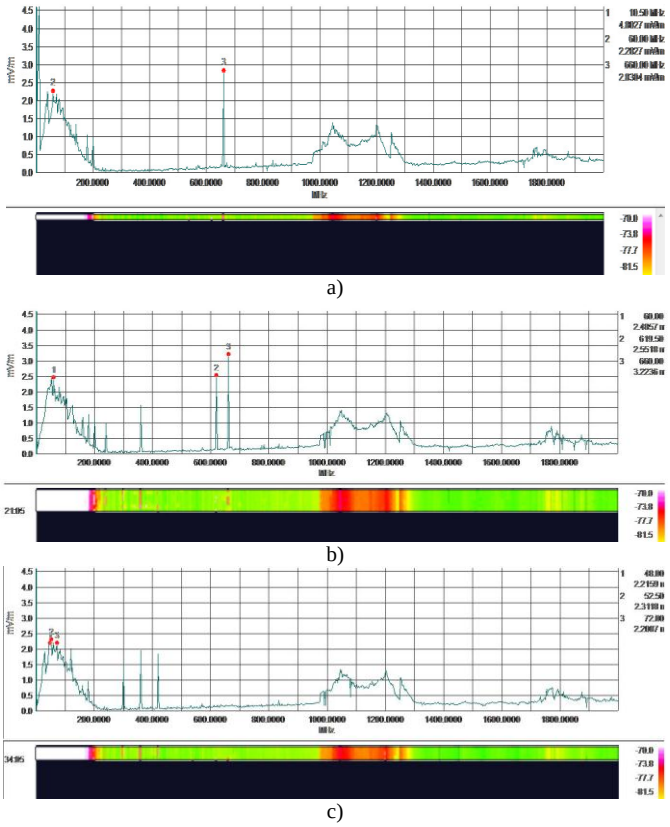

a)

b)

c)

Fig. 7. 0.4 ml of water droplet corona discharge performed.
a) 1,5 cm b) 2 cm c) 2.5 cm

Certain frequencies up to a value for each of the graphics from baseline were recorded. Each of graphs 1, 2, 3, numbered values represent values equivalent to examine the corona discharge between the electrodes.

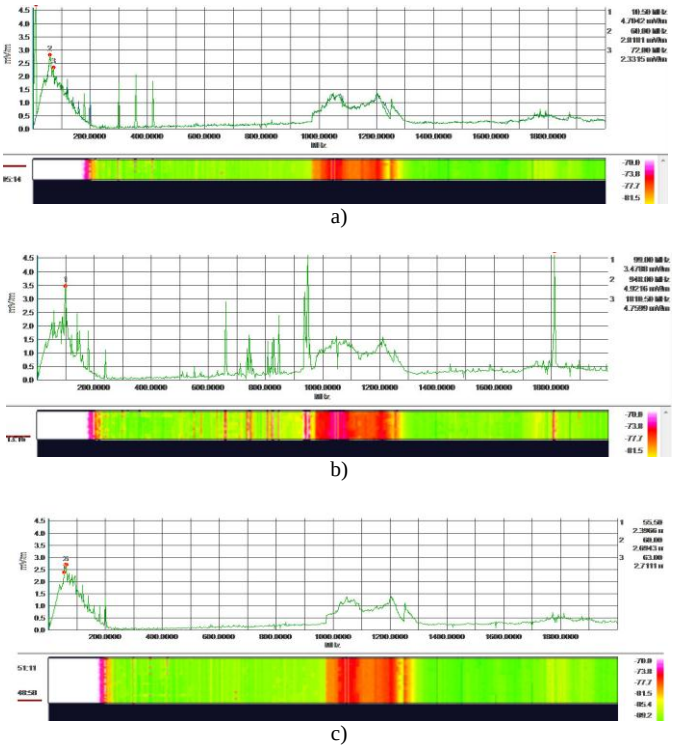

a)

b)

c)

Fig. 8. 0.6 ml of water droplet corona discharge performed.
a) 1,5 cm b) 2 cm c) 2.5 cm

This, the number 1 is taken as the reference value. Detection environment of any signal from the RF antenna 2, 3 number values are affected. Base on this value, so the first number. Figure 6 (a) graph, the distance between the electrodes 1.5 cm. are set to the test when there are Obtained. Here, value is based on the number 1, the electric field exceeds a value greater portion of the value that the chart.

Figure 6 (b) the distance between the electrodes 2 cm. When set to a value compared to the decrease observed in the number 1.Figure 6 (c) distance between the electrodes 2,5 cm. When the experiment, the resulting chart, the number 1 has been observed value decreased slightly. Figures 7 and 8 as a reference in the chart, the number 1 examine the values in the same way, with increasing distance between electrodes, the electric field is low the increased volume of water droplets, however, observed that the electric field. Figures 6, 7 As can be seen in the graphs are examined, the electric field increases, the increase in the volume of water droplets understood. The resulting graphs were compatible with the theory [21-34].

IV. Results and discussions

This experimental study, with the help of RF technique for water droplets between corona discharge of discharge has been observed. During the experiment, the distance between the water droplets, corona discharge, arc discharge, and finally set to turn into a short circuit. In this study, the value of 5 kV corona discharge starts, the applied voltage is taken as approximately 5KV experiments, the distance between the water droplets 1,5-2-2,5 cm. made to. The results obtained in this study, is understood to be in harmony with the theory. [30-34] Using RF sensor used in this study, the frequency of the electric field and between the aggregates are obtained directly. As you can see in Figure 6, 7 and 8 as you increase the distance between the electrodes, an electrical field is decreasing. Therefore, distance between the electrodes is of great importance. As seen in previous studies, the water droplets on the high-voltage corona discharge over time, cause the electrical field there is increasing. Corona discharge, affecting not only the distance between the water droplets, where the volumes of the drops are important. Having made the experiment, 0.2 ml, 0.4 ml, 0.6 ml volume drops were used.

V. CONCLUSIONS

In this study, 0-200000 MHz. in the range of 1, 2, 3 numbers of the values is taken as the reference value of the number 1 and the electrodes by the distance to the volume of the water, the number 1 electrical field value changes were observed. Volume of 0.2 ml of water droplets and the distance between the electrodes 1.5 cm. graphical examination of the electrical field increases, which increases the volume of water is understood. RF electric field sensing to see the experiment, ie, the horn antenna is used. 0 to 2.5 GHz. frequency spectrum analyses of the results show the properties of the discharge. Under normal conditions, to obtain data from the corona discharge, it can be difficult to observe.

To perform this procedure, the horn antenna horn antenna is used through LCS program, were obtained and interpreted in the desired graphics. According to the obtained graphs, the corona discharge monitor, high-voltage lines feature before losing in the dielectric insulators, is important to take the necessary precautions. According to the information obtained from this experiment, the RF sensors can be observed using the discharge of high-voltage lines.

This information is a high voltage transmission lines, corona discharge before they happen, transmission lines is placed 1 meter away from the radio-frequency detection device, if lines occurring on the corona discharge, the chances of observing reveals to intervene. In addition, the isolators to observe events occurring on a discharge, several types of sensors can be used, operating similarly to the RF technology. Thus, the discharge events detected with the help of sensors is saved to the computer; the necessary measures can be taken without harming Isolator.

References

[1] Kueffel, E.; Abdullah, M.: “High Voltage Engineering Pergamon Pres”, (1970).

[2] Nasser, E.: “Fundamentalsof Gaseous Ionizahun and Plasma Electronics, Wiley Interscience” Newyork, (1971).

[3] Özkaya M.: “Yüksek Gerilim Tekniğinde Deşarj Olayları”, İstanbul, (1988).

[4] Brown, S.C.: “Basic Data Of Plasma PhysicsThe M.I.T. Press” , (1959).

[5] Kuffel, E.; Zaengi, W.S.; Kuffel, J.:“High Voltage Engineering, Fundamentals”, (2006).

[6] Kuffel, E.;Zaengi, W.S.; Kuffel, J.: “High Voltage Engineering”, (1996).MCGraw – Hill – USA

[7] Rumeli, A.: “Kirli İzole Yüzeylerde Deşarjların Yayılımı ve Atlama” Elektrik Mühendisliği, (1973). 199: 419-427.

[8] Rumeli, A.; Hızal, M.; Demir, Y.: “Analytical Estimation of Flashover Performances of Polluted Insulators” ISPPISD, Madras.(1981).

[9] Mackevich, J.;Shah,M.: “Polymer outdoor insulating materials Part I: Comparison of porcelain and polymer electrical insulation”IEEE Electrical Insulation Magazine, (1997)5-12.

[10] Gorur, R.;Karady G.; Jagota A.; Shah M.; Yates A.: “Agingin silicone rubber used for outdoor insulation”IEEE Transactionson Power Delivery, (1992)525-538.

[11] Zhu, Y.;Otsubo M.; Honda C.: “Behavior of water dropletone electrically stressed polymeric coating surface”Surface and Coatings Technology, Feb. (2007)5541-5546.

[12] Phillips, A.;Childs D.;Schneider H.: “Aging of nonceramicinsulators due to corona from water drops”IEEE Transactionson Power Delivery, (1999)1081-1089.

[13] Gorus, R.;Cherney E.; Hackam R.: “The AC and DC performance of polymeric insulating materials under accelerated aging in a fogchamber”IEEE Transactions on Power Delivery, (1988) 1892-1902.

[14] Meyer, L.;Jayaram S.; Cherney E.: “Correlation of damage, dry band arcing energy, and temperature in inclined plane testing of silicone rubber for outdoor insulation”IEEE Transactionson Dielectrics and Electrical Insulation, (2004) 424-432.

[15] El-Hag, A. H.: “Leakage current characterization for estimating the conditions of non-ceramic insulators' surfaces,” Electric Power Systems Research, Mar. (2007) 379-384.

[16] Kumagai, S.;Yoshimura N.: “Leakage current characterization for estimating the conditions of ceramic and polymeric insulating surfaces”IEEE Transactions on Dielectrics and Electrical Insulation, (2004) 681-690.

[17] Lopes, I.;Jayaram S.; Cherney E.: “A method for detecting the transition from corona from water droplets to dry-band arcing on silicone rubber insulators” IEEE Transactions on Dielectrics and Electrical Insulation, (2002) 964-971.

[18] Fernando, S. C.;Wong K. L.; Rowe W. S. T.: “RF radiation from corona discharge between two water droplets on epoxy and silicone-rubber

surfaces" Proceedings of Asia-Pacific Microwave Conference, , (2011) 1582-1585.
[19] Sarathi, R.;Nagesh G.: "UHF technique for identication of discharges initiated by liquid droplet in epoxy nano composite insulation material under ac voltages" Journal of Physics D:Applied Physics, Vol. 41, 155407, (2008).
[20] Higashiyama, Y.;Yanase S.; Sugimoto T.: "DC corona discharge from water droplets on a hydrophobic surface" Journalof Electrostatics, (2002) 351-360.
[21] Imano, A.;Beroual A.: "Study of the behavior of AC discharges of water drops on both conducting and dielectric solid surfaces" IEEE Transactions on Dielectrics and Electrical Insulation, (2010) 1569-1575.
[22] Rowland, S. M.;Lin F. C.: "Stability of alternating current discharges between water drops on insulation surfaces" Journalof Physics D: Applied Physics, (2006) 3067-3076.
[23] Fernando, S. C.;Wong K. L.; Bojovschi A.; Rowe W. S. T.:"Detection of GHz frequency components of partial discharge in various media"Proceedings of 16th International Symposiumon High Voltage Engineering (ISH 2009), Cape Town, South Africa, (2009)687-692.
[24] El-Kishky, H.;Gorur R.: "Electric field computation on an insulating surface with discrete water droplets"IEEE Transactions on Dielectrics and Electrical Insulation, (1996) 450-456.
[25] Guan, Z.;Wang L.; Yang B.; Liang X.; Li Z.: "Electric field analysis of water drop corona" IEEE Transactions on Power Delivery, (2005)964-969.
[26] Fujii, O.;Honsali K.;Mizuno Y.;Naito K.: "A basic study on the effect of voltage stress on a water droplet on a silicone rubber surface" IEEE Transactions on Dielectrics and Electrical Insulation,(2009) 116-122.
[27] Gao, H.;Jia Z.; Mao Y.; Guan Z.; Wang L.: "Effect of hydrophobicity on electric field distribution and discharge salong various wetted hydrophobic surfaces" IEEE Transactionson Dielectrics and Electrical Insulation, (2008)435-443.
[28] Zhu, Y.;Otsubo M.; Honda C.; Hashimoto Y.; Ohno A.:"Mechanism for change in leakage current waveform on a wet silicone rubber surface - A study using a dynamic 3-D model" IEEE Transactions on Dielectrics and Electrical Insulation, (2005)556-565.
[29] Kim, S.;Cherney E.; Hackam R.: "Effect of dryband arcing on the surface of RTV silicone rubber coatings" IEEE International Symposium on Electrical Insulation, (1992)237-240.
[30] Qıu, Y.: "Simple Expression of Field Nonuniformity Factor for Hemispherically Capped Rod-Plane Gaps" IEEE Trans. Elect. Insul. Vol. EI-21 No:4, 673 - 675. (1986).
[31] Azer, A.A.;Comsa, A.P.:"Influence of Field Nonuniformity on the Breakdown Characteristic of SF6" IEEE Trans,EI.8., 136 - 142. (1973).
[32] Nagata, M.;Yokoı, Y.; Mıyachı, I.: "Electrical Breakdown Characteristics in High Temperature Gases" Elect.Eng. Japan, Vol.97, 1 - 6. (1977).
[33] HABAŞ.: "Özel Gazlar -Argon Gazı ve diğerleri" Katalog, Bahriye Cad.No:199, Kasımpaşa, İstanbul (2002).
[34] Haykin, S.: "Neural Networks a Comprehensive Foundation", PrenticeHall, N. J., (1999).

Taner Dindar (Feb'87) received B.Sc. and M.Sc. degrees from Marmara University Department of Electrical Education in Istanbul, Turkey, in 2009 and 2012 respectively. He is currently working at Ankara University, Ankara, Turkey. He worked as a lecturer in Arel University, Department of Electricity from 2011 to 2012 in Istanbul, Turkey. His research interest includes the high voltage systems, energy applications, and control systems.

N. Fusun Oyman Serteller received her B.Sc., M.Sc. degrees from the Istanbul Technical University (ITU), and Ph.D. degree from the Marmara University, Electrical Engineering Department, in 1988, 1993 and 2000 respectively. Between 1990 and 1994, she worked at Balikesir University. She is currently Associate professor of electrical and electronics engineering department at Marmara University. Him research interests are electrical machines, electrical power systems and high voltage energy systems.

Tahir Cetin Akinci was born in Pınarbası in Turkey. He graduated from Electrical Engineering department at Klaipeda University. He received M.Sc. and Ph.D. degrees from Marmara University of Istanbul, Turkey, in 2002 and 2009 respectively. He is currently assistant professor of electrical and electronics engineering department at Kirklareli University. His research interests are signal processing, control systems, electrical power systems, non-linear dynamical systems, soft computing and condition monitoring techniques.

The Connection between real-ω and real-k Approaches in an Absorbing Medium

Mehmet Emre Taşgın

***Abstract*—We investigate the transmission and reflection of a pulse that is incident from air on to an absorbing medium of frequency dependent dielectric. In the literature solution on the absorbing part is expressed as the fourier integral over all real frequency (ω) range, with corresponding complex wave-vectors $k = k_R(\omega) + ik_I(\omega)$. We show that, the solution in the absorbing part must be written as the Fourier sum of all real wave-vectors (k), with the corresponding complex frequencies $\omega = \omega_R(k) + i\omega_I(k)$. Then, we try to show that these two approaches result in different function, in space and time, for the transmitted pulse. On the contrary, we show that two approaches give the same result.**

On the other hand, we manage to derive a mathematical connection between the fourier components of the two approaches. This makes the comparison of the two types of group velocities accessible; with fixed position and with fixed time. We calculate a velocity in two different ways: using the i) real-ω and ii) real-k approaches. Then we compare the two results and decide if the velocity definition is reliable or not. This paper is the complementary work leading to Ref. [1]

***Index Terms*—group velocity, dispersive medium, superluminal propagation, real frequency, complex frequency, pulse reshape.**

I. Introduction

We consider the problem of pulse transmission from air to an absorbing medium of complex dielectric susceptibility $\epsilon(\omega) = \epsilon_R(\omega) + i\epsilon_R(\omega)$ which gives a complex index $n(\omega) = n_R(\omega) + in_I(\omega)$.

The solution of the Maxwell equations in complex indexed medium is given, [2], [3], by the integral sum of the real frequency fourier components such as

$$E(x,t) = \int_{-\infty}^{\infty} d\omega e^{-i\omega t} \quad \Big(C_1(\omega)e^{in(\omega)\omega x/c} + D_1(\omega)e^{-in(\omega)\omega x/c}\Big). \quad (1)$$

In section II-A we show that, in the general solution of the Maxwell equations in complex indexed medium, wave-vector k must be treated real. Treating k as a real variable brings out the complexity of the frequency ω. Furthermore, according to the usual model of absorption, as well as the polarization, this phenomenon is a behavior due to the time response of the atoms. This brings out the decision that the solutions must decay in time, locally.

M.E. Tasgin is with the Department of Electrical & Electronics Engineering, Kırklareli University, Kırklareli, Karahıdır 39020 Turkey and Center for Advanced Research, Kırklareli University, Kırklareli, Karahıdır 39020 Turkey e-mail: metasgin@kirklareli.edu.tr.

In contrast to the literature solution (1), we show that the general solution must be in the form of

$$E(x,t) = \int_{-\infty}^{\infty} dk e^{ikx} \left(C_2(k)e^{i\frac{ck}{n(k)}t} + D_2(k)e^{-i\frac{ck}{n(k)}t}\right), \quad (2)$$

where $n(k)$ is the index as a function of the real wave-vector k, treated in section II-B.

After then, we try to show the difference in between the two approach; real-ω approach and real-k approach. We use the boundary conditions(BC) in order to establish a connection between the fourier components of the two approaches in section III. The suspicion of the inequality of two approaches originates from the following decision. The equality of the sum of the fourier components at the boundary

$$\int_{-\infty}^{\infty} d\omega D_1(\omega)e^{-i\omega t} = \int_{-\infty}^{\infty} dk D_2(k)e^{-i\frac{ck}{n(k)}t} \quad (3)$$

does not imply the equality of the electric fields

$$\int_{-\infty}^{\infty} d\omega D_1(\omega)e^{i\omega n(\omega)x/c}e^{-i\omega t} = \int_{-\infty}^{\infty} dk D_2(k)e^{ikx}e^{-i\frac{ck}{n(k)}t} \quad (4)$$

in whole space and time. Carrying the integration over complex ω space may change the result of the two integrals in (4), due to the enclosed poles or branch cuts of $D_1(\omega)$, $D_2(k)$ or $n(k)$.

In section IV we try to show the difference of two approaches. For the cases, we considered here, there occurs no difference between results of the two approaches. However, we limited the behaviors of the functions such as the index $n(\omega)$ and the frequency distribution of the incident pulse $A(\omega)$. In example we limited $A(\omega)$ to convergent to zero at all infinities in the whole complex plane. This excludes the Gaussian functions, in example. Furthermore, in some dielectric mediums, created using three level systems, index $n(\omega)$ may exhibit strange behaviors, out of the lorentzian type.

So that, there exists the possibility of the presence of deviation from the equivalence of the two approaches for other types of incident pulse shapes.

Beyond the discussion of the equivalence/inequality of the two approaches, we managed to establish a connection between the fourier components of the two approaches. This opens the feasibility of some research topics, discussed in several papers.

Reference [4] examined the group velocity of a pulse, propagating in an absorbing medium. They derived the average

of the time $\langle t\rangle_x$ that describes where the pulse is in time, for a given space point x. They also announced, eighth reference in this paper, that they would publish a second paper, where they were going to treat the average pulse position $\langle x\rangle_t$ for a given time. They, however, did not publish such a paper. We performed this study, which is very very similar to the method discussed in [4]. The result of $\langle t\rangle_x$ contains the fourier components in real-ω approach $D_1(\omega)$. The result of $\langle x\rangle_t$, however, contains the fourier components in the real-k space $D_2(k)$. Since the two approaches have been unable to be connected, they could not compare the velocity from the two approaches. This is the probable reason for not to publish.

Being established the connection, we plan to investigate average pulse position $\langle x\rangle_t$ and compare the results with the $\langle t\rangle_x$ of reference [4]. For a beginning research we observed that, see figure 9, we showed the group velocity in the two approaches are different. Tracking the propagation of the pulse position (v_2) always results in higher average velocity than the tracking of the arrival time (v_1). This is going to be considered in a separate report.

In the band structure calculations for the frequency dependent dielectric materials, the method of k-real (complex-ω) is also used, [5], in order to compare the results with the ω:complex(k:real) method. The parallel behavior is exhibited. However, the direct relationship between the band structures were not derived.

A proper definition of the group velocity in complex indexed medium, whether uniform or not, has not been established yet. Whatever the formula for a group velocity is, it must generate the same results in both approaches. The closer values of the velocities in two approaches, the generated formula of group velocity is closer to reality.

II. MAXWELL EQUATIONS IN ABSORBING MEDIUM

A. Realness of k

In this section we show that the solution of the Maxwell equations in an absorbing medium is the Fourier integral of real k vectors and complex frequency ω.

Maxwell equations are

$$\begin{array}{ll} \nabla\cdot\mathbf{D}=0 & \nabla\cdot\mathbf{B}=0 \\ \nabla\mathbf{E}=-\frac{\partial\mathbf{B}}{\partial t} & \nabla\mathbf{H}=\frac{\partial\mathbf{D}}{\partial t}. \end{array} \tag{5}$$

For auxiliary magnetic field field we assume vacuum permeability $\mathbf{H}=\frac{\mathbf{B}}{\mu_0}$. Displacement field depends on the the electric field as

$$\mathbf{D}(x,t)=\epsilon_0\mathbf{E}(x,t)+\int_{-\infty}^{\infty}\chi(\tau)\mathbf{E}(x,t-\tau)d\tau. \tag{6}$$

The physical interpretation of equation (6) is as follows. Electron, about the atomic or molecular core, response to the applied electric field in a finite time which is less than the frequency of the light. This creates an electric dipole moment oscillating in time and a magnetization at later times . The dipole moment $\mathbf{M}(x,t)$ at time t, generated by the applied electric field $\mathbf{E}(x,t-\tau)$ at time $t-\tau$, superposes with the the electric field $\mathbf{E}(x,t)$ at time t. Absorbtion of the incident $\mathbf{E}$ field is modelled as the interference with the dipole moment of the medium. This shows, even before attempting to solve Maxwell equations, that the attenuation shall be considered in time.

Due to causality, $\chi(\tau)=0$ for $\tau<0$. dielectric function becomes

$$\mathbf{D}(x,t)=\epsilon_0\mathbf{E}(x,t)+\int_{0}^{\infty}\chi(\tau)\mathbf{E}(x,t-\tau)d\tau. \tag{7}$$

Now, lets solve the Maxwell equations (5) more carefully. Using the third and the fourth equations in (5) we obtain the wave equation

$$\nabla^2\mathbf{E}(x,t)=\frac{1}{c^2}\frac{\partial^2\mathbf{E}}{\partial t^2}+\frac{1}{c^2}\int_0^{\infty}\chi(\tau)\frac{\partial^2\mathbf{E}}{\partial t^2}(x,t-\tau)d\tau \tag{8}$$

for the electric field. Since there is no source $\nabla\cdot\mathbf{E}=0$. We reduce our problem to one dimension, assuming normal incidence. We separate the equation into two, by separation of variables $E(x,t)=E_1(x)E_2(t)$, in time and in space

$$-c^2k^2E_2(t)=\frac{d^2E_2(t)}{dt^2}+\int_0^{\infty}\chi(\tau)\frac{d^2E_2}{dt^2}(t-\tau)d\tau \tag{9}$$

$$-k^2E_1(x)=\frac{d^2E_1(x)}{dx^2}. \tag{10}$$

k^2 is the separation constant, which we have equated to the $-\frac{1}{E_1(x)}\frac{\partial^2E_1(x)}{\partial x^2}$. The solution of space equation (10) is straight forward $E_2(x)=A_2cos(kx)+B_2sin(kx)$ with $E_2(x)$ real.

On the time equation (9) we apparently see that k^2 must be real, since both $\chi(t)$ and $E_2(t)$ are real. Note that the condition for $E(x,t)=E_1(x)E_2(t)$ to be real is both $E_1(x)$ and $E_2(t)$ are to be real. After fixing(choosing) a k value, due to equation (10), we must solve equation (9) for this k value.

To be able to determine $E_2(t;k)$, we Fourier expand the time function of electric field and the dielectric susceptibility as

$$E_2(t)=\textstyle\int_{-\infty}^{\infty}E_2(\omega)e^{-i\omega t}d\omega \quad , \tag{11}$$

$$\chi(\tau)=\textstyle\int_{-\infty}^{\infty}\chi(\omega)e^{-i\omega\tau}d\omega \tag{12}$$

with $E_2(-\omega)=E_2^*(\omega)$ and $\chi(-\omega)=\chi^*(\omega)$. Putting (12) in (9) we determine that $E_2(\omega;k)=0$ for all ω, except for the $\bar{\omega}$ with $\bar{\omega}^2(1+\chi(\bar{\omega}))=c^2k^2$. This equation has two solutions $\bar{\omega}_{1,2}=\pm|\bar{\omega}|$, since $\chi(\omega)$ is symmetric function. (This is also valid for complex ω case when $\omega_R\to-\omega_R$ and $\omega_I\to\omega_I$.)

Then solution, for a fixed k value, is $E_2(t;k)=C_2e^{i|\omega(k)|t}+D_2e^{-i|\omega(k)|t}$. C_2 and D_2 are totally unconnected, except that $E(x,t)$ must be real.

Note that, the form of this solution $E_2(t;k)$ is independent of the solution we chose for $E_1(x)$.

If we use $E_1(x)=cos(kx)$ or $E_1(x)=sin(kx)$, the time solution would be $E_2(t;k)=\mathrm{Re}\{C_2\}cos(\omega(k)t)+\mathrm{Im}\{C_2\}sin(\omega(k)t)$. The solution equivalently can be written in the form

$$\begin{aligned} E_1(x)E_2(t)=e^{ikx}(C_2e^{i|\omega(k)|t}+D_2e^{-i|\omega(k)|t}) \\ +e^{-ikx}(C_2^*e^{-i|\omega(k)|t}+D_2^*e^{i|\omega(k)|t}). \end{aligned} \tag{13}$$

The most general solution, which may contain any k, can be written as

$$E_b(x,t) = \int_{-\infty}^{\infty} dk e^{ikx} \Big(\quad C_2(k) e^{i\omega(k)t} + D_2(k) e^{-i\omega(k)t} \quad \Big), \quad (14)$$

not as

$$E_a(x,t) = \int_{-\infty}^{\infty} d\omega e^{-i\omega t} \Big(\quad C_1(\omega) e^{-ik(\omega)t} + D_1(\omega) e^{ik(\omega)t} \quad \Big). \quad (15)$$

For real $\chi(\omega)$ functions (14) and (15) are equivalent. They are only scaled versions of each other. When $\chi(\omega)$ is complex, however, for a given incident pulse the transmitted pulse(so reflected) may differ in two approaches.

B. Index $n(k)$ and real-k integration

Since ω and k are dependent on each other via $\omega n(\omega) = ck$, we may write equations (14) and (15) as

$$E_b(x,t) = \int_{-\infty}^{\infty} dk e^{ikx} \Big(\quad C_2(k) e^{ickt/n(k)t} + D_2(k) e^{-ickt/n(k)} \quad \Big), \quad (16)$$

$$E_a(x,t) = \int_{-\infty}^{\infty} d\omega e^{-i\omega t} \Big(\quad C_1(\omega) e^{-i\omega n(\omega)x/c} + D_1(\omega) e^{i\omega n(\omega)x/c} \quad \Big). \quad (17)$$

For real $\epsilon(\omega) = n^2(\omega)$, $n(k)$ and $n(\omega)$ are the same within only a transform of the arguments $k \rightarrow \omega n(\omega)/c$. When $\epsilon(\omega)$ is complex, however, $n(k)$ and $n(\omega)$ differs functionally. Moreover, $n(k)$ can not be determined analytically due to the nonlinearity in $n(\omega)$.

When k is constrained to be real, we find index $n(\omega)$ as follows. Equation $n(\omega)\omega = ck$ is now separated into two equations

$$\omega_R n_I + \omega_I n_R = 0 \qquad \text{and} \qquad \omega_R n_R + \omega_I n_I = ck \quad . \quad (18)$$

Since $n_R(\omega)$ and $n_I(\omega)$ are given functions of ω, ω_R and ω_I are solved computationally for a given value of real k. Then, these ω_R and ω_I values are substituted in $n(\omega_R + i\omega_I)$ in order to determine the index value for the real k value, $n(k) = n_R(k) + in_I(k)$.

In figure 1a we plotted the real and imaginary parts of index with respect to real k. And in figure 1b we depicted the corresponding $\omega_R(k)$ and $\omega_I(k)$ values for the real parameter space $k = -2 \ldots 2$. We observe similar properties for $n(k)$, $n_R(-k) = n_R(k)$ and $n_I(-k) = -n_I(k)$, as it is for $n(\omega)$. A zoomed version of $n(k)$ is plotted in figure 2, that is compared with $n(\omega)$. We see that $n(k)$ and $n(\omega)$ are almost the same except that $n(k)$ is little bit greater at both n_R and n_I peaks.

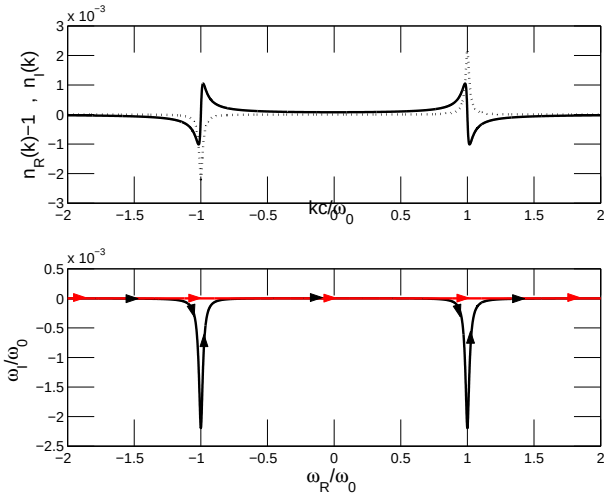

Fig. 1. (a) Complex index as a function of real-k. (b) Corresponding complex frequency $\omega(k) = \omega_R(k) + i\omega_I(k)$ values. This is the real-k integration path $\int_C d\omega$, represented in the complex-ω plane. Red line is the real-ω integration path.

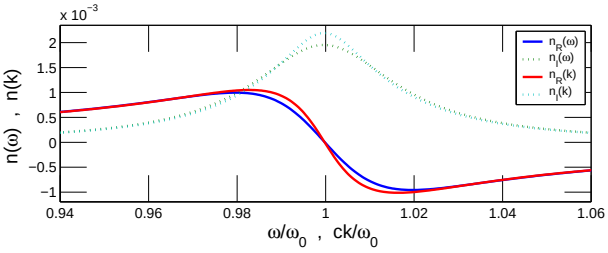

Fig. 2. Complex index for real-ω values $n(\omega)$ and for real-k values. $n(k)$ also exhibits lorentzian type behavior, although analytically not achievable.

C. Integration path in the complex ω plane:

In order to be able to compare functions (16) and (17), we write (14) as

$$\int_C d\omega \left(\frac{dk}{d\omega}\right) e^{i\omega n(\omega)x/c} \Big(\quad C_2\left(\frac{\omega n(\omega)}{c}\right) e^{-i\omega t} + D_2\left(\frac{\omega n(\omega)}{c}\right) e^{i\omega t} \quad \Big) \quad (19)$$

Integration is in the complex ω plane, on the line of constraint k is real. The curve is given in figure 1b with black line. Black arrows indicate the direction of integration, whose limits approaches the real ω axis. The integration with real ω in 17 is drawn with a red line, which is on the real axis. The direction of real ω integration is also indicated with red arrows.

In the next sections we determine the coefficients $D_1(\omega)$, $D_2(k) \equiv D_2\left(\frac{n(\omega)\omega}{c}\right)$ and investigate the difference of functions $E_a(x,t)$ (real ω) and $E_b(x,t)$ (real k).

III. Pulse transmission through an Absorbing Medium

In this section we investigate the pulse transmission through an absorbing medium in 1D. We solve the boundary match problem for the two approaches expressed by electric fields (15) for real ω and (16) for real k.

$n=1$	$n(\omega)=n_R(\omega)+in_I(\omega)$
$E_L(x,t)=$ $\int_{-\infty}^{\infty}d\omega A_1(\omega)e^{i(kx-\omega t)}$ $+\int_{-\infty}^{\infty}d\omega B_1(\omega)e^{i(kx+\omega t)}$	$E_R(x,t)=$ $\int_{-\infty}^{\infty}d\omega D_1(\omega)e^{i(k_1(\omega)x-\omega t)}$
$k=\omega/c$	$k_1=\omega n(\omega)/c$

Fig. 3. The pulse $A(\omega)$, travelling to right, is incident on the plane interface from the air $n=1$. There exist a reflected wave $B_1(\omega)$ on the LHS. On the RHS there is only right travelling wave with frequency components $D_1(\omega)$. The solution on the RHS is considered in real-ω approach.

$n=1$	n=const.
$E_L(x,t)=$ $\int_{-\infty}^{\infty}dkA_2(k)e^{i(kx-\omega t)}$ $+\int_{-\infty}^{\infty}dkB_2(k)e^{i(kx+\omega t)}$	$E_R(x,t)=$ $\int_{-\infty}^{\infty}dkD_2(k)e^{i(kx-\omega_1 t)}$
$\omega=ck$	$\omega_1=ck/n$

Fig. 4. Real-k approach for the constant dielectric. Two approaches are equivalent for real $n(\omega)$.

In subsection III-A we determine the fourier coefficients for real ω case, which we use them to determine $E_a(x,t)$ in the absorbing medium.

In subsection III-B we determine the fourier coefficients for real k case, which we use them to express $E_b(x,t)$. However, we perform this approach in two steps.First for constant dielectric ϵ case, in order to show the equivalence between the two approaches for real $n(\omega)$ case (part III-B1). Second for complex index $n(\omega)$, where two approaches depart from each other (part III-B2).

A. Real ω Approach

We assume a plane interface, see figure 3 , between air $n=1$ and an absorbing medium of complex dielectric $n(\omega)=n_R(\omega)+in_I(\omega)$. Since the incident wave approach from the left(L), there is no left travelling wave on the RHS.

We apply the boundary conditions(BC) $E_{aL}(0,t)=E_{aR}(0,t)$ and $\frac{\partial E_{aL}}{\partial x}(0,t)=\frac{\partial E_{aR}}{\partial x}(0,t)$ to obtain the equations at $x=0$ as

$$\int_{-\infty}^{\infty}d\omega A_1(\omega)e^{-i\omega t}+\int_{-\infty}^{\infty}d\omega B_1(\omega)e^{i\omega t}=\int_{-\infty}^{\infty}d\omega D_1(\omega)e^{-i\omega t} \quad (20)$$

$$\int_{-\infty}^{\infty}d\omega\omega A_1(\omega)e^{-i\omega t}-\int_{-\infty}^{\infty}d\omega\omega B_1(\omega)e^{i\omega t}=\int_{-\infty}^{\infty}d\omega\omega D_1(\omega)e^{-i\omega t} \quad (21)$$

We use the sufficient condition that the integrands are equal for each frequency ω component. Then, fourier components are given by

$$B_1(\omega)=\frac{1-n(\omega)}{1+n(\omega)}A_1(\omega),$$
$$D_1(\omega)=\frac{2}{1+n(\omega)}A_1(\omega). \quad (22)$$

The behavior of the transmitted wave in space and time, is then, given by

$$E_{aR}(x,t)=\int_{-\infty}^{\infty}d\omega\frac{2}{1+n(\omega)}e^{i(n(\omega)\omega x/c-\omega t)} \quad , \quad (23)$$

where each frequency component decay in space with exponential $e^{-n_I(\omega)\omega x/c}$. However the physical intuition (in addition to mathematics) tells that each frequency component must decay in time. This is easily seen by considering an oscillating dipole, which has no interaction with the neighboring dipoles. Since absorption is a local interference effect, the solution must decay in time for a fixed position. One may also tell that equation (23) is only a representation and the decay in time is transferred to the an effective decay in space. We will see in the next section, however, that real k solution differs from (23).

B. Real k Approach

1) Constant Dielectric Case: ϵ : In this part we introduce the real k approach and we show the equivalence (and indicate the reasons of equivalence) between the two approaches when index n is real, see figure 4.

When dielectric response is constant and real, the dispersion $ck=n\omega$ relation comes out only as a scaling transformation between ω and k.

Applying the same BCs, $E_{bL}(0,t)=E_{bR}(0,t)$ and $\frac{\partial E_{bL}}{\partial x}(0,t)=E_{bL}(0,t)=E_{bR}(0,t)$ and $\frac{\partial E_{bR}}{\partial x}(0,t)$, we obtain the integral equations

$$\int_{-\infty}^{\infty}dkA_2(k)e^{-ikct}+\int_{-\infty}^{\infty}dkB_2(k)e^{ikct}=\int_{-\infty}^{\infty}dkD_2(k)e^{-i\frac{k}{n}ct}, \quad (24)$$

$$\int_{-\infty}^{\infty}dkkA_2(k)e^{-ikct}-\int_{-\infty}^{\infty}dkkB_2(k)e^{ikct} \quad (25)$$
$$=\int_{-\infty}^{\infty}dk\frac{k}{n}D_2(k)e^{-i\frac{k}{n}ct} \quad (26)$$

For only mathematical reasons we may define frequency transformations $\omega=ck$ on the LHS and $\omega_1=\frac{ck}{n}$ on the RHS. Equations transform to

$$\frac{1}{c}\int_{-\infty}^{\infty}d\omega A_2(\quad\frac{\omega}{c}\quad)e^{-i\omega t}+\frac{1}{c}\int_{-\infty}^{\infty}d\omega B_2(k)e^{i\omega t}=\frac{n}{c}\int_{-\infty}^{\infty}d\omega_1 D_2(\frac{n\omega_1}{c})e^{-i\omega_1 t}, \quad (27)$$

$$\frac{1}{c^2}\int_{-\infty}^{\infty}d\omega\,\omega A_2(\frac{\omega}{c})e^{-i\omega t}-\frac{1}{c^2}\int_{-\infty}^{\infty}d\omega\omega B_2(k)e^{i\omega t}=\frac{n^2}{c^2}\int_{-\infty}^{\infty}d\omega_1\omega_1 D_2(\frac{n\omega_1}{c})e^{-i\omega_1 t}. \quad (28)$$

Since ω and ω_1 are dummy variables we equate the integrands to obtain the relations

$$A_2\left(\frac{\omega}{c}\right)+B_2\left(-\frac{\omega}{c}\right)=nD_2\left(\frac{n\omega}{c}\right) \quad (29)$$

$n=1$	$n(\omega)\equiv n_R(k)+in_I(k).$
$E_L(x,t)=$ $\int_{-\infty}^{\infty}dkA_2(k)e^{i(kx-\omega t)}$ $+\int_{-\infty}^{\infty}dkB_2(k)e^{i(kx+\omega t)}$	$E_R(x,t)=$ $\int_{-\infty}^{\infty}dkD_2(k)e^{i(kx-\omega_1 t)}$
$\omega=ck$	$\omega_1=ck/n(k)$

Fig. 5. Same configuration of 3, but this time problem is treated with the real-k approach: RHS is expressed as the sum over real-k plane waves of fourier coefficients $D_2(k)$.

$$\omega A_2\left(\frac{\omega}{c}\right)-\omega B_2\left(-\frac{\omega}{c}\right)=n^2\omega D_2\left(\frac{n\omega}{c}\right) \tag{30}$$

between the fourier components. In 30 ω cancels. However, we kept ω in order to remind the reader that $\omega=ck$ on the LHS, but it is $\omega=\frac{ck}{n}$ on the RHS. Consequently the fourier components are calculated to be

$$\begin{aligned} B_2\left(\frac{\omega}{c}\right)&=\frac{1-n}{1+n}A_2\left(\frac{\omega}{c}\right),\\ D_2\left(\frac{n\omega}{c}\right)&=\frac{2}{n(1+n)}A_2\left(\frac{\omega}{c}\right). \end{aligned} \tag{31}$$

Solution of $D_2(k)$ seems different than real ω result (22). However, if it is put in the form $nD_2\left(\frac{n\omega}{c}\right)=\frac{2}{1+n}A_2\left(\frac{\omega}{c}\right)$, it is seen that

$$\int_{-\infty}^{\infty}dkD_2(\omega)e^{ikx-\frac{k}{n}ct}=\int_{-\infty}^{\infty}d\omega\frac{2}{1+n}e^{i\omega x/c-\omega t}. \tag{32}$$

When n is real the results (31) and (22) are equivalent, in determining $E_a(x,t)\equiv E_b(x,t)=E(x,t)$. However, the usual physical interpretation "Frequency does not change for light changing medium between dielectrics." here transforms to only a mathematical scaling transformation which cannot be performed in the complex $\epsilon(\omega)$ case.

2) Complex (frequency-dependent) Dielectric Case: $\epsilon(\omega)=\epsilon_R(\omega)+i\epsilon_I(\omega)$: In this part we discuss the pulse transmission/propagation into/through an absorbing medium. We extend the real-k approach to frequency dependent complex index, $n(\omega)=n_R(\omega)+in_I(\omega)$. We determine the integral equations connecting the fourier components $A_2(k)$, $B_2(k)$ and and $D_2(k)$. The explicit connection, however, is not straightforward to obtain as it is in the real-ω approach. This is left to section IV.

The solutions on the LHS and RHS, see figure 5, are given by

$$\begin{aligned} E_{bL}(x,t) &= \int_{-\infty}^{\infty}dkA_2(k)e^{i(kx-kct)}\\ &\quad+\int_{-\infty}^{\infty}dkB_2(k)e^{i(kx+kct)} \end{aligned} \tag{33}$$

$$E_{bR}(x,t)=\int_{-\infty}^{\infty}dkD_2(k)e^{i\left(kx-\frac{k}{n(k)}ct\right)}\quad. \tag{34}$$

Applying the BC.s $E_{bL}(0,t)=E_{bR}(0,t)$ and $\frac{\partial E_{bL}}{\partial x}(0,t)=\frac{\partial E_{bR}}{\partial x}(0,t)$, as usual, we obtain the integral equations

$$\begin{aligned} \int_{-\infty}^{\infty}dkA_2(k)e^{-ikct} &+ \int_{-\infty}^{\infty}dkB_2(k)e^{ikct}\\ &=\int_{-\infty}^{\infty}dkD_2(k)e^{-i\frac{k}{n(k)}ct}, \end{aligned} \tag{35}$$

$$\begin{aligned} \int_{-\infty}^{\infty}dkkA_2(k)e^{-ikct} &+ \int_{-\infty}^{\infty}dkkB_2(k)e^{ikct}\\ &=\int_{-\infty}^{\infty}dkkD_2(k)e^{-i\frac{k}{n(k)}ct} \end{aligned} \tag{36}$$

This time, however, the fourier components $A_2(k)$ and $B_2(k)$ cannot be connected to $D_2(k)$ easily. This is because we cannot equate the integrands directly, as it is in real-ω approach III-A, or with a scaling transformation, as it is in constant index case III-B1.

One may try to perform the transformation $\omega=ck$ an the LHS and $\omega_2=\frac{ck}{n(k)}$ on the RHS. This time, however, the integral on the RHS transform to a line integration over the complex ω_2 plane as is mentioned in subsection II-B. So, integrands cannot be equalized.

C. The Connection between Fourier Components $D_2(k)$ and $D_1(\omega)$

The incoming pulses are common in both approaches. So that we equate

$$\int_{-\infty}^{\infty}dkA_2(k)e^{i(kx-ckt)}=\int_{-\infty}^{\infty}d\omega A_1(\omega)e^{i(\omega x/c-\omega t)} \tag{37}$$

in order to obtain the relation $\frac{1}{c}A_2(k)=A_1(\omega)$.

Before solving equations (35) and (36) for $D_2(k)$ explicitly, it is not possible to obtain $B_2(k)$ in terms of $A_2(k)$. Without any proof, however, we take

$$B_2(k)=\frac{1-n(k)}{1+n(k)}A_2(k)\quad. \tag{38}$$

This is because we aim to show that the resultant electric fields $E_{aR}(x,t)$ and E_{bR} are different in the absorbing medium. Equation (38) corresponds to taking fourier coefficients equal on the LHS.

When the fourier components on the LHS are the same, functional behavior of $E_{aL}(x,t)$ and $E_{bL}(x,t)$ also match due to scaling transformation $\omega=ck$. Then, the integrals of fourier coefficients on the RHS are also equal

$$\int_{-\infty}^{\infty}dkD_2(k)e^{-i\frac{k}{n(k)}ct}=\int_{-\infty}^{\infty}d\omega D_1(\omega)e^{-i\omega t}. \tag{39}$$

Due to the complexity of the transformation $\omega_2=\frac{ck}{n(k)}$, integrands are not able to be equalized. Furthermore, due to the line integration over the complex ω_2 plane, the presence of equation

$$\begin{aligned} \int_C d\omega\left(\frac{dk}{d\omega}\right)\quad D_2\quad\left(\frac{\omega n(\omega)}{c}\right)e^{-i\omega t}\\ =\int_{-\infty}^{\infty}d\bar{\omega}D_1(\bar{\omega})e^{-i\bar{\omega}t} \end{aligned} \tag{40}$$

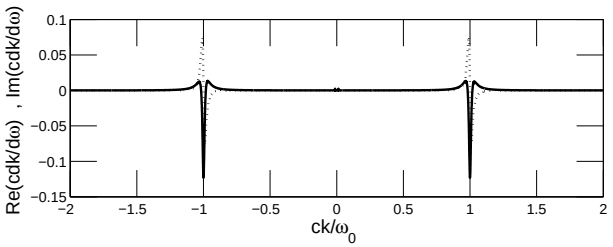

Fig. 6. The behavior of $\frac{dk}{d\omega}$ for real-k case. The real part is symmetric, the imaginary part is anti-symmetric.

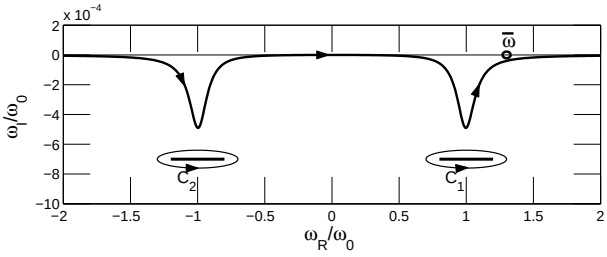

Fig. 7. Real-k integration path, $\int_c d\omega$, in the complex-ω plane.The contours $C_{1,2}$ are the branch cuts of lorentzian $n(\omega)$. There exists no pone nor branch cut of $D_2\left(\frac{n(\omega)\omega}{c}\right)$ in between the curve C and the real-ω axis. The $\bar{\omega}$ is the single pole of equation (47) .

originating from equation (39), *does not imply* the equality

$$\int_C d\omega \left(\frac{dk}{d\omega}\right) \quad D_2 \quad \left(\frac{\omega n(\omega)}{c}\right) e^{i(k(\omega)x-\omega t)} = \int_{-\infty}^{\infty} d\bar{\omega} D_1(\bar{\omega}) e^{i(k(\bar{\omega})x-\bar{\omega}t)}, \quad (41)$$

in general. This is because of the possibility of including any pole or branch cut of $D_2\left(\frac{n(\omega)\omega}{c}\right)$. The bar symbol refers to the reality of frequency.

IV. Difference Between Two Approaches

In the previous section we obtained a direct connection between he fourier components of real-ω approach $D_1(\omega)$ and the ones for the real-k approach $D_2(k)$, at equation (40). In this section we aim to show that this connection leads to different functions for the transmitted pulses $E_{aR}(x,t)$ and $E_{bR}(x,t)$, in the absorbing medium.

We assume that $D_2\left(\frac{n(\omega)\omega}{c}\right)$ converges to zero at all infinities, as $|\omega| \to \infty$. WE make this assumption to be able to use the contour integral formalism; that integration over infinite circles does not contribute.

If ω, on the LHS of equation (40) were real we could use the Dirac delta function formula $\int_{-\infty}^{\infty} e^{-(\omega-\bar{\omega})t} dt = \delta(\omega-\bar{\omega})$ in order to connect $\left(\frac{dk}{d\omega}\right) D_2\left(\frac{n(\omega)\omega}{c}\right)$ to $D_1(\omega)$. The existence of imaginary part of ω, however, makes the time integral divergent. Above, bar symbol $\bar{\omega}$ implies the reality of the variable.

In order to overcome this difficulty we integrate for a finite time, $t = T \ldots T$, after then we take the limit $T \to \infty$. The fourier component of the real-ω approach is given in terms o the real-k approach as

$$2\pi D_1(\bar{\omega}) = \lim_{T\to\infty} \int_C \quad d\omega \quad \left(\frac{dk}{d\omega}\right) D_2\left(\frac{n(\omega)\omega}{c}\right) \times \int_{t=-T}^{T} dt e^{-i(\omega-\bar{\omega})t}, \quad (42)$$

which transforms to

$$2\pi D_1(\bar{\omega}) = \lim_{T\to\infty} \int_C \quad d\omega \quad \left(\frac{dk}{d\omega}\right) D_2\left(\frac{n(\omega)\omega}{c}\right) \times \frac{e^{i(\omega-\bar{\omega})T} - e^{-i(\omega-\bar{\omega})T}}{i(\omega-\bar{\omega})} \quad (43)$$

when the time integration is carried out.

In equation (43) we obtained $D_1(\bar{\omega})$ in terms of $D_2\left(\frac{n(\omega)\omega}{c}\right)$. So, our strategy becomes to place (43) into the solution for the real-ω approach

$$E_{aR}(x,t) = \int_{-\infty}^{\infty} d\bar{\omega} D_1(\bar{\omega}) e^{i(k(\bar{\omega})x-\bar{\omega}t)} \quad (44)$$

to be able to compare $E_{aR}(x,t)$ with the real-k approach solution

$$E_{bR}(x,t) = \int_C d\omega \left(\frac{dk}{d\omega}\right) D_2\left(\frac{n(\omega)\omega}{c}\right) e^{i(k(\omega)x-\omega t)} \quad (45)$$

where integration path C is depicted in figure 1 that is not closed. Equation (45) originates from equation (34).

A. $D_2\left(\frac{n(\omega)\omega}{c}\right)$ has no pole , no branch cut

If $D_2\left(\frac{n(\omega)\omega}{c}\right)$ does not have any pole nor branch cut, see figure 7, integrand in equation (43) has pole only at $\omega = \bar{\omega}$ and branch cut below the real-k contour due to $\left(\frac{dk}{d\omega}\right)$. The $\omega = \bar{\omega}$ pole contributes if real-k contour is closed up for $e^{i(\omega-\bar{\omega})T}$ term and branch cuts contribute if if real-k contour is closed down for $e^{-i(\omega-\bar{\omega})T}$ term. We obtain the relation

$$D_1(\bar{\omega}) = \left(\frac{dk}{d\omega}\right)_{\omega=\bar{\omega}} D_2\left(\frac{n(\bar{\omega})\bar{\omega}}{c}\right) - \lim_{T\to\infty} \sum_{1,2} \oint_{C_{1,2}} d\omega \left(\frac{dk}{d\omega}\right) D_2\left(\frac{n(\omega)\omega}{c}\right) \frac{e^{-i(\omega-\bar{\omega})T}}{2\pi i(\omega-\bar{\omega})}. \quad (46)$$

When we put (46) into (44), electric field for the real-ω approach becomes

$$E_{aR}(x,t) = \int_{-\infty}^{\infty} d\bar{\omega} \left(\frac{dk}{d\omega}\right)_{\omega=\bar{\omega}} D_2\left(\frac{n(\bar{\omega})\bar{\omega}}{c}\right) e^{i(k(\bar{\omega})x-\bar{\omega}t)} - \lim_{T\to\infty} \sum_{1,2} \oint_{C_{1,2}} d\omega \left(\frac{dk}{d\omega}\right) D_2\left(\frac{n(\omega)\omega}{c}\right) \times \times \frac{e^{-i\omega T}}{2\pi i} \int_{-\infty}^{\infty} d\bar{\omega} \frac{e^{i\bar{\omega}T}}{(\omega-\bar{\omega})}. \quad (47)$$

The last integral of the last term of (47) is evaluated by closing the contour up. Defined by $C_{1,2}$ contours, ω is always below the real-ω line. So that, the second term in (47) is zero. Then, electric field for the real-ω approach comes out to be

$$E_{aR}(x,t) = \int_{-\infty}^{\infty} d\bar{\omega} \left(\frac{dk}{d\omega}\right)_{\bar{\omega}} D_2\left(\frac{n(\bar{\omega})\bar{\omega}}{c}\right) e^{i(k(\bar{\omega})x-\bar{\omega}t)} \quad (48)$$

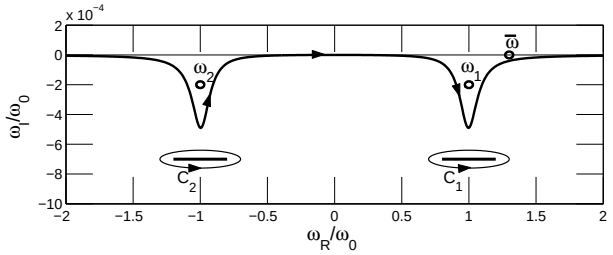

Fig. 8. Real-k integration path, $\int_c d\omega$, in the complex-ω plane. We assume that $D_2\left(\frac{n(\omega)\omega}{c}\right)$ has two symmetric poles at $\omega_1 = \omega_{1R} - i\omega_{1I}$ and $\omega_1 = -\omega_{1R} - i\omega_{1I}$. Equation (51) has three poles at $\omega_{1,2}$ and $\bar{\omega}$.

which is equal to the real-k approach one

$$E_{bR}(x,t) = \int_C d\omega \left(\frac{dk}{d\omega}\right) D_2\left(\frac{n(\omega)\omega}{c}\right) e^{i(k(\omega)x-\omega t)} \quad , \tag{49}$$

because there is no pole nor branch cut of $D_2\left(\frac{n(\omega)\omega}{c}\right)$ in between the integration paths of (48) and (49). In this case both approaches give the same result.

B. $D_2\left(\frac{n(\omega)\omega}{c}\right)$ has pole in between the integration lines

We assume, in difference to the previous case IV-A, that $\left(\frac{dk}{d\omega}\right) D_2\left(\frac{n(\omega)\omega}{c}\right)$ has pole between the two integration lines, see figure 8. If it has a pole at $\omega_1 = \omega_{1R} - i\omega_{1I}$, due to the symmetry property, there must be another pole at $\omega_2 = -\omega_{1R} - i\omega_{1I}$. Then we may express $\left(\frac{dk}{d\omega}\right) D_2\left(\frac{n(\omega)\omega}{c}\right)$ as

$$\left(\frac{dk}{d\omega}\right) \quad D_2 \quad \left(\frac{n(\omega)\omega}{c}\right) = \frac{F(\omega)}{[\omega - (\omega_{1R} - i\omega_{1I})][\omega - (-\omega_{1R} - i\omega_{1I})]} \tag{50}$$

where $F(\omega)$ has the symmetry as $\omega_R \to -\omega_R$. Note that ω_I has same symmetry as $\omega_R \to -\omega_R$.

Closing the contours up, for $e^{i(\omega-\bar{\omega})T}$, 3 poles contribute to $D_1(\omega)$ in (43). Closing the contour down, for $e^{-i(\omega-\bar{\omega})T}$ term, only branch cuts due to $\left(\frac{dk}{d\omega}\right)$ contribute. We obtain

$$\begin{aligned} D_1(\bar{\omega}) &= \left(\frac{dk}{d\omega}\right)_{\bar{\omega}} D_2\left(\frac{n(\bar{\omega})\bar{\omega}}{c}\right) \\ &+ 2\pi i \frac{F(\omega_{1R} - i\omega_{1I})}{2\omega_{1R}} \frac{e^{i(\omega_{1R}-\bar{\omega})T} e^{\omega_{1I}T}}{2\pi i(\omega_1 - \bar{\omega})} \\ &+ 2\pi i \frac{F(-\omega_{1R} - i\omega_{1I})}{-2\omega_{1R}} \frac{e^{i(-\omega_{1R}-\bar{\omega})T} e^{\omega_{1I}T}}{2\pi i(\omega_2 - \bar{\omega})} \\ &- \lim_{T\to\infty} \sum_{1,2} \oint_{C_{1,2}} d\omega \left(\frac{dk}{d\omega}\right) D_2\left(\frac{n(\omega)\omega}{c}\right) \frac{e^{-i(\omega-\bar{\omega})T}}{2\pi i(\omega - \bar{\omega})} \end{aligned} \tag{51}$$

When this is put into equation (44) the last term gives zero, since $e^{i\bar{\omega}T}$ is closed up of the real-ω axis. Due to the symmetry property $F(\omega_1) = F(\omega_2)$. Fourier component of the real-ω case becomes

$$\begin{aligned} D_1 \quad (\bar{\omega}) &= \left(\frac{dk}{d\omega}\right)_{\bar{\omega}} D_2\left(\frac{n(\bar{\omega})\bar{\omega}}{c}\right) \\ + \quad & \frac{F(\omega_1)}{2\omega_{1R}} e^{\omega_{1I}T} e^{-i\bar{\omega}T} \times \\ & \times \left(\frac{e^{i\omega_{1R}T}}{(\omega_{1R} - i\omega_{1I} - \bar{\omega})} - \frac{e^{-i\omega_{1R}T}}{(-\omega_{1R} - i\omega_{1I} - \bar{\omega})}\right) \end{aligned} \tag{52}$$

We put (52) into (44) to determine the electric field for the real-ω approach as

$$\begin{aligned} E_{aR} \quad (x,t) &= \left(\frac{dk}{d\omega}\right)_{\bar{\omega}} D_2\left(\frac{n(\bar{\omega})\bar{\omega}}{c}\right) e^{i(k(\bar{\omega})x-\bar{\omega}t)} \\ + \quad & \lim_{T\to\infty} \frac{F(\omega_1)}{2\omega_{1R}} e^{\omega_{1I}T} \int_{-\infty}^{\infty} d\bar{\omega} e^{-i\bar{\omega}T} e^{i(k(\bar{\omega})x-\bar{\omega}t)} \\ & \times \left(\frac{e^{i\omega_{1R}T}}{(\omega_{1R} - i\omega_{1I} - \bar{\omega})} - \frac{e^{-i\omega_{1R}T}}{(-\omega_{1R} - i\omega_{1I} - \bar{\omega})}\right) \end{aligned} \tag{53}$$

Since T $to\infty$, due to the $e^{-i\bar{\omega}T}$ term real $\bar{\omega}$ integration is closed down. The contour includes two poles at $\bar{\omega} = \omega_{1R} - i\omega_{1I}$ and $\bar{\omega} = -\omega_{1R} - i\omega_{1I}$ and two branch cut loops $C_{1,2}$. Branch cuts occur due to the $e^{ik(\bar{\omega})}$ term. Each branch cut is marked with two points $\omega_{b1} = \omega_{bR1} - i\omega_{bI}$, $\omega_{b2} = \omega_{bR2} - i\omega_{bI}$ for the contour C_1 and $\omega_{b3} = \omega_{bR3} - i\omega_{bI}$, $\omega_{b4} = \omega_{bR4} - i\omega_{bI}$ for the contour C_2. All have same imaginary part. Electric field becomes

$$\begin{aligned} E_{aR}(x,t) &= \int_{-\infty}^{\infty} d\bar{\omega} \left(\frac{dk}{d\omega}\right)_{\bar{\omega}} D_2\left(\frac{n(\bar{\omega})\bar{\omega}}{c}\right) e^{i(k(\bar{\omega})x-\bar{\omega}t)} \\ &+ \lim_{T\to\infty} \frac{F(\omega_1)}{2\omega_{1R}} \left(e^{ik(\omega_1)x-\omega_1 t} - e^{ik(\omega_2)x-\omega_2 t}\right) \\ &+ \lim_{T\to\infty} \frac{F(\omega_1)}{2\omega_{1R}} e^{\omega_{1I}T} e^{-\omega_{bI}T} \\ &\times \left(\int_{\omega_{bR1}}^{\omega_{bR2}} d\omega_{bR} f(\omega_{bR}) + \int_{\omega_{bR1}}^{\omega_{bR2}} d\omega_{bR} f(\omega_{bR})\right), \end{aligned}$$

where the integrals on the last term are carried over the two sides of the each branch cut line. The last term does not contribute, because $\lim_{T\to\infty} e^{\omega_{1I}T} e^{-\omega_{bI}T} = 0$ since $|\omega_{bI}| > |\omega_{1I}|$.

Then the electric field for the real-ω approach (54) is the same with the real-k approach

$$E_{bR}(x,t) = \int_C d\omega \left(\frac{dk}{d\omega}\right) D_2\left(\frac{n(\omega)\omega}{c}\right) e^{i(k(\omega)x-\omega t)}. \tag{55}$$

This is because, the open contour C, joined with the reverse real axis integration, also contains the poles $\omega_{1,2}$.

In this case, too, no difference between the two approaches exists.

V. Average Energy Flow of Optical Pulses in Dispersive Medium

Peatross et. al. [4] analytically derived an expression for the average velocity of a pulse in an absorbing medium. They used the Poynting vector to calculate the average time

$$\langle t \rangle_x = \frac{\int_{-\infty}^{\infty} dt\ t\ S(x,t)}{\int_{-\infty}^{\infty} dt S(x,t)} \tag{56}$$

at which the pulse is on the space point, let it be a detector, x. WE simplified the problem to 1D.

The same problem can be treated in a different point of view: Average spatial position

$$\langle x\rangle_t = \frac{\int_{-\infty}^{\infty} dx\ x\ S(x,t)}{\int_{-\infty}^{\infty} dx S(x,t)} \tag{57}$$

where the pulse is at time t.

One may calculate the pulse velocity referring both to (56) and (57). If Poynting vector average is a good identity to determine the group velocity of a signal, then these two approaches must give similar velocities.

When the index of the medium is complex, (56) is easily treated in the real-ω approach [4] since $S(x,t)$. is easily fourier transformed. Average position (57), however, is easily treated in the real-k approach.

Since the mathematical procedure relating the fourier coefficients $E(x,\omega)$ and $E(k,x)$ has not been studied in a complex indexed medium, however, two group velocity could not be compared.

Being derived the aforementioned connection in the previous subsection III-C, we managed to compare the time arrival velocity (from (56)) and pulse center propagation velocity from (from (57)).

In subsections V-A and V-B we shortly mention the velocity derivation using the real-ω and real-k approaches, respectively. In subsection V-C we compare the two velocities, nothing that they belong to the same pulse.

A. $\langle t\rangle_x$ Real-ω Approach

Since the time average is considered we expend the electric field and magnetic field as

$$\begin{aligned} E(x,t) &= \frac{1}{\sqrt{2\pi}}\int_{-\infty}^{\infty} d\omega E(x,\omega)e^{-i\omega t},\\ H(x,t) &= \frac{1}{\sqrt{2\pi}}\int_{-\infty}^{\infty} d\omega H(x,\omega)e^{-i\omega t}, \end{aligned} \tag{58}$$

where $H(x,\omega) = \frac{k}{\omega}E(x,\omega)$. Then we can write the average Poynting vector(flux) as the frequency component summation

$$\int_{-\infty}^{\infty} dt S(x,t) = \int_{-\infty}^{\infty} d\omega E(x,\omega)H^*(x,\omega), \tag{59}$$

and the average time

$$\int_{-\infty}^{\infty} dt\ t\ S(x,t) = -i\int_{-\infty}^{\infty} d\omega \frac{\partial E(x,\omega)}{\partial\omega}H^*(x,\omega), \tag{60}$$

where we have used the integration by parts, $E(x,\omega = \pm\infty) = 0$, and $t = \frac{1}{-i}\frac{\partial e^{-i\omega t}}{\partial\omega}$.

Time of arrival of a signal from a source at position x_0 to the detector at position x_0 is given by $\Delta t = \langle t\rangle_x - \langle t\rangle_{x_0}$. When we express the temporal dependence explicitly as

$$E(x,\omega) = e^{ik\Delta x}E(x_0,\omega), \tag{61}$$

$$H(x,\omega) = e^{ik\Delta x}H(x_0,\omega) \tag{62}$$

the arrival time becomes

$$\begin{aligned} \Delta t &= -i\times\\ &\times \Big[\frac{e^{-2k_I\Delta x}\int_{-\infty}^{\infty} d\omega\mathcal{F}(\omega;\Delta x,x_0)H^*(x_0,\omega)}{e^{-2k_I\Delta x}\int_{-\infty}^{\infty} d\omega E(x_0,\omega)H^*(x_0,\omega)} \qquad (63)\\ &\quad -\frac{\int_{-\infty}^{\infty} d\omega\frac{\partial E(x_0,\omega)}{\partial\omega}H^*(x_0,\omega)}{\int_{-\infty}^{\infty} d\omega E(x_0,\omega)H^*(x_0,\omega)},\Big] \qquad (64) \end{aligned}$$

where

$$\mathcal{F}(\omega;\Delta x,x_0) = \left\{\left(\frac{\partial k}{\partial\omega}\Delta x\right)E(x_0,\omega) + \frac{\partial E(x_0,\omega)}{\partial\omega}\right\}. \tag{65}$$

This results in a simple arrival time velocity(inverse)

$$\frac{1}{v_1} = \frac{\Delta t}{\Delta x} = \frac{\int_{-\infty}^{\infty} d\omega\frac{\partial k}{\partial\omega}S(x_0,\omega)}{\int_{-\infty}^{\infty} d\omega S(x_0,\omega))}, \tag{66}$$

where complex harmonic Poynting vector is defined as $S(x_0,\omega) = E(x_0,\omega)H^*(x_0,\omega)$. Note that wave-vector k is complex.

B. $\langle x\rangle_t$ Real-k Approach

When the spatial average is considered we expend the electric field and magnetic field as

$$E(x,t) = \frac{1}{\sqrt{2\pi}}\int_{-\infty}^{\infty} dkE(k,t)e^{ikx}, \tag{67}$$

$$H(x,t) = \frac{1}{\sqrt{2\pi}}\int_{-\infty}^{\infty} dkH(x,\omega)e^{ikx}, \tag{68}$$

where $H(k,t) = \frac{k}{\omega}E(k,t)$, again. Then we can write the average Poynting vector(flux) as the frequency component summation

$$\int_{-\infty}^{\infty} dxS(x,t) = \int_{-\infty}^{\infty} dkE(k,t)H^*(k,t), \tag{69}$$

and the average spatial pulse position

$$\int_{-\infty}^{\infty} dx\ x\ S(x,t) = i\int_{-\infty}^{\infty} dk\frac{\partial E(k,t)}{\partial k}H^*(k,t), \tag{70}$$

where we have used the integration by parts, $E(k=\pm\infty,t) = 0$, and $x = \frac{1}{i}\frac{\partial e^{ikx}}{\partial k}$.

The change of the pulse center position from at time t_0 to at time t is given by $\Delta x = \langle x\rangle_t - \langle x\rangle_{t_0}$. When we express the temporal dependence explicitly as

$$E(k,t) = e^{-i\omega\Delta t}E(k,t_0), \tag{71}$$

$$H(k,t) = e^{-i\omega\Delta t}H(k,t_0), \tag{72}$$

we obtain the pulse center propagation velocity

$$v_2 = \frac{\Delta x}{\Delta t} = \frac{\int_{-\infty}^{\infty} dk\frac{\partial\omega}{\partial k}S(k,t_0)}{\int_{-\infty}^{\infty} dkS(k,t0))}. \tag{73}$$

complex Poynting vector is defined as

$$S(k,t_0) = E(k,t_0)H^*(k,t_0). \tag{74}$$

Now, frequency ω is complex.

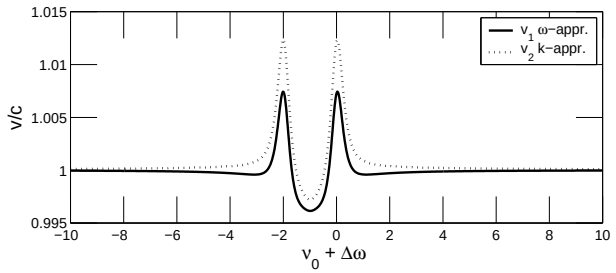

Fig. 9. (solid-line) Group velocity calculated by Poynting vector average $\langle t\rangle_{x_0}$ for fixed position x_0. Treated in real-ω approach. (dotted-line) Group velocity calculated by Poynting vector average $\langle x\rangle_{t_0}$ for fixed time x_0. Treated in real-k approach.

C. Comparison of the Velocities

We assume fourier distributions $D_1(\omega)$ and $D_2(k)$ which does not have any poles nor branch cuts in between the integration paths depicted in figure 1. Then we are able to use the identity (46), $D_1(\bar{\omega}) = \left(\frac{dk}{d\omega}\right)_{\bar{\omega}} D_2\left(\frac{\bar{\omega} n(\bar{\omega})}{c}\right)$. Note that the second term in (46) approaches zero as $T \to \infty$, since all ω on $C_{1,2}$ are complex.

The fourier components are $E(x_0,\omega) \equiv D_1(\omega)$ and $E(k,t_0) \equiv D_2(k)$. Magnetic field components are $H(x_0,\omega) \equiv \frac{k(\omega)}{\omega} D_1(\omega) = n(\omega) D_1(\omega)$ and $E(k,t_0) \equiv \frac{k}{\omega(k)} D_2(k) = n(k) D_2(k)$. Then the first velocity becomes

$$v_1 = \frac{\int_{-\infty}^{\infty} d\bar{\omega} n^*(\bar{\omega}) |D_1(\bar{\omega})|^2}{\int_{-\infty}^{\infty} d\bar{\omega} n^*(\bar{\omega}) \frac{dk}{d\omega}(\bar{\omega}) |D_1(\bar{\omega})|^2} \quad , \tag{75}$$

where $\bar{\omega}$ indicates the reality of the frequency.

Since there is no pole between the integration paths, Fig. 7, second velocity can be written as

$$\begin{aligned} v_2 &= \frac{\int_C d\omega \frac{dk}{d\omega} \frac{d\omega}{dk} n^*(\omega) |D_2(k(\omega))|^2}{\int_C d\omega \frac{d\omega}{dk} n^*(\omega) |D_2(k(\omega))|^2} \\ &= \frac{\int_{-\infty}^{\infty} d\bar{\omega} n^*(\bar{\omega}) |D_2(k(\bar{\omega}))|^2}{\int_{-\infty}^{\infty} d\bar{\omega} \frac{d\omega}{dk}(\bar{\omega}) n^*(\bar{\omega}) |D_2(k(\bar{\omega}))|^2} \quad . \end{aligned} \tag{76}$$

If we use (46) as $D_2(k(\bar{\omega})) = \left(\frac{d\omega}{dk}\right)_{\bar{\omega}} D_1(\bar{\omega})$, we transform v_2 into the form

$$v_2 = \frac{\int_{-\infty}^{\infty} d\bar{\omega} n^*(\bar{\omega}) \left|\frac{d\omega}{dk}(\bar{\omega})\right|^2 |D_1(\bar{\omega})|^2}{\int_{-\infty}^{\infty} d\bar{\omega} \frac{d\omega}{dk}(\bar{\omega}) n^*(\bar{\omega}) \left|\frac{d\omega}{dk}(\bar{\omega})\right|^2 |D_1(\bar{\omega})|^2} \quad . \tag{77}$$

Since v_2, in equation (77), is written in terms of the fourier coefficients of the real-ω approach, we are able to compare the results of the two velocities (75) and (77).

For the frequency spectrum we chose a lorentzian distribution $D_1(\omega) = \frac{1}{[\omega-(\nu_0+\Delta\omega-i\zeta)][\omega-(-\nu_0-\Delta\omega-i\zeta)]}$, whose poles are below the lorentzian index $n(\omega) = \frac{[\omega-(\beta_0-i\rho)]^{1/2}[\omega-(-\beta_0-i\rho)]^{1/2}}{[\omega-(\nu_0-i\rho)]^{1/2}[\omega-(-\nu_0-i\rho)]^{1/2}}$, since $\zeta > \rho$. We used $\rho = \gamma/2$ and $\nu_0^2 = \omega_0^2 + \rho^2$, which are defined in [2].

The numerical results are depicted in figure 9. We observe that real-k approach (77) results in higher velocity everywhere than real-ω approach (75).

Then, the velocity of the center of pulse propagation in spatially is always greater than the average arrival time velocity.

We plan to check the similar velocities for defined as the energy average.

D. Why to treat $\langle t\rangle_x$ and $\langle x\rangle_t$ in different approaches?

In section V-A, while calculating the time average $\langle t\rangle_x$, we used the real-ω approach. In section V-B, while calculating position average $\langle x\rangle_t$, we preferred to use the real-k approach. This parallelism, at first, may seem like that; we performed the calculation of the same quantity in the two approaches and found different results. This is a misunderstanding.

The true story is as follows. After we showed the equivalence of the two approaches, in section IV, we calculated the two different quantities $\langle t\rangle_x$ and $\langle x\rangle_t$. The first is analytically trackable in the real-ω approach, second is in the real-k approach.

As an example we try to treat spatial average $\langle x\rangle_t$ in the real-ω approach, and show the dead-end. Starting from equation (57) we fourier expand the electric fields with real-ω's

$$\begin{aligned} \int_{-\infty}^{\infty} dx\, x\, S(x,t) &= \frac{1}{2\pi} \int_{-\infty}^{\infty} dx \int_{-\infty}^{\infty} d\omega_1 \int_{-\infty}^{\infty} d\omega_2 \times \\ &\times \frac{1}{i} \frac{\partial e^{ik(\omega_1)x}}{\partial k(\omega_1)} e^{-i\omega_1 t} E(\omega_1) e^{ik(\omega_2)x} e^{-i\omega_2 t} \frac{k(\omega_2)}{\omega_2} E(\omega_2), \end{aligned} \tag{78}$$

which can be put in to the form, using similar arguments as in equation (64),

$$\begin{aligned} \Delta x &= \int_{-\infty}^{\infty} dx \int_{-\infty}^{\infty} d\omega_1 \int_{-\infty}^{\infty} d\omega_2 \left(\frac{\partial \omega_1}{\partial k(\omega_1)} \Delta t\right) E(\omega_1) \\ &\times \frac{k(\omega_2)}{\omega_2} E(\omega_2) e^{ik(\omega_1)x} e^{-i\omega_1 t} e^{ik(\omega_2)x} e^{-i\omega_2 t} \ . \end{aligned} \tag{79}$$

This is, however, cannot be simplified further. Because integral

$$\int_{-\infty}^{\infty} dx e^{ik(\omega_1)x} e^{ik(\omega_2)x} \neq 2\pi\delta(k_1 - k_2) \ , \tag{80}$$

since k_1 and k_2 are now complex. Furthermore, this integral diverges. In order to make a progress in (79), one already has to study the mathematics of the previous sections.

ACKNOWLEDGMENT

I acknowledge support from TÜBİTAK-KARİYER Grant No. 112T927 and TÜBİTAK-1001 Grant No. 110T876. I specially thank T. Çetin Akıncı and Ş. Serhat Şeker for their motivational support.

REFERENCES

[1] M.E. Taşgın, Phys. Rev. A **86**, 033833 (2012).
[2] J.D. Jackson, *Classical Electrodynamics*(Wiley, Newyork, 1998), 3rd ed., pp. 336, 348
[3] M. Tanaka, M. Fujiwara, and Hideo Ikegami, Phys. Rev. A, **34**, 4851 (1986)
[4] J. Peatross, S.A. Glasgow, and M. Ware, Phys. Rev. Lett. **84** 2370 (2000)
[5] V. Kuzmiak and A.A. Maradudin, Phys. Rev. B **55**, 7427 (1997).
[6] M. Fleischhauer, C.H. Keitel, M.O. Scully, C. Su, B.T. Ulrich, and S.Y. Zhu, Phys. Rev. A **46**, 1468 (1992).
[7] M.O. Scully and M.S. Zubairy, *Quantum Optics* (Cambridge University Press, Cambridge, 1997).

Mehmet Emre Taşgın received the B.S. degree in physics from Bilkent University, Ankara, Turkey, in 2003 and the Ph.D. degree in physics from Bilkent University, Ankara, Turkey, in 2009. He performed a one year post-doc at Koç University, İstanbul, Turkey, in 2010. He did another one year post-doc in the College of Optics, at University of Arizona, Tucson, AZ, USA, in 2011. Starting from 2012, he is an Asst. Prof. in the Department of Electrical and Electronics Engineering at Kırklareli University, Kırklareli, Turkey. His research interests are quantum optical properties cold atoms, photonic crystals, quantum measurements, spin-squeezing, and electromagnetically induced transparency-like effects in solar cells.

A Measurement System for Solar Energy in Kırklareli

S. Görgülü* S. Kocabey

***Abstract* – This study is focused on the investigation of PV-panel performance in terms of the solar radiation and temperature. For this purpose, a data collection system is established in campus of Kirklareli University and the collected data depending on the seasonal variations are analyzed as well as collection. The collected data set contain of electrical current, voltage, solar radiation and temperature hence, the data are presented by a computer interface.**

Index Terms—**Solar energy, measurement system, PV-panel, data collection.**

I. INTRODUCTION

THE increase in demand for energy in the World, harms of the fossil fuels to the environment and the increase in their prices as they run short increase the demand for the renewable energy sources [1]. At last decade, the solar energy and its related applications began to get an importance in energy environments. The solar energy has essentially two different applications. In this manner, one of them is heat production and another one is electrical energy production.

Photovoltaic cells are semiconductor substances that directly convert sunlight into electrical energy. Photovoltaic cells work based on photovoltaic principle which means that electrical voltage arises when light falls into them. The source of the electrical energy given by the cell is the solar energy on the surface. Solar energy can be converted into electrical energy with a 5% to 30% productivity according to the structure of the photovoltaic cell. Many solar cells are series or parallel connected in order to increase the power output and installed onto a space which structure is called as photovoltaic module [2]. With the advancing technology, manufacturing technologies of the PV chips have also developed and the productivity has been raised.

For the design and implementation of the solar energy systems solar radiation values are needed [3,4]. In Turkey, yearly sunshine duration on avarage is 2640 hours/year and yearly total solar energy on average is 1311 kwh/m^2.

Despite the high solar energy potential of Turkey, this potential cannot be evaluated sufficiently. Appropriate values are needed for the determination of the solar energy potential. In this study, solar energy measurement of Kirklareli is investigated by designing a measuring system.

* S. Gorgulu is is with the Electrical-Electronics Engineering Department, Technology Faculty, University of Kırklareli, Kırklareli, Turkey, (e-mail: sertac.gorgulu@kirklareli.edu.tr).

II. GENERAL PRINCIPLES OF THE MEASUREMENT SYSTEM

In the experimental system formed, there are 40w PV panels of 32 cells and a resistor unit where the energy produced is consumed. In the measurement system, there are a thermometer which is to measure the surface temperature and air temperature on the panel, a multimeter to measure the current and voltage values and a solarimeter to measure the solar radiation values.

40W PV panel has 32 cells. Short circuit current of PV is 2.75A, open circuit voltage is 19.48V, maximum power current is 2.53A and maximum power voltage is 15.84V. Multimeter accuracy is 0.06%, voltage range is 0.01mV to 1000VDC, current range is 0.01μA to 20A. Solarimeter irrigation measuring range is 1-1300 W/m^2, accuracy is 5%. Thermometer operating temperature range is -40 to +260°C, accuracy is ±0.2°C,

Thermometer Multimeter Solarimeter

Fig.1. Measurement devices

III. DATA COLLECTION

Measurement system can be seen on Fig. 2. Measurements are every 60 seconds and continue 24 hours straight. All devices record data and these data are transferred to the computer. The transfer is made after all the values are zero in order not to have data loss.

Measurements' transfer to the computer is started manually but the transfer to the computer from the devices is conducted automatically with the relevant program. The losses occurred when the multimeters transfer data is completed by tracking on the device and the data is recorded completely.

Data transfer program image of the multimeters could be seen on Fig. 3.

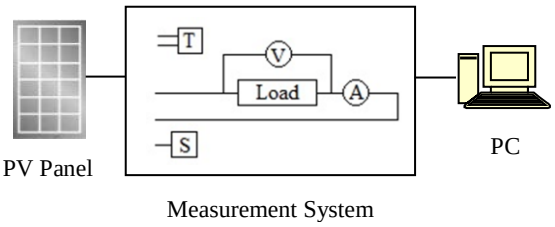

Fig.2. Measurement system

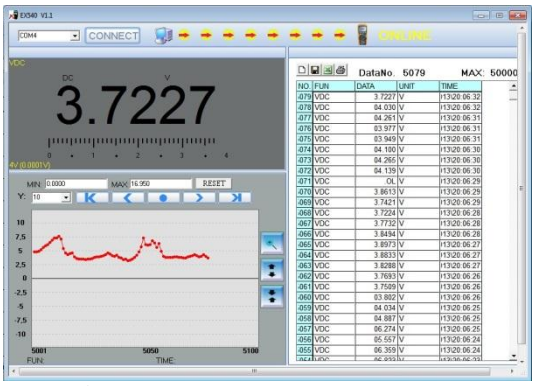

Fig. 3. Program for multimeter

Thermometer's data transfer image could be seen on Fig. 4.

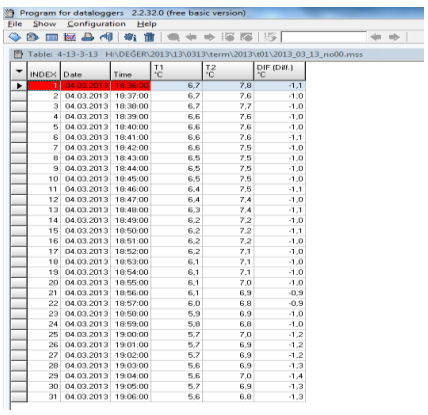

Fig 4. Datalogger program for thermometer

Solarimeter's data transfer program image could be seen on Fig. 5.

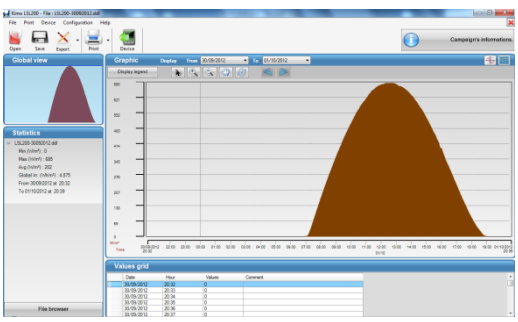

Fig.5. Program for solarimeter

Data kept at all devices are transferred to computers with their own programs. The data transferred to the computer are recorded in an Excel document. The data in excel are aggregated in one document and daily files are constituted.

IV. CONCLUSIONS

Determination of the solar energy potential works is important as they will lead the solar energy investments. A location's solar energy potential is determined with the evaluation of the data of the measurements taken. Optimum conduction of the PV system investments which is of foreign origin and have high first installation cost are aimed with the accurate analysis of the data. In this study, the measurement system that is formed to collect solar radiation, temperature, current and voltage values for Kirklareli is introduced. The data of the measurement system are important for the determination of the solar energy potential of Kirklareli.

V. ACKNOWLEDGEMENTS

This study is supported by Scientific Research Board of Kırklareli University with project number KÜBAP-03.

REFERENCES

[1] C.P. Jacovides, F.S. Tymvios, V.D. Assimakopulous, N.A. Kaltsounides, Comparative study of various correlations in estimating hourly diffuse fraction of global solar radiation, Renewable Energy, 31 (2006) 2492-2504.
[2] http://www.eie.gov.tr (January 2013)
[3] U. Amoto, V. Cuomo, F. Fontana, C. Serio, P. Silverstrini, behavior of hourly solar ırradiance in the Italian climate, Solar Energy 40(1) (1988) 65-79.
[4] L. Wenxian, A general correlation for estimating the monthly average daily direct radiation incident on a horizontal surface in Yunnan Province, China, Solar Energy 41(1) (1988) 1-3.

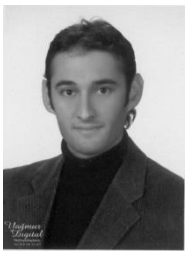

Sertaç GÖRGÜLÜ was born in Karabük in 1978. He graduated from Marmara University, Technical Education Faculty in 2001. In 2002, he started to work as a research assistant in Marmara University. He completed his M.Sc. degree in 2004. He worked as a lecturer at Kırklareli University between 2009-2011. He had his Ph.D. degree from Marmara University in 2011. He has been working as an Assistant Professor at Kırklareli University since 2011.

Süreyya KOCABEY was born in 1973 in Susurluk-Turkey. He received the B.Sc., M.Sc. and Ph.D. degrees from Marmara University. From 1996 to 2009, he worked at Marmara University as a Research Assistant. He has been working at the Electrical - Electronics Engineering Department of Kırklareli University, Turkey as an Assistant Professor since 2009.

Short-Time Fourier Transform for Different Impulse Measurements

E. Onal , J. Dikun

***Abstract*—The aim of this paper is to point out the advantages of the use of the time-frequency analysis in the digital processing of the waveforms recorded in the high voltage impulse tests. Impulse voltage tests are essential to inspect and test insulation integrity of high voltage apparatus. The measured waveforms in practice may contain oscillations and overshoots due to contribution of different noise sources. The different methods incorporating signal-processing method such as wavelets and Short Time Fourier Transform are proposed for failure identification. It is now possible to distinguish failure during lightning tests as well as chopped lightning impulse tests. The method is experimentally validated on a transformer winding. Obtained voltage waveforms usually have some sort of interferences originated from the different sources. These interferences have to be removed from the original impulse data in order to evaluate the waveform characteristics precisely. In this paper two impulse signal are given concerned with the methods used for the time-frequency analysis. The impulse signals are at the pressure of 1 and 3 bar. In this study pressure of the signal are taken as a parameter. Signals are compared according to pressure by using time frequency analysis. Time-frequency analysis is powerful signal processing tool in order to recognize the noise of impulse voltage data. Thus the sources of the noise can be found and eliminated.**

Index Terms—**Impulse Voltage, Time-Frequency Analysis, Short-Time Fourier Transform.**

I. INTRODUCTION

IMPULSE voltage test on high-voltage equipment is essential to evaluate the insulation integrity and to identify the ability to withstand over-voltages encountered during operation. The significance of chopped impulse application is of paramount importance in impulse testing of transformer. The measured waveforms in practice may contain oscillations and overshoots due to contribution of different noise sources. One of the major challenges of impulse voltage and current measurements is the existence of noise that affects the precise identification of impulse parameters. The measurement of lightning impulses with superimposed overshoot or oscillation has been the subject of extensive studies in the last few years in light of results of an important study [1-2] with regard to the relationship of the effective peak voltage and the overshoot frequency. The main findings of the study are the test voltage equation for the determination of the effective peak voltage. The evaluation of the overshoot and the test voltage from an output waveform is performed with the residual filtering method. Basically the evaluation of the high voltage impulse signals consists on the evaluation of the peak amplitude (U_{max}) and three time parameters (T_1: Front time, T_2: Time to half value for full impulse and T_c: Cut-off time). When the level of disturbance in signals is low, computation of these parameters are also quite simple but when the disturbance level rises, they get much more difficult. In terms of frequency contents, there are three kinds of disturbance: Oscillation on the test circuit, electromagnetic disturbance and digitizer noise. The results show that those three disturbance types have different frequency characteristics [3]. The oscillations due to the test circuit have frequency above 500kHz, the electromagnetic disturbance usually is characterized by frequencies in the range of several hundreds of kilohertz (more than 500kHz) up to a few megahertz (less than 10MHz) and the digitizer noise that come from digitizers used in high voltage test halls and these frequencies are clearly above 10MHz. Taking this information into account, the standard states that the evaluation of the HV impulse parameters must be based on the low voltage part of high voltage signal that is actually applied to the equipment under test. The characterization of HV impulses is based on the evaluation peak and time parameters so their spectrum is important to detect the presence of disturbance. Thus, all of the disturbances having frequency above 500 kHz can be removed from the low voltage part before the evaluation of the impulse parameters. For this reason it is very important to know the sources and eliminate the noises [4].

The attention of many researchers has been focused on the disturbances caused by the combination of a high rate of rise of impulses with the stray capacitances and inductances that are present in the circuit. The measuring circuit, as well as the generating circuit, should be as free as possible from oscillations and overshoot. Oscillations can only be accepted if it is certain that they are produced by the test object in connection with the high voltage circuit. It is necessary to ensure that they are generated in the measuring system, e.g. in the low voltage arm of the divider. For this reason in this study, the effect of impulse voltage at the pressure of 1 and 3 bars are considered. It is important to examine the above atmospheric pressure because circuit breakers are used in high pressure like 2-3 bars. It has many advantages over existing methods, since it does not assume any model for estimating the mean-curve, is interactive in nature, suitable for full and chopped impulses, does not introduce distortions due to its application, is easy to implement and does not call for changes to existing standards.

E.Onal is with the Electrical Engineering Department, Istanbul Technical University (I.T.U.), Maslak, Istanbul, 34469, Turkey, (e-mail: eonal@itu.edu.tr).

J.Dukin is with the Electrical Engineering Department, Klaipeda University, Bijūnų 17, 91225, Klaipėda, Lithuania, (e-mail: jeldik@bk.ru).

II. TIME-FREQUENCY ANALYSIS

In this section, mathematical background to be used in this application is focused on the Short-Time Fourier Transform (STFT) techniques and coherence analysis which is presented as cross spectral property between two signals [5].

A. Short-Time Fourier Transform

The signal to be transformed is multiplied by a window function which is defined for a short time period and then it can be represented by the integral form of the classical Fourier transform sliding the window function along the time axis. In application there are so many window type, however, one of the most popular one is "Hanning type windowing". The shape of this window function is appeared as a Gaussian function at around the zero value [6]. In this manner, Short-Time Fourier Transform of a given signal x(t) is described as below:

$$\mathrm{STFT}\{x(t)\} \equiv X(\tau,\omega) = \int_{-\infty}^{\infty} x(t)\omega(t-\tau)e^{-j\omega t}\,dt \qquad (1)$$

For discrete case, STFT of discrete time domain signal x[n] is given by the following equality

$$\mathrm{STFT}\{x[n]\} \equiv X(m,\omega) = \sum_{n=-\infty}^{\infty} x[n]\,\omega[n-m]e^{-j\omega n} \qquad (2)$$

III. MEASUREMENT SYSTEM AND DATA

The lightning impulse voltages used in this study are produced by a 1 MV, 50 kJ, Marx type impulse generator (Fig. 2). The voltages are measured by means of a capacitive divider and a HIAS 743 digital oscilloscope with 12 bit real vertical resolution at 120 Mega sample / sec. All data have sample frequency of 1 Giga sample /sec. Experimental set-up is shown in Fig. 1. The present paper describes a study of two full impulse signal analysis of Sulphur-hexafluoride (SF6) at the pressure of 1 and 3 bar. Sulphur-hexafluoride gas due to its exceptional insulating and arc-extinguishing properties has been widely employed as insulation of high voltage power apparatus.

Signals are carried out using rod-plane electrode with a rod diameter of 1 mm and electrode gap spacing is 5 cm. Rod electrode is connected to high voltage while plane electrode is earthed. Electrodes are mounted in a pressure vessel of 120 mm diameter and 600 mm length. The full impulse signals are shown in figure 3 and figure 4 for the pressure of 1 and 3 bar respectively. All measurements of the experimental study are given in IEC standard.

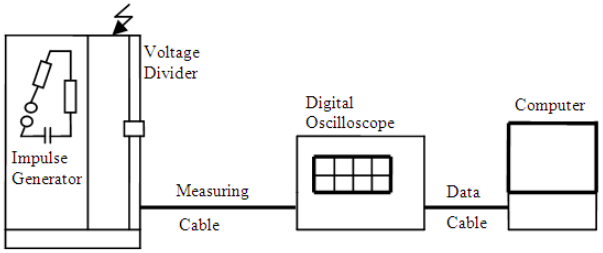

Fig. 1. Experimental set up

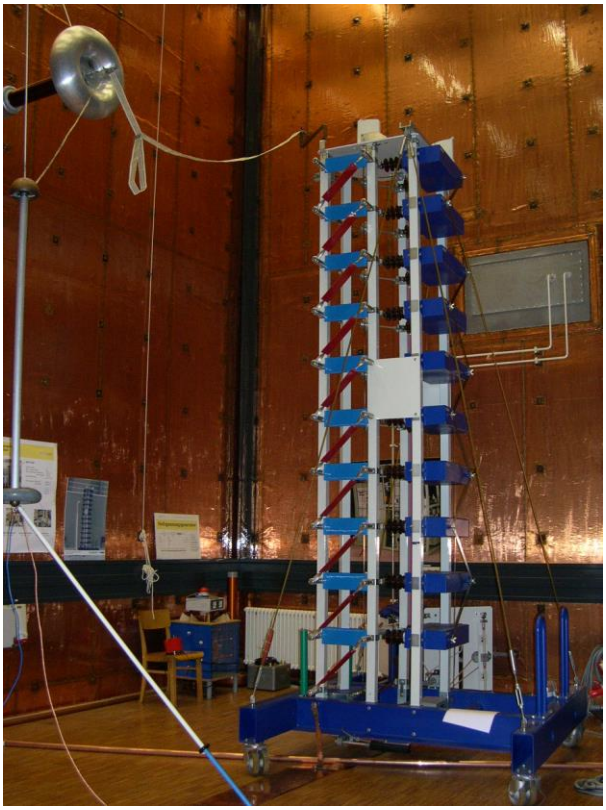

Fig.2. 1 MV Marx impulse generator

T1 and Umax values of the signals which have the pressure of 1 bar and 3 bar are 0.968 µs, 167.1 kV and 0.997 µs, 286.5 kV respectively. The signal evaluation of the pressure value in time-frequency analysis is carried out by using STFT. The impulse signals are compared over a wide range from 0 to 500 MHz, which is the spectrum of the impulse.

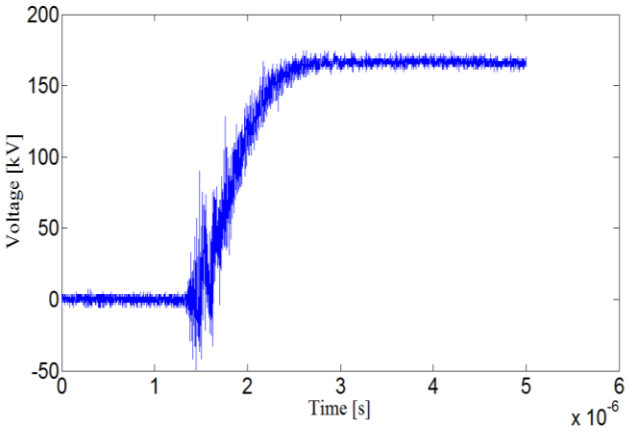

Fig. 3. Full Impulse Voltage Signal for the pressure of 1 bar

These spectrums are shown in figure 5 and figure 6. When the spectrums are examined, it is shown that especially in the range of frequency of 0-4 MHz frequencies are the same and predominant. There are the weak same frequencies which have between 4-500 MHz for two signals. The reason of this is that the frequencies in this range belong to test circuit. In some cases, the oscillations or the overshoot can be eliminated or reduced by improving the electric circuit.

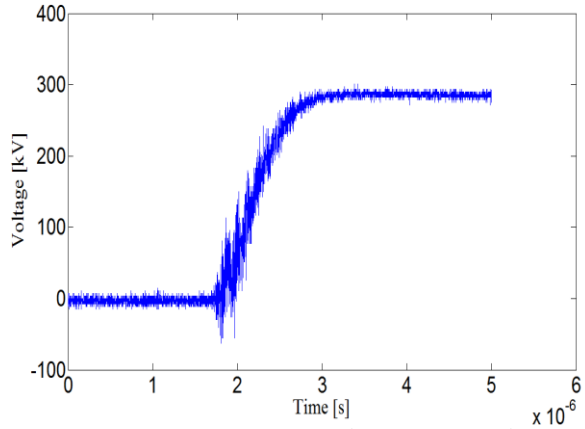

Fig. 4. Full Impulse Voltage Signal for the pressure of 3 bars

It is difficult to establish traceability of the test results and compare them with those of other high-voltage (HV) testing laboratories. All the disturbances with frequencies above 500 kHz must be removed from the lightning voltage waveform before the evaluation of the impulse parameters [7-9]. Removal of noise with low frequency is comparatively difficult as to removal of noise with high frequency.

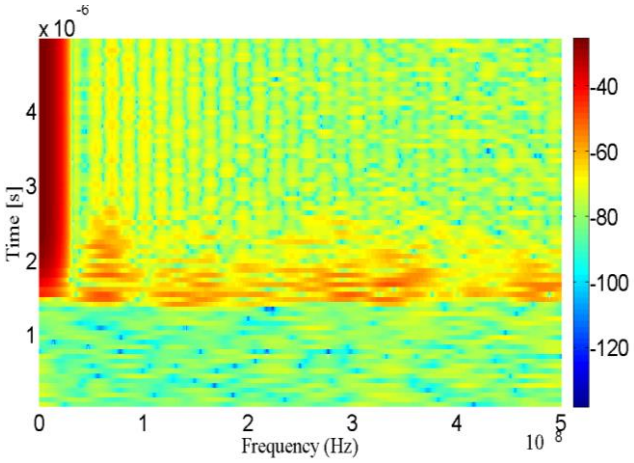

Fig. 4. Time-Frequency Analysis for Impulse Voltage Signal for the pressure of 1 bar

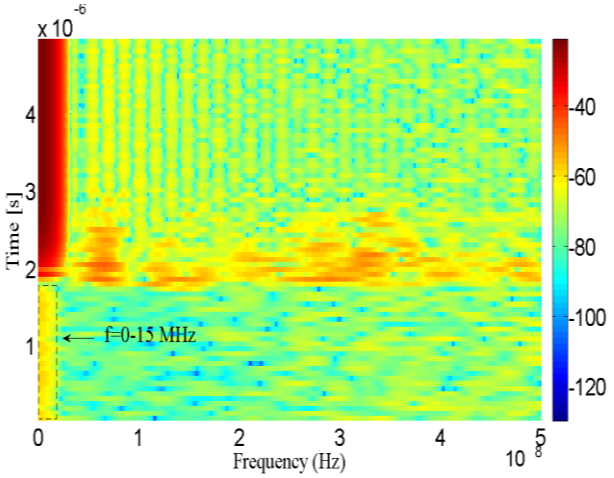

Fig. 5. Time-Frequency Analysis for Impulse Voltage Signal for the pressure of 3 bars

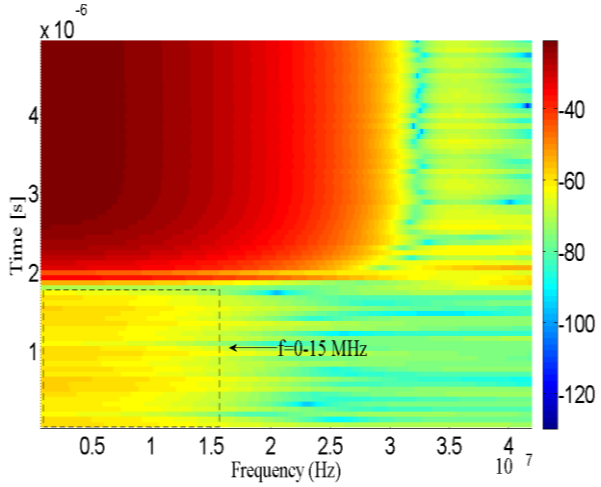

Fig. 6. Detailed Time-Frequency Analysis for Impulse Voltage Signal for the pressure of 3 bars

According to these spectrums, the most important difference in spectrum analysis is shown between the frequency range of 0- 15 MHz. As seen from figure 5, for impulse voltage signal which has the pressure of 3 bar, the frequencies between 0 and 15 MHz are more intensive compared to than that of 1 bar at the time range of 0-2 μs. This case is shown in figure 6 clearly. The common frequencies for the two signals are in the range of 4-500 MHz. These frequencies are occurred at the time range of 1.5 μs-2.5 μs and 2-2.5 μs for the pressure of 1 and 3 bar respectively. These frequencies belong to electromagnetic disturbance and digitizer disturbance coming from environmental. This can be eliminated by using filter and shielding as much as possible. This time range corresponds to the rise time of impulse signals. At this range, corona discharges begin between electrodes before the breakdown phenomena. Corona discharges cause the distortion in the circuit. Electromagnetic interferences radiated from a high voltage impulse generator are mainly caused by the discharges occurring in air gaps, which are used to switching on the impulse generator. Effect of these interferences increases with increase of the applied voltage and decreases with go away the generator. The measuring circuit, as well as the high-voltage generator, should produce or cause as few oscillations and overshoots as possible. Oscillations can only be accepted if it is certain that they are produced by the device under test in connection with the high-voltage generator. It is necessary to ensure that they are generated in the measuring system, e.g. in the low voltage arm of the divider. The increasing pressure creates frequencies which have the range of 0-15 MHz at between 0-1.5 μs. The space charges are pushed back at the time range of 0-1.5 μs for 3 bars. This pressure range can make easy to ionization and weaken the links of SF6 molecules.

IV. CONCLUSIONS AND DISCUSSIONS

When the interference level is high enough, it might not be possible to distinguish signal parameters from the recorded data. One of the major challenges of impulse voltage and current measurements is the existence of noise that affects the precise identification of impulse parameters [10-12]. In some

cases noise interfacing with the measured data can be strong necessitating utilization of de-noising algorithms on measured data, where conventional filtering is inadequate as in the case of white noise [13-14]. This time-frequency analysis has been proven to give quick and reliable results and helps to find the frequency of disturbance. In this study the disturbances noises which are approximately at front of the signal can be reduced by shielding. The electromagnetic interferences in the circuit and the digital recorder quantization noise have been predominant source of error. For our electrode system, the peak of frequency of distortions which has the above 15 MHz belong the digitizers and environmental. As mentioned before, the reason of these situations can be disturbance depending on electrode system. This caused more distortion peaks due to the corona phenomena before the breakdown. The aim of this analysis to determine frequency content of the disturbances whether a given frequency component corresponds to a disturbance that should be removed or not. It can be said that corona begins around the rod electrode. However as in many practical situations, a transient electromagnetic interference can enter the measuring circuit at the divider low-voltage arm, or penetrate through the coaxial cable sheath and the digital recorder enclosure. Ideally, all these devices shall be protected by a perfect electromagnetic shield, but in reality its shielding efficiency decreases with frequency. In this study, the disturbance effect of impulse signal can be reduced in some degree by using shielding cabinet.

ACKNOWLEDGMENT

Authors present their deepest appreciates to Prof. Dr. Serhat Seker from Istanbul Technical University in Turkey and Prof. Stefan Tenbohlen from IEH Stuttgart University in Germany.

REFERENCES

[1] IEC 60060-1, "High Voltage Test Techniques - Part 1 : General Definitions and Test requirements", *Int. Electrotech. Comm*., 1989.

[2] L. Angrisani, P. Daponte, C. Dias, A. Vale, "Advanced Processing Techniques of High- Voltage Impulse Test Signals" *IEEE Trans. on Instrumentation and Measurement*, Vol. 47, No. 2, April 1998.

[3] Standard Techniques for High Voltage Testing, *IEEE Standard 4*, 1995.

[4] F. Garnacho et al., "Evaluation Procedures for Lightning Impulse Parameters in case of Waveforms with Oscillations and/or Overshoot" *IEEE Trans. On Power Delivery*, vol. 12, no. 2, pp. 640 - 649, 1997.

[5] F. Harris, "On the Use of Windows for the Harmonic Analysis with the Dicrete Fourier Transform" in Proceedings of the IEEE, Vol. 66, No.1, pp. 51-83, January 1978.

[6] Z. Kara, J. Dikun, E. Onal, "Time-Frequency Analysis for Different Impulse Voltages" *ISSD2013, 4th International Symposium on Sustainable Development*, Bosnai and Herzegovina, May 2013.

[7] Y. Li and J. Rungis, "Evaluation of parameters of lightning impulses with overshoot," *13th Int. Symp. High Voltage Engineering*, Delft, The Netherlands, Aug. 25 29, 2003.

[8] F. Gamacho et al., "Evaluation of lightning impulse voltages based on experimental results" *Electra*, no. 204, pp. 3 1 - 38, 2002

[9] P. L. Lewin, T. N. Tran, D. J. Swaffield, J. K. Hällström "Zero-Phase Filtering for Lightning Impulse Evaluation: A k-factor Filter for the Revision of IEC60060-1 and -2" *IEEE Trans. on Power Delivery*, Vol. 23, No. 1, January 2008.

[10] E. Onal, O. Kalenderli, S.Seker, **"**Multi-Resolution Wavelet Analysis for Chopped Impulse Voltage Measurements and Feature Extraction" *IEEE Trans on Dielectrics and Insulations*, July 2008.

[11] J. Rungis and Y. Li, "Precision digital filters for high voltage impulse measurement systems," *IEEE Trans. Power Del.*, vol. 14, no. 4, pp. 1213–1220, Oct. 1999.

[12] E. Gockenbach, K. Hackemack, P.Werle, **"**A contribution to the evaluation of lightning impulses with oscillations or overshoot near the peak',, *Intern. Symposium on High Voltage Engineering*, Bangalore, paper no. 7-3, 2001.

[13] O. Altay, O. Kalenderli, "Interference Removal on Impulse Voltage and Current Measurements with Wavelet Analysis," *2012 International Conference on High Voltage Engineering and Application*, Shanghai, China, September, 17-20, 2012.

[14] D. Custodio, A. Almeida do Vale, "High Performance Digital Processing of High Voltage Impulses based on Time-Frequency Analysis," *10th Mediterranean Electrotechnical Conference* Melecon, pp. 766-769, Vol. 2, 2000**.**

Emel Önal was born in Istanbul, Turkey. She received B.Sc., M.Sc. and Ph.D. degrees from Istanbul Technical University (ITU) in Electrical and Electronics Faculty in Istanbul, Turkey. She worked as a visiting researcher at IEH Stuttgart University about GIS technology and transformers between 2006 and 2007. Her interest areas are in the areas of discharge phenomena, generation and measurement of high voltages. She is currently working as associate professor in electrical engineering department at ITU.

Jelena Dikun was born in Klaipeda, Lithuania. She received P.B. from Klaipeda Business and Technology College in Electrical Engineering Faculty (2005-2009) and B.Sc. from Klaipeda University in Electrical Engineering Faculty (2009 – 2011). In present, she continues her education in Electrical Engineering Faculty of Klaipeda University to obtain the M.Sc degree. She visited as a trainee Istanbul Technical University between October 21 and November 22, 2012 that provided by projects JUREIVIS and "Lithuanian Maritime Sectors' Technologies and Environmental Research Development". Her areas of interest are the study of electric and magnetic fields.

Balkan Journal of Electrical & Computer Engineering
BAJECE
International Referred Indexed Journal

ISSN: 2147- 284X
Vol: 1
No: 1
Year: April 2013

CONTENTS

JOURNAL OF
ELECTRICAL & COMPUTER ENGINEERING
(International Referred Indexed Journal)

Contact
www.bajece.com
e-mail: editor@bajece.com
bajece@bajece.com

Phone: +90 288 214 05 14
Fax: +90 288 214 05 16
Kirklareli University,
Engineering Faculty,
Department of Electrical & Electronics Engineering,
39020, Kirklareli-Turkey.